



Preventing Voltage Collapse with Protection Systems that Incorporate Optimal Reactive Power Control

Final Project Report

Power Systems Engineering Research Center

*A National Science Foundation
Industry/University Cooperative Research Center
since 1996*





Power Systems Engineering Research Center

**Preventing Voltage Collapse with Protection
Systems that Incorporate Optimal
Reactive Power Control**

Final Project Report

Project Team

**Venkataramana Ajjarapu, Project Leader, Iowa State University
A.P. Sakis Meliopoulos, Georgia Institute of Technology**

PSERC Publication 08-20

October 2008

Information about this project

For information about this project contact:

Venkataramana Ajjarapu
Department of Electrical and Computer Engineering
Iowa State University
Ames, IA 50010
Tel: 515-294-7687
Fax: 515-294-4263
Email: vajjarap@iastate.edu

Power Systems Engineering Research Center

This is a project report from the Power Systems Engineering Research Center (PSERC). The Power Systems Engineering Research Center (PSERC) is a multi-university Center conducting research on challenges facing the electric power industry and educating the next generation of power engineers. More information about PSERC can be found at the Center's website: <http://www.pserc.org>.

For additional information, contact:

Power Systems Engineering Research Center
Arizona State University
577 Engineering Research Center
Box 878606
Tempe, AZ 85287-8606
Phone: 480-965-1643
Fax: 480-965-0745

Notice Concerning Copyright Material

PSERC members are given permission to copy without fee all or part of this publication for internal use if appropriate attribution is given to this document as the source material. This report is available for downloading from the PSERC website.

© 2008 Iowa State University and Georgia Institute of Technology.
All rights reserved.

Acknowledgements

This is the final report for the Power Systems Engineering Research Center (PSERC) research project S-28 titled “Optimal Reactive Power Control against Voltage Collapse Incorporating Protection System.” We express our appreciation for the support provided by PSERC’s industrial members and by the National Science Foundation’s Industry / University Cooperative Research Center program under the grants NSF EEC-0002917 at Iowa State University and NSF EEC-0080012 at Georgia Institute of Technology.

The authors wish to recognize their postdoctoral researchers and graduate students that contributed to the research and creation of the reports:

Iowa State University

- Hua Bai

Georgia Institute of Technology

- George Stefopoulos, GRA
- Dr. George Cokkinides

The authors thank all PSERC members for their technical advice on the project, especially the industry advisors for the project:

- Ali Chowdury – CAISO
- Jianzhong Tong – PJM
- Mahendra Patel – PJM
- Floyd Galvan – Entergy
- Sharma Kolluri – Entergy
- Bruce Fardanesh – NYPA
- Chetty Mamandur – CAISO

Executive Summary

In recent years, new attention has been given to system disturbances that have cascaded due to voltage instabilities and to unwanted relay operations. Unwanted relay operations due to voltage instabilities and transients have not been well understood. In this project, voltage instability phenomena were studied to develop a comprehensive approach for mitigating the effects of voltage transients and instabilities on designed operation of a protection system. The comprehensive framework covers monitoring, predicting, and assessing system performance for secure power system operation. The developed framework and methodology provide advanced tools use optimal control strategies that can be used to avoid voltage collapse with respect to system-wide voltage instability and undesired protection system operations. The project's specific objectives were:

- to develop realistic models that accurately model voltage dynamics and their effects on protective schemes
- to develop fast and flexible schemes for assessment of voltage stability and relay status
- to develop optimal strategies to prevent voltage instability and maintain adequate relay margins.

The project objectives were accomplished in two integrated steps.

1. Optimal Strategies to Maintain Adequate Voltage Stability and Relay Margins (Volume I)

In this step of the project, we identified schemes for fast and flexible assessment of voltage stability and relay status. Then we developed optimal strategies for maintaining adequate voltage stability and relay margins.

Voltage stability margin (VSM) assessment for online monitoring is a challenging problem computationally. We developed a predictor and corrector based framework to estimate VSM at local buses. The framework applies a Thevein Equivalent method as a predictor to approximate the maximum power that can be transferred. Since Thevein Equivalent is a linear approximation, it cannot consider system operational constraints which cause the VSM estimate by the predictor to be too optimistic. This optimistic estimate especially occurs when the load level is far away from the maximum loading point. We applied a corrector to adjust the predicted VSM to a more realistic value.

The new predictor and corrector based approach can address “what if” questions in an online environment. For example, from the present operating condition, the approach can predict the future margin under various contingencies and scenarios. To assess the effects on the protection system, the relay margin is applied to determine the intended relay status and identify critical relays after contingencies. According to the operating criteria for post-contingency security, the voltage stability margin and relay margin should be maintained at adequate levels. An optimal reactive power control scheme is developed to prevent voltage instability and relay margin violations. Operators can use this information for possible control actions against voltage instability. We tested our approach on a New England 39-bus system. We simulated various contingencies and scenarios. The predictor

and corrector based VSM estimation was very fast and accurate. Based on the relay margin of each relay, critical relays were identified in the test system under several different operating conditions. By performing the optimal reactive power control after contingencies, the system voltage profile, the voltage stability margin at load buses, and the relay margins were improved to insure that system operating criteria were met after any of the contingencies.

Our research provides a proof of concept of the proposed framework. In future work we can test the developed tools on a large utility system. With the above framework, we used existing control sources to maintain relevant margins. In future work, we can identify where and how much supply of additional control sources would be needed when the existing control sources are not adequate to meet system operating criteria.

2. Incorporating Relays in a Power System Model with Dynamic Loads for Voltage Transient and Stability Analyses (Volume II)

Relay operation due to transient voltage phenomena is unneeded if the voltage transient is stable and the system will eventually return to normal voltages. If relay operation did happen in these cases it will deteriorate system conditions and may result in a cascading series of relay operations and eventual system collapse. Therefore relay operation must be inhibited if the voltage transient represents a stable event.

In the second step of this project, we studied the impact of voltage transients and voltage instabilities with an integrated power system simulation model that explicitly represents the load dynamics (mainly motor loads) and the dynamics of reactive power sources. Examples of reactive power sources include generators, over and under exciter limiters, and static VAR sources. The power system model was augmented with relay models. Two specific relays were modeled: (a) overcurrent relays and (b) distance relays.

Two test systems were developed to demonstrate use the augmented simulation model for analysis of voltage instabilities and protective systems. The results illustrated that voltage instabilities during recovery from disturbances can cause excessive current flows that may affect the operation of overcurrent relays and of the impedance seen by distance relays. Distance relays are especially vulnerable to mis-operation because these phenomena exhibit simultaneously low voltages and high currents creating the possibility of load encroachment. The level of these phenomena is dependent upon the specific circuit parameters, and the type and amount of dynamic loads. As a result, it is difficult to develop general guidelines for predicting the level and impact of these phenomena.

Based on these results, we conclude that the proper way to apply the proposed methodology is to study specific systems that are heavily loaded with motor type loads. The prototype power system simulation model has the capability to model a limited number of relays since the objective of the project was to simply demonstrate the feasibility of the approach. To achieve the capability of modeling and comprehensively studying the response of a system, we recommend that the developed methodology be augmented with a full set of relays and further developed into a commercial grade computer program.

Optimal Strategies to Maintain Adequate Voltage Stability and Relay Margins

Volume 1

Project Team

Venkataramana Ajjarapu, Project Leader, Iowa State University

Information about this project

For information about this project contact:

Venkataramana Ajjarapu
Department of Electrical and Computer Engineering
Iowa State University
Ames, IA 50010
Tel: 515-294-7687
Fax: 515-294-4263
Email: vajjarap@iastate.edu

Power Systems Engineering Research Center

This is a project report from the Power Systems Engineering Research Center (PSERC). The Power Systems Engineering Research Center (PSERC) is a multi-university Center conducting research on challenges facing the electric power industry and educating the next generation of power engineers. More information about PSERC can be found at the Center's website: <http://www.pserc.org>.

For additional information, contact:

Power Systems Engineering Research Center
Arizona State University
577 Engineering Research Center
Box 878606
Tempe, AZ 85287-8606
Phone: 480-965-1643
Fax: 480-965-0745

Notice Concerning Copyright Material

PSERC members are given permission to copy without fee all or part of this publication for internal use if appropriate attribution is given to this document as the source material. This report is available for downloading from the PSERC website.

**© 2008 Iowa State University and Georgia Institute of Technology.
All rights reserved.**

Table of Contents

1. Introduction.....	1
1.1 Background	1
1.2 Motivation	2
1.3 Present Status of the Knowledge.....	3
1.4 Power System Protection: A Review	4
1.5 Practical Criteria for Relay Margin and Voltage Stability	5
1.5.1 Dynamic Security Assessment Criteria.....	5
1.5.2 Relay Margin Criteria for Post-Contingency Stability.....	5
1.5.3 Power – Voltage (P-V) Curves.....	5
1.6 Power System Voltage Stability: A Review.....	7
1.7 Overview of Voltage Stability with respect to Maximum Loading	8
1.8 Report Organization	9
2. Theoretical Methodology.....	10
2.1 Relay Status Evaluation using Relay Margin.....	10
2.1.1 Relay Margin and Relay Staying Time	10
2.1.2 Relay Margin Ratio and Relay Staying Time Ratio.....	13
2.1.3 Identification of Critical Relays	14
2.1.4 Critical Relay Identifications by the Power Flow and Time Domain Simulation	15
2.2 Proposed Predictor-Corrector Framework for VSM Calculation.....	16
2.2.1 Introduction	16
2.2.2 Overview of VSM Calculation.....	17
2.2.3 Problem Formulation.....	17
2.2.4 VSM Predictor.....	18
2.2.5 VSM Corrector.....	20
2.2.6 Identification of VSM by Predictor and Corrector.....	22
3. Optimal Control Strategy against Voltage Instability.....	23
3.1 Introduction	23
3.2 Overview	23
3.3 Formulation of the Optimal Control Strategy	23
3.3.1 Control Objective	23
3.3.2 System Constraints	23
3.3.2.1 Load Voltage Limit	23
3.3.2.2 Relay Margin Limit	24
3.3.2.3 Voltage Stability Margin Limit	24
3.3.2.4 On Load Tap Changer (OLTC) Limit	24
3.3.2.5 Shunt Capacitor Limit	25
3.3.3 Mathematical Formulation of the Optimization.....	25
3.4 Overall Framework of Optimal Control Strategy.....	27
4. Numerical Results.....	28
4.1 Numerical Results for Identification of Critical Relays.....	28
4.1.1 23-bus Test System Description.....	28
4.1.2 Numerical Results	29
4.1.3 Conclusions	31

Table of Contents (continued)

4.2	Numerical Results for VSM Calculation.....	32
4.2.1	New England 39-bus Test System Description.....	32
4.2.2	Numerical Results	32
4.2.3	Conclusions	35
4.3	Numerical Results for Optimal Reactive Power Control	36
4.3.1	Numerical Results	36
4.3.2	Conclusions	41
4.3.3	Future Work	41
	References.....	42
	Project Publications	44

List of Figures

Figure 1 Voltage collapse sequence by additional tripping by protective relays	3
Figure 2 Typical P-V curve for voltage stability limit.....	6
Figure 3 Transmission line with mho relays.....	10
Figure 4 Illustration of relay margin of mho relay with $\alpha=0$	12
Figure 5 Illustration of relay staying time of mho relay with $\alpha=0$	13
Figure 6 Flowchart of identifying critical relays by RMR and RSTR.....	15
Figure 7 Critical relay identification by power flow and time domain simulation.....	16
Figure 8 Idea of predictor-corrector based VSM identification.....	18
Figure 9 Load bus and Thevenin equivalent system.....	19
Figure 10 Flowchart of VSM correction by the corrector	21
Figure 11 Identification of VSM by predictor and corrector.....	22
Figure 12 Framework of optimal control strategy against voltage collapse.....	27
Figure 13 One-line diagram of the 23-bus test system	28
Figure 14 Impedance swing trajectory of relay 153-154_2 for contingency 1	30
Figure 15 Relay margin trajectory of relay 203-154 for contingency 1	31
Figure 16 New England 39-bus system	32
Figure 17 Predictor-corrector based VSM identification with contingency	34
Figure 18 Predictor-corrector based VSM identification with load increase	35
Figure 19 System voltage profile before and after optimal control (2-25 outage case) ...	36
Figure 20 Voltage stability margin before and after optimal control (2-25 outage case).	38
Figure 21 Relay margin before and after optimal control (2-25 outage case)	38
Figure 22 System voltage profile before and after optimal control (26-29 outage case) .	39
Figure 23 Voltage stability margin before and after the optimal control (26-29 outage case)	40
Figure 24 Relay margin before and after optimal control (26-29 outage case)	40

List of Tables

Table 1 Relay ranking for contingency 1 in 23-bus test system	29
Table 2 Relay ranking for contingency 2 in 23-bus test system	29
Table 3 Relay ranking for contingency 3 in 23-bus test system	30
Table 4 Numerical results for the VSM calculation	33
Table 5 Optimal reactive power control variable settings	37

1. Introduction

1.1 Background

The primary motivation for this project arises from the critical need to provide fast calculation of voltage stability margin (VSM) and quick identification of critical relays using real-time measurements. To achieve this objective one needs analytical tools to enhance power system voltage stability incorporating protection systems.

Wide area blackouts in power systems are considered as system-wide events caused by combination of diverse events such as severe system faults, excessive load demand, and human/machine errors. In the 1996 WSCC blackout voltage collapse played a major role. In the 2003 Northeast blackout even though it is not directly related to voltage collapse, reactive power played an important role in the blackout. According to 2003 US-Canada outage task force, reactive power supplies in the Northeast were exhausted but the need for reactive power continued to rise as peak load increased. The conclusion is that proper reactive power management would have helped to prevent the initial system events and therefore would have delayed or possibly might even have prevented the resulting blackout. In the experience of most system blackouts, the initiating event was a protection device operation that played a very important role in triggering cascading events and finally wide-area voltage collapse. This direct impact of protection system on the phenomenon suggests that integration of protection systems into a unified framework for control determination against voltage collapse.

This project proposes a comprehensive framework to monitor, predict, and assess the system performance for secure power system operation, considering reactive power aspects and protection schemes applied in power systems. The proposal provides advanced tools that can be used to avoid voltage collapse with respect to system-wide voltage instability as well as undesirable protective operation. In addition, the proposal provides a framework for fast, flexible and reliable calculation of voltage stability margin, which are composed of predictor, predicting the VSM directly by using Thevenin Equivalent method and corrector, correcting the VSM to be close to the true maximum loadability point. Particularly, the project first applied the concept of relay margin to evaluate relay status and identify critical relays with different system contingencies. Then the project develops a novel predictor and corrector based framework to calculate voltage stability margin quickly, flexibly and accurately. Finally we propose an optimal reactive power control scheme which incorporates the constraints of voltage stability margin and relay margin to maintain voltage stability. Since the system protection scheme is integrated in the system model, the method proposed here can also identify adequacy or deficiency of control resources in the system.

1.2 Motivation

The security of a bulk power system is threatened when it is loaded near to its maximum capacity. Voltage instability and undesirable protective relay operation¹ are two major interrelated phenomena that occur when the system is under stress. As reported in many voltage collapse incidents [1-3], when the system experiences excessive voltage drop after one or more severe faults, high loading conditions on system components tend to operate protective relays and to further trip the corresponding components, leading to spreading of cascading events of tripping. The lack of reactive power during heavy loading conditions may trigger field limiters and overload protection to trip the generators. Undoubtedly, this directly contributes to wide-area blackouts.

Even though it is not hard to find interrelation between voltage collapse and system component protection, however, there are very few references to come up with countermeasure both considering system wide voltage collapse as well as undesirable protective operation. Generally, control determination for voltage stability enhancement first detects the margin boundary with the given direction of load increase and then calculates control strategies by applying the optimal reactive power control framework. However, the control strategies may fail when another severe tripping due to protective operation occurs. Thus, consideration of protection actions is required when deciding control strategies against voltage collapse.

One of the main objectives in this project is to determine control strategies for preventing further tripping events resulting from unwanted protective actions that make systems more vulnerable in terms of voltage stability. Fig. 1 illustrates the sequence of the events that are mainly concerned in this project. In the normal state, the system is operated at the point 'a'. After N-1 (or N-k) contingency, if the system is transiently stable, short-term dynamics settles down to the point 'b', and because of load recovery dynamics, the equilibrium of the short-term dynamics moves along the $P-V$ curve of N-1 case. If the long-term load characteristic is constant power as shown in Fig. 1, equilibrium point of total system dynamics will reach the point 'c' and settles down. However, during the transition from the point 'b' to 'c', if one of the protective relays of main transmission facilities violates its normal operational limits or seriously exceeds its own rating, another event of tripping happens. If the trip of the transmission facility is in a set of severe contingencies, the systems may be in great danger, and it may lead to cascading events resulting in voltage collapse.

¹ Undesired relay operation is here defined by action of protective relay that happens without any faults in the systems and causes inappropriate trippings leading to aggravate situation during voltage instability.

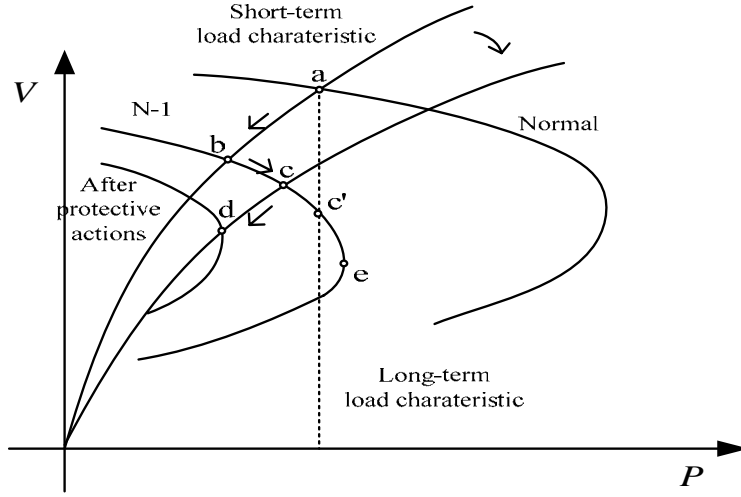


Figure 1 Voltage collapse sequence by additional tripping by protective relays

1.3 Present Status of the Knowledge

To prevent these kinds of events caused by undesired protective actions, adequate setting of relay parameters in the corresponding protection equipment is required. In the recent deregulated environment, however, flow patterns and system states are constantly changing and fixed settings of these parameters cannot cover all the possible undesired actions. In reference [4], an adaptive scheme for preventing unintended trips of zone 3 distance relay is proposed, which can be implemented on modern numerical relays. However, this scheme itself cannot remove the fundamental problem of low voltage and high reactive current. In reference [5], system protection scheme with coordination of protection and system requirement is emphasized to form a defense plan against system breakdown due to prohibitive cost of wide area blackouts. A scheme of adaptive wide area protection for mitigating voltage collapse has been proposed by some researchers by applying a fuzzy inference system. The system inputs are fault detection, VSI (voltage stability index), and signals from component protection devices.

This project considers optimal reactive power control strategy including voltage stability margin and relay margin constraints to prevent system from voltage collapse and unwanted protective actions. The framework includes fast identification of critical relays in the system after contingencies, quick identification of voltage instability by predictor-corrector based voltage stability margin calculation, and determination of optimal countermeasure against voltage collapse; i.e., the determination of optimal control measures to force the system out of the voltage instability region and conditions of undesired protective actions.

1.4 Power System Protection: A Review

The blackout events are reported in many countries all over the world. From these reports, we know that the protection system has played an important role. The transmission protection device operation is usually the initial trigger of the cascading events. Since the transmission lines are exposed to the natural environment, they are vulnerable to lightening and tree branches touching the lines which cause a permanent short circuit fault.

Protective relays are the main components of modern protection systems and the main task of protective relays is to trip associated circuit breakers (i.e., transmission lines, generators, transformers, etc.) in response to faults or other conditions for which the protection system is designed. The protective relays are designed to be autonomous and they can make use of the locally measured signals supplied by remote terminal data over pilot channels. Usually, backup relays are also provided which in general operate more slowly and disconnect a larger portion of power system. It has been pointed out that, in many cascading events, the relays of protection systems are activated in undesired manner. Some relays, such as zone 3 distance relays, are sensitive to power flow redistribution due to contingency or switch operation out of the protected region, and thus may be undesirably activated to trip lines and machines in power systems.

From the designed functions of protective relays, we know that the relay philosophy is biased towards dependability which means that if there is a fault in the system, the primary relay should operate to clear the fault. This bias towards high dependability inevitably leads to a reduction in security of the protection system. In other words, with the protection system that is designed to be highly dependable, it is more prone to false trip when no trips are warranted. Therefore, there is a conflict between the dependability of protection system and security of power system which has not been solved successfully [6]. As the modern power system is undergoing fundamental changes, such as those brought on by open access and deregulation, we must reexamine this traditional protection philosophy, especially when power systems are nowadays operating under stressed conditions which are very close to the operation threshold of power systems. After a disturbance in a power system, distance relays can observe the power swing of the system according to the relay impedance trajectory mapped on the R-X plane. Distance relays have a great possibility to trip during the unstable power swings. Traditionally, we consider it as severe enough to cause system insecurity, when there is a swing trajectory entering zone 1 of distance relays [7]. Blocking relays during unstable power system perturbation is the often used strategy to prevent possible undesired relay actions. However, from the system aspect, blocking itself can not improve the system operating condition. Further more, blocking will reduce the dependability of the protection system. Therefore, blocking strategy can not solve the problem essentially. There is one straightforward way to detect the possible undesired relay tripping after a disturbance, which is to include the tripping logic of protective relays in the transient stability program [8]. However, this method can not provide information about the importance of relay settings with respect to the power system perturbation. Relay margin proposed in [9] is applied as a measure of closeness of a system trajectory to relay tripping zones.

1.5 Practical Criteria for Relay Margin and Voltage Stability

1.5.1 Dynamic Security Assessment Criteria

Based on the regional council (WSCC) guidelines [10], criteria for dynamic security assessment typically include:

- Inertial stability criteria. This concerns mainly the evolution of relative machine angles and frequencies.
- Voltage excursions (dip or rise) beyond specified threshold level and duration. This includes separate voltage excursion threshold/duration pairs for voltage dip and voltage rise, and maximum/minimum instantaneous excursion threshold.
- Relay margin criteria. These are defined for pre-disturbance and post disturbance conditions. If relay margin is violated for more than a maximum specified time after the disturbance, it is identified as insecure.
- Minimum damping criteria. For a designated list of contingencies, if the post disturbance system exhibits oscillations, they must be positively damped (decreasing in amplitude).

1.5.2 Relay Margin Criteria for Post-Contingency Stability

According to Reliability Standards and Security Criteria of IESO of Ontario [11], the following relay margin requirements should be satisfied to ensure post-contingency stability:

“Following fault clearance or the loss of an element without a fault, the margin on all instantaneous and timed distance relays those affect the integrity of the grid, including generator loss of excitation and out-of-step relaying at major generating stations, must be at least 20 and 10 percent, respectively.

The margin on all other relays whose operation would not affect the integrity of the grid, such as 115 kV or radial 230 kV circuit protections, generator loss of excitation and out-of-step protections on small generating units, those associated with transformer backup protections, must be at least 15 percent on all instantaneous relays and zero percent on all timed relays having a time delay setting less than or equal to 0.4 seconds.

For those relays having a time delay setting greater than 0.4 seconds, the apparent impedance may enter the timed tripping characteristic, provided that there is a margin of 50 percent on time. For example, the apparent impedance does not remain within the tripping characteristic for a period of time greater than one-half of the relay time delay setting. The margin on all system relays, such as change of power relays, must be at least 10 percent.”

1.5.3 Power – Voltage (P-V) Curves

To generate the P-V curve, loads should be modeled as constant MVA. In specific situations, if good data is available, voltage dependent loads and tap-changer action may be modeled in detail to assess the system voltage performance following the contingency and automatic equipment actions but before manual operator intervention. Power flow

programs can be used to generate a P-V curve. In certain situations it may be desirable to manually generate a P-V curve to take into account specific remedies available.

A sample P-V curve is shown below. The critical point of the curve, or voltage instability point, is the point where the slope of the P-V curve is vertical. As illustrated, the maximum acceptable pre-contingency power transfer must be the lesser of:

- a pre-contingency power transfer (point a) that is 10% lower than the voltage instability point of the pre-contingency P-V curve, and
- a pre-contingency transfer that results in a post-contingency power flow (point b) that is 5% lower than the voltage instability point of the post-contingency curve

The P-V curve is dependent on the power factor. Care must be taken that the worst case P-V curve is used to identify the stability limit.

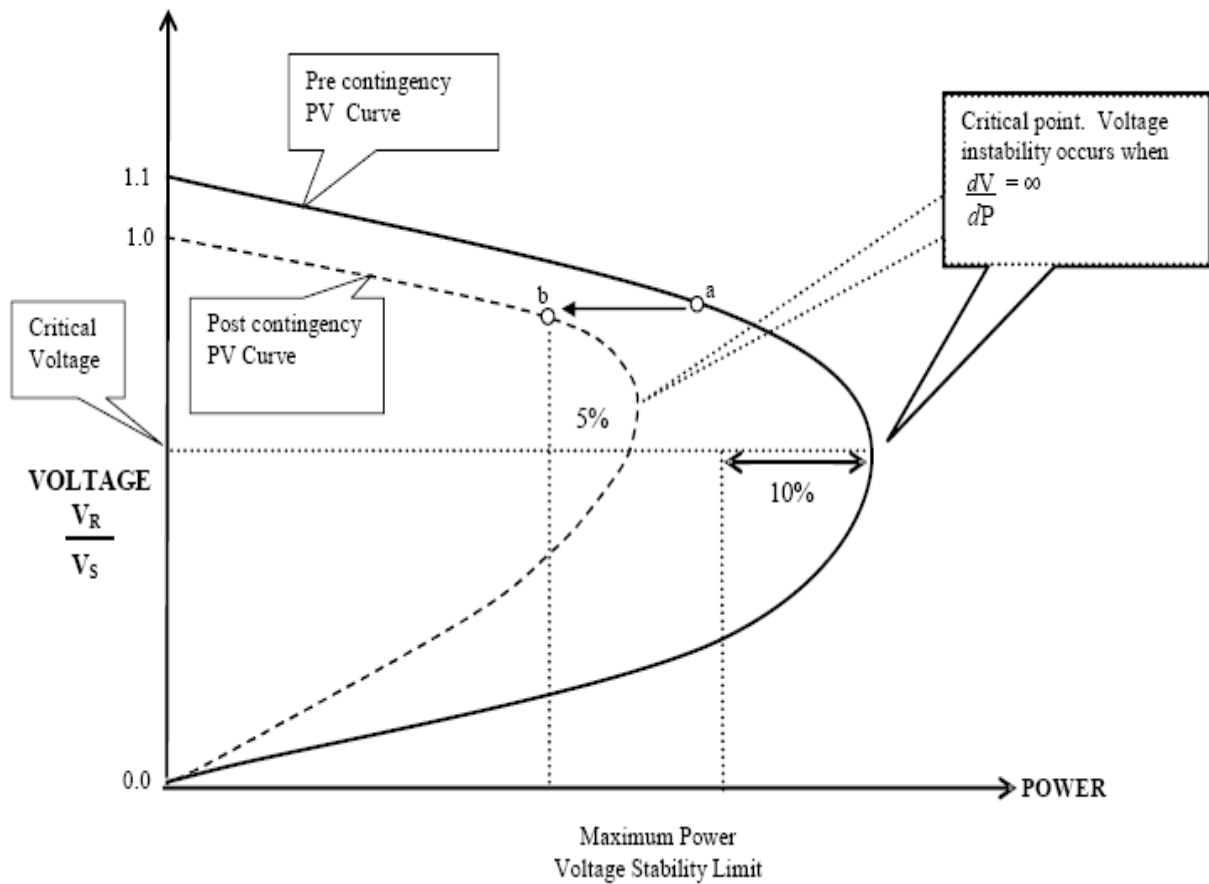


Figure 2 Typical P-V curve for voltage stability limit

1.6 Power System Voltage Stability: A Review

Voltage stability is defined as follows:

Voltage stability refers to the ability of a power system to maintain steady voltages at all buses in the system after being subjected to a disturbance from a given initial operating condition. The term voltage collapse is also often used. It is the process by which the sequence of events accompanying voltage instability leads to a blackout or abnormally low voltages in a significant part of the power system. Reference [12] provides details related to various stability phenomena and definitions. The following sections provide information related to voltage stability and security from that reference [12]

Based on the size of the disturbance, voltage stability can be further classified into the following two subcategories:

- Large-disturbance voltage stability refers to the system's ability to maintain steady voltages following large disturbances such as system faults, loss of generation, or circuit contingencies.
- Small-disturbance voltage stability refers to the system's ability to maintain steady voltages when subjected to small perturbations such as incremental changes in system load.

The time frame of interest for voltage stability problems may vary from a few seconds to tens of minutes. Therefore, voltage stability may be either a short-term or a long-term phenomenon.

- Short-term voltage stability involves dynamics of fast acting load components such as induction motors, electronically controlled loads, and HVDC converters. The study period of interest is in the order of several seconds.
- Long-term voltage stability involves slower acting equipment such as tap-changing transformers, thermostatically controlled loads, and generator current limiters. The study period of interest may extend to several or many minutes, and long-term simulations are required for analysis of system dynamic performance

Security of a power system refers to the degree of risk in its ability to survive imminent disturbances (contingencies) without interruption of customer service. It relates to robustness of the system to imminent disturbances and, hence, depends on the system operating condition as well as the contingent probability of disturbances. System security may be further distinguished from stability in terms of the resulting consequences. For example, two systems may both be stable with equal stability margins, but one may be relatively more secure because the consequences of instability are less severe.

The analysis of security relates to the determination of the robustness of the power system relative to imminent disturbances. There are two important components of security analysis. For a power system subjected to changes (small or large), it is important that when the changes are completed, the system settles to new operating conditions such that no physical constraints are violated. This implies that, in addition to the next operating conditions being acceptable, the system must survive the transition to these conditions. Hence, there are two types of analysis related to security:

- Static security analysis: the steady-state analysis of post-disturbance system conditions to verify that no equipment ratings and voltage constraints are violated.
- Dynamic security analysis: This involves examining different categories of system stability.

1.7 Overview of Voltage Stability with respect to Maximum Loading

The voltage instability process is characterized by a monotonic voltage drop, which is slow at first and becomes abrupt after some time. Voltage collapse occurs when the system is unable to meet the demand, and the phenomenon is characterized by the loss of control of the voltage levels in a power system. Voltage instability and even voltage collapse situations have become more likely to occur, imposing important limitations to power systems operation [13]. Voltage collapse is generally precipitated by one of the following types of system disturbances: load variations, contingencies, or a combination of them. The knowledge of the reactive power reserve condition is of paramount importance in the operation of a transmission network and will strongly affect the reliability of power systems [14].

Voltage stability is an essentially dynamic phenomenon, and the system's behavior depends on the models of the loads and other system components. However, the analysis based on static approaches presents some practical advantages over the dynamical approaches [15]. Analysis based on static approaches has been widely used, since it provides results with acceptable accuracy and little computational effort. These features are desirable in restrictive environments from the computational effort standpoint, such as in a real-time operation environment.

Voltage stability security margins must be determined in operational planning and real-time operation in order to best utilize the available system components [16]. Finding a voltage stability index had become an important task for many voltage stability studies. Many researchers proposed voltage stability indices based on information about the proximity to voltage collapse, such as those based on the Jacobian matrix minimum singular value [17] among others. The continuation method is widely known as a very powerful, though slow, method to estimate systems maximum loading points [18]. Sensitivity techniques have shown to be very useful for determining the voltage stability margins, which can be given in terms of MW, Mvar or MVA [19]. Other research works have focused on maximizing the real power transfer before voltage collapse takes place, for instance, after a strategic reactive load allocation [20]. An alternative approach for determining the maximum loadability using interior point was proposed in [21]. Recently an increase in the loadability of power systems through real power losses minimization has been proposed [22].

Security margins to voltage collapse in parameter space provide important analysis information and can be determined by simple computational procedures while maintaining a good accuracy. Several algorithms have been developed to detect how close a system is to voltage collapse [18], [22]. All of these algorithms assess the distance between the present loading and the maximum loading point in parameter space.

1.8 Report Organization

This report focuses on using relay margin to evaluate relay status and identify critical relays after contingencies and using the proposed predictor-corrector based framework to identify voltage stability margin. The optimal reactive power control strategy which incorporate the voltage stability margin and relay margin can then be used for preventive control.

Section 2 provides the description of the relay margin concept and the proposed predictor-corrector based framework for VSM calculation. The procedures of applications of relay margins and voltage stability margins to identify critical relays and voltage instability in the system are also provided.

Section 3 provides the details about the optimal reactive power control framework and the mathematic model. Especially, the relay margin and voltage stability margin which have been derived in section 2 are incorporated in the optimization model to maintain certain required margins. Also, the other security limits including transmission line thermal limits, bus voltage limits, generator capacity limits are incorporated in the optimization model.

Section 4 deals with the case study carried out on the New England 39-bus system. Based on the relay margin of each relay, the critical relay has been identified. The proposed predictor-corrector based framework for VSM identification is tested using this test system. The optimal reactive power control method is applied to improve the system voltage stability and relay margin after several contingencies.

2. Theoretical Methodology

2.1 Relay Status Evaluation using Relay Margin

Power system protection at the transmission system level is based on distance relays. Distance relays are applied for both apparatus protection and system protection. Significant power flow oscillations can occur on a transmission line or a network due to major disturbances like faults and subsequent clearing. Relay margin related information can be used to evaluate relay status and identify critical relays in the transmission system.

2.1.1 Relay Margin and Relay Staying Time

Traditionally, the impedance based relay margins are mainly used to quantify the closeness of a system trajectory to a relay zone. However, relay margin can also be formulated as a function of the bus voltage instead of the line impedance. This way we can detect the effectiveness of controls applied to power systems for preventing possible undesired relay tripping more efficiently. The relay status during system disturbances can also be quantified based on the information of relay margin ratio and relay staying time ratio.

Figure 3 is used to illustrate the voltage based relay margin. We consider that the offset coefficient α of mho relay is usually close to 0, so the 3-zone characteristic of mho relay can be shown in Figures 4 and 5.

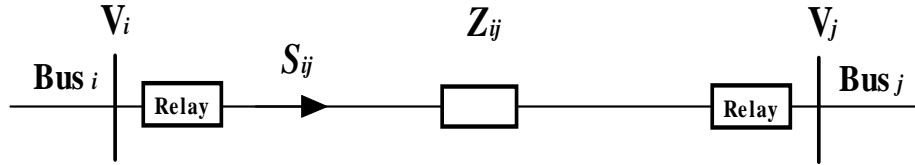


Figure 3 Transmission line with mho relays

From Figure 3, we know that the apparent impedance seen by a relay at bus i , along a transmission line between buses i and j is given as follows,

$$Z_{ij}(v_i, v_j, \delta_i, \delta_j) = \frac{v_i \angle \delta_i}{\frac{v_i \angle \delta_i - v_j \angle \delta_j}{R_{ij} + jX_{ij}}} \quad (1)$$

where v_i and δ_i are the voltage magnitude and angle at bus i , and R_{ij} and X_{ij} are the transmission line resistance and reactance.

From the design logic of distance relays, we know that the tripping of a distance relay depends on: whether the system trajectory enters the relay tripping zone, which

zone of the three zones is entered and how long the trajectory stays in one particular tripping zone. The relay at bus i along the line between buses i and j will operate when

$$|Z_{ij} - \sigma| \leq |\sigma| \quad (2)$$

where

$$\sigma = \frac{\lambda}{2}(R_{ij} + jX_{ij}) \quad (3)$$

is the center of the circle corresponding to the mho relay characteristic in Figure 4.

According to the design scheme of 3-zone distance relay, each protection zone is designed to protect a different range of the transmission line which is referred as λ in equation (3). From the relay setting, we know that usually $\lambda=0.8$ is set for zone 1 and $\lambda=1.2$ for zone 2. Zone 3 setting depends on various factors and λ for zone 3 is usually much higher than zone 2. When the zone 1 of a distance relay in the transmission system is entered during a particular disturbance, the corresponding relay will trip the line instantaneously. If the system trajectory enters the other two zones, it must stay in the zones longer than the pre-set time before the relay tripping operation is activated. However, the transmission system is considered as vulnerable any time when the three zones are entered by system trajectory.

In order to evaluate the relay status during system disturbance, the concept of relay margin is proposed in [8] and it can be applied to evaluate whether some relays in the system are going to initiate the tripping operations. According to the original definition of relay margin in [8], we make some adjustments about the variable. We define the relay margin (RM) as the distance of system trajectory to the zone 3 of distance relay which can be seen directly by the red line in Figure 4. The mathematical formulation of RM can be expressed by

$$RM = |Z_{ij} - \sigma| - |\sigma| \quad (4)$$

$$RM = \left| Z_{ij} - \frac{\lambda}{2}(R_{ij} + jX_{ij}) \right| - \left| \frac{\lambda}{2}(R_{ij} + jX_{ij}) \right| \quad (5)$$

$$RM = \left| \frac{v_i \angle \delta_i}{v_i \angle \delta_i - v_j \angle \delta_j} (R_{ij} + jX_{ij}) - \frac{\lambda}{2}(R_{ij} + jX_{ij}) \right| - \left| \frac{\lambda}{2}(R_{ij} + jX_{ij}) \right| \quad (6)$$

Therefore, the relay operating criteria expressed as (2) can be written as

$$RM(v_i, v_j, \delta_i, \delta_j, R_{ij}, X_{ij}, \lambda) \leq 0 \quad (7)$$

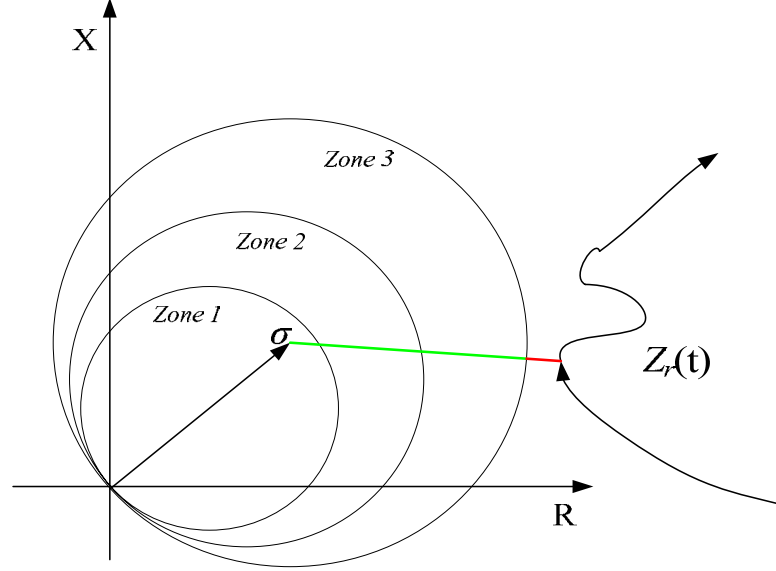


Figure 4 Illustration of relay margin of mho relay with $\alpha=0$

When the system trajectory enters the three zones of distance relay during a system disturbance, we also need to know whether staying time of the trajectory in one particular zone exceeds the preset time for relay tripping. Therefore, we define the relay staying time (RST) as the maximum staying time of a trajectory within one particular zone of relay. Figure 3 shows the relay staying time directly.

The formulation of RST is defined as

$$RST = \max[(t_2 - t_1), (t_4 - t_3), \dots, (t_{2j} - t_{2j-1})] \quad (8)$$

where j is the number of times entering one particular zone.

After the relay margin and relay staying time are defined in this part, in the next section we can apply these two variables to propose two new indexes for evaluating relay status during system disturbances and identifying critical relays.

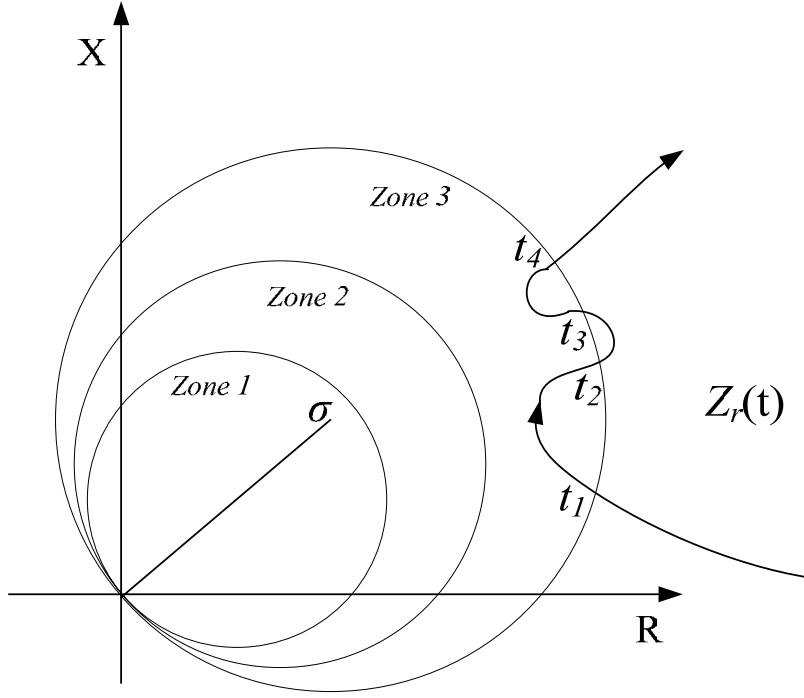


Figure 5 Illustration of relay staying time of mho relay with $\alpha=0$

2.1.2 Relay Margin Ratio and Relay Staying Time Ratio

We propose the following relay margin ratio (RMR). For a contingency “ c ”, the following scalar which corresponds to the minimum relay margin value of relays over the interested time span divided by the relay margin of pre-contingency state is defined as,

$$RMR(c, r) = \frac{\min_t RM(c, r, t)}{RM_0} \quad (9)$$

It will be referred to as RMR which samples the smallest relay margin over the time span ($t=0, 1, \dots, n_t$) divided by the relay margin of pre-contingency state (RM_0) for each relay. The proposed RMR provides a relative value of the current relay margin compared with the pre-contingency relay margin. Actually, by applying the RMR we have given a reference to the current relay margin compared with the pre-contingency state. The threshold of RMR is less than or equal to 1 and greater than or equal to 0. If the RMR value is less than 0, it means that the relay tripping zone is entered by system trajectory and instead of using RMR, the following proposed RSTR will be applied to evaluate relays.

Similarly to the definition of RMR, we also propose a scalar for evaluating the system trajectory staying time within the relay tripping zones which is relay staying time ratio (RSTR). The RSTR is defined as,

$$RSTR(c, r, t) = \frac{RST(c, r, t)}{T_{set}} \quad (10)$$

where T_{set} is the relay pre-set time which is the maximum time for a system trajectory staying within tripping zones before the relay operate. If the value of RSTR is greater than 1, then the relay will initiate the tripping signal.

2.1.3 Identification of Critical Relays

After a contingency, if the tripping zones of some relays are entered, RSTR will be calculated and applied to rank the corresponding relays in a descending order to obtain the set of the most vulnerable relays (MVR). Otherwise, relays will be ranked by RMR in an ascending order to obtain the set of the potentially most vulnerable relays (PMVR). When the system operation condition is changed, some MVRs and PMVRs may change. The above procedure will solve the problem of identification of critical relays. Therefore, we only need to simulate the relay functionality of those critical relays for system stability analysis. Figure 6 shows the procedure of identifying critical relays by RMR and RSTR.

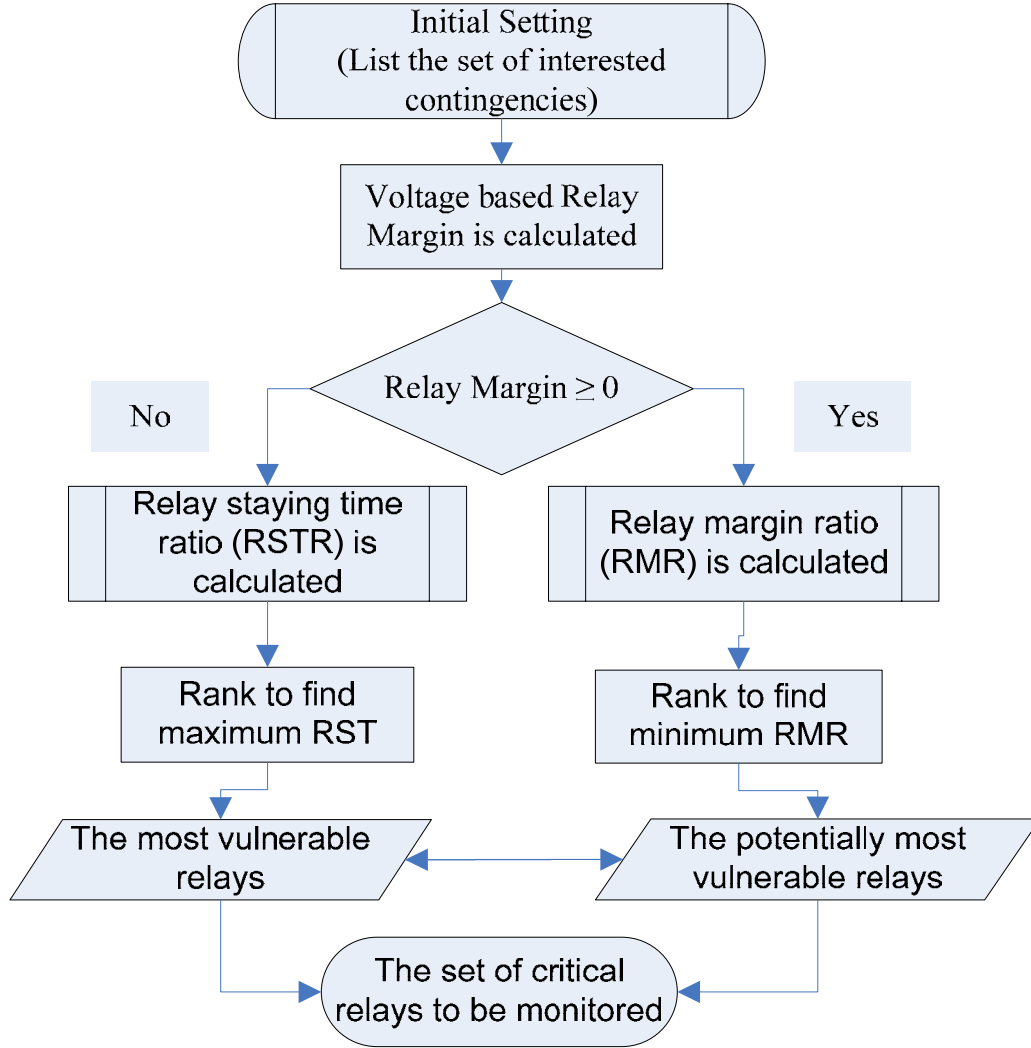


Figure 6 Flowchart of identifying critical relays by RMR and RSTR

2.1.4 Critical Relay Identifications by the Power Flow and Time Domain Simulation

The critical relay identification results by power flow and time domain simulation are different. The details are published in our first of paper of our publication references.

As shown in the Figure 7, the relay margin calculation based on the power flow basically calculates the relay margin at the two points (a and b) on the impedance trajectory which is obtained by the time domain simulation. Point a refers to the pre-contingency state and point b refers to the post-contingency state. Therefore, the power flow based relay margin calculation is just a snapshot of the time domain simulation at one time instant.

The time domain simulation based relay margin calculation can capture all the relay margin values at all the time instants in the time interval. For the identification of critical

relay based on time domain simulation, the minimum relay margin in the interested time interval is picked up for each relay and used to rank them.

Therefore, the time domain simulation based critical relay identification is able to consider the transient period which cannot be done by power flow based analysis. In the optimal control part of this project, we apply the power flow based relay margin calculation. In the next phase of work, we plan to formulate a dynamic optimization model to incorporate the time domain simulation based relay margin as a constraint.

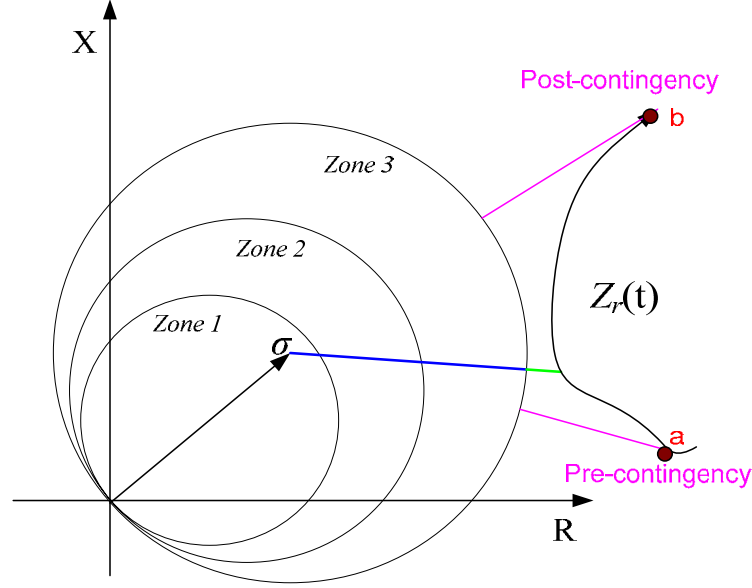


Figure 7 Critical relay identification by power flow and time domain simulation

2.2 Proposed Predictor-Corrector Framework for VSM Calculation

2.2.1 Introduction

This section introduces a fast, flexible and reliable method for identification of voltage stability margin (VSM) using local measurements. The proposed method is based on a predictor-corrector framework. The predictor first derives the Thevenin's impedance at load bus which is used to predict the VSM. The corrector then applies binary search and power flow convergence evaluation to correct the overestimated VSM value by predictor to draw the system back onto the feasibility boundary. Simulation results for a 39-bus test system are shown in the numerical result part which indicates that the proposed method is able to provide a fast calculation of voltage stability margin with a good accuracy.

2.2.2 Overview of VSM Calculation

Recently, there is an increasing concern about power system voltage collapse since less regulated power flow patterns and increased utilization of transmission facilities could more frequently violate system security conditions [23, 24].

Practical loading limits may be encountered by thermal limits of transmission lines, the requirement of maintaining bus voltages within certain limits or the generator reactive power limits. It is possible, well before any theoretical limit is reached, some system constraints may be violated. VSM identification should take into account various system constraints. The VSM could be identified using continuation [18], direct method [25], point of collapse [26] and optimization [27] methods. We propose a new method based on a predictor-corrector (P-C) framework to identify VSM using local measurements. Initially, measured voltage and current are used to estimate Thevenin's impedance for deriving the prediction of VSM. Since Thevenin equivalent is a linear approximation, VSM predictor gives an overestimated value of the maximum loading. The VSM corrector, aiming to draw the system back to the feasibility boundary, applies the binary search algorithm and power flow convergence evaluation to correct the VSM obtained by the predictor.

2.2.3 Problem Formulation

The load flow equations can be written in terms of state variables X and a parameter S as:

$$f(X, S) = f(X) - S = 0 \quad (11)$$

$$S = P_{\max} + jQ_{\max} \quad (12)$$

$$P_{\max} = P_{\text{predictor}} + P_{\text{corrector}} \quad (13)$$

$$Q_{\max} = pf \times P_{\max} \quad (14)$$

$$VSM_P = P_{\max} - P_L \quad (15)$$

where S is the nodal power injection vector, P_{\max} is the nodal real power injection vector, Q_{\max} is the nodal reactive power injection vector after the prediction and correction. pf is the load power factor vector, $P_{\text{predictor}}$ is the nodal real power injection vector after the prediction, $P_{\text{corrector}}$ is the nodal real power injection vector after the correction, P_L is the present load vector and VSM_P is the voltage stability margin vector in term of real power.

Initially, $P_{predictor}$ is derived by the VSM predictor to guess maximum power point. Then, $P_{corrector}$ uses this initial guess to converge to the actual maximum point P_{max} . Fig. 8 shows the basic idea about the predictor-corrector based VSM identification.

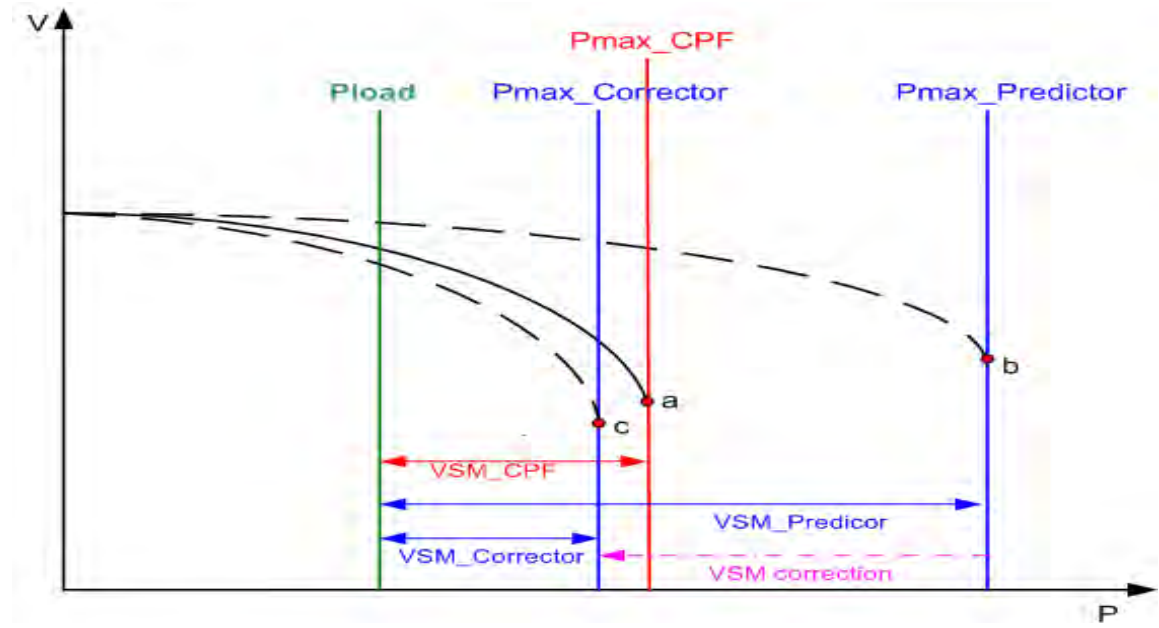


Figure 8 Idea of predictor-corrector based VSM identification

2.2.4 VSM Predictor

The predictor is derived based on Thevenin equivalent. A load bus and rest of the system treated as a Thevenin equivalent is shown in Fig. 9. The predictor-corrector based framework deals with the voltage stability margin calculation from the point of view of local load bus. The main motivation is to estimate how much more power at the local load bus can be increased based on current generation, load level and system operating condition.

The Thevenin equivalent is applied to treat the other parts of the system besides the local load bus as an equivalent system which is made up by an equivalent voltage source \bar{E}_{Th} and an equivalent impedance \bar{Z}_{Th} . Then the original power system is equivalently transformed into a two-bus system. We know that the maximum loadability occurs when the load impedance equals to the network impedance as shown by equations (16)-(18). Therefore, the VSM predictor based maximum load ($P_{predictor}$) is expressed in equation (18). To get the VSM prediction from the Thevenin equivalent, we need to have the local measurements (voltage and current) of the local load bus from the system measurement devices, such as PMU or EMS.

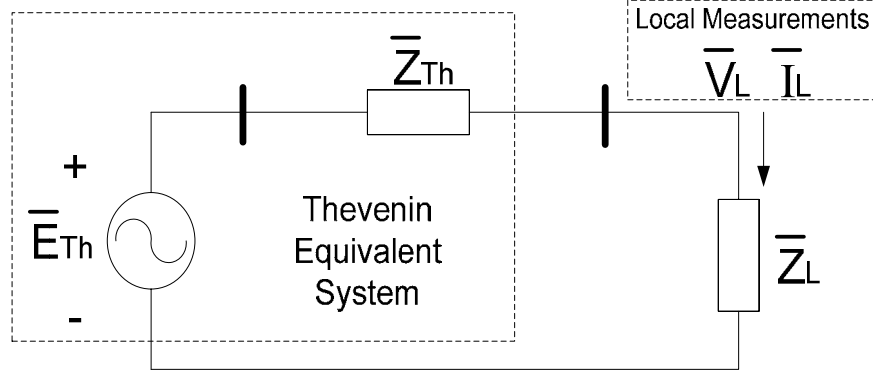


Figure 9 Load bus and Thevenin equivalent system

By Kirchoff's law and reference [28]:

$$\frac{\bar{E}_{Th} - \bar{V}_L}{\bar{Z}_{Th}} = \bar{I}_L = \left(\frac{P + jQ}{\bar{V}_L} \right)^* \Rightarrow P + jQ = \frac{\bar{V}_L * (\bar{E}_{Th} - \bar{V}_L)^*}{\bar{Z}_{Th}^*} \quad (16)$$

$$\text{Maximal Power Transfer} \Leftrightarrow \bar{V}_L = (\bar{E}_{Th} - \bar{V}_L)^* \quad (17)$$

$$P_{predictor} + jQ_{predictor} = \frac{(\bar{V}_L)^2}{\bar{Z}_{Th}^*} \quad (18)$$

For the tracking of Thevenin equivalent, equations (19) and (20) are used,

$$\bar{E}_{Th} = \bar{V}_L + \bar{Z}_{Th} * \bar{I}_L \quad (19)$$

$$\begin{bmatrix} 1 & 0 & -c & d \\ 0 & 1 & -d & -c \end{bmatrix} \begin{bmatrix} E_r \\ E_i \\ R_{Th} \\ X_{Th} \end{bmatrix} = \begin{bmatrix} a \\ b \end{bmatrix} \quad (20)$$

where $\bar{E}_{Th} = E_r + jE_i$, $\bar{V} = a + jb$, $\bar{I} = c + jd$, $\bar{Z}_{Th} = R_{Th} + jX_{Th}$. Two or more measurements taken at different times are required to solve for unknown parameters: E_r , E_i , R_{Th} , X_{Th} . For the online tracking of Thevenin equivalent

parameters, there are several parameters identification methods can be used, such as least square method, Kalman Filter method etc.

Since there are several system measurement devices available, it opens up an opportunity to make use of these measurement data to update the system status and monitor the system stability on line. Given the measurement data from the system load bus, the VSM predictor can quickly predict the voltage stability margin at load buses. This ensures that when the new measurement data is arrived, the last calculation of VSM has already been finished and the new measurements can be continuously used to update the VSM value at local load buses. Being able to apply the real time measurements to predict the VSM on line has several advantages compared with the traditional used offline study method, such as continuation power flow method. One obvious advantage is that, the assumption of load increase pattern is not needed as the load increase information can be obtained and updated by the real time measurements. Therefore, this VSM predictor makes the digital computer calculation based power system analysis results closer to the real power system situations.

2.2.5 VSM Corrector

Since VSM Predictor using Thevenin equivalent which is only a linear approximation (it can not consider the system constraints, such as, thermal limits of transmission lines, requirements of maintaining bus voltages within certain ranges, and limits of generator reactive power output limits) the VSM values at local load buses are over estimated. The VSM corrector is proposed to correct the VSM by predictor and provide a better estimate for VSM. By taking power flow convergence as an indicator, the VSM corrector sets $P_{predictor}$ obtained by the VSM predictor and P_L of the present load as the upper and lower bounds for the search space of P_{max} . Binary search algorithm, which is fast and robust, is used to update $P_{corrector}$ and search for P_{max} which draws the system back onto the feasibility boundary. Fig. 10 shows the flowchart of VSM correction by the corrector.

Since the corrector involves power flow convergence evaluation, it is able to incorporate transmission line thermal limits, bus voltage limits, and generator reactive power limits in the process of VSM correction. The power flow convergence evaluation requires that the updated power flow data being available from the system state estimator. During the process of VSM correction, the forecasted load for the next 24 hour or possible contingencies can also be incorporated to calculate the VSM. Thus several scenarios which the system may face in the next day can be considered to correct the VSM obtained by the predictor. Therefore, the corrector makes the VSM calculation being able to incorporate system constraints for online operation and consider possible system scenarios for the next day planning.

Overall, the predictor-corrector based framework is able to provide fast, flexible and reliable VSM calculation using the system real time measurements from local load buses. The numerical section will provide the test results of the proposed method for VSM calculation. It validates that the predictor- corrector based framework is suitable for online calculation of VSM. The following section provides the procedure of using the

proposed predictor-corrector method to identify VSM using local measurements which may give a clear idea about how to implement it in the real system.

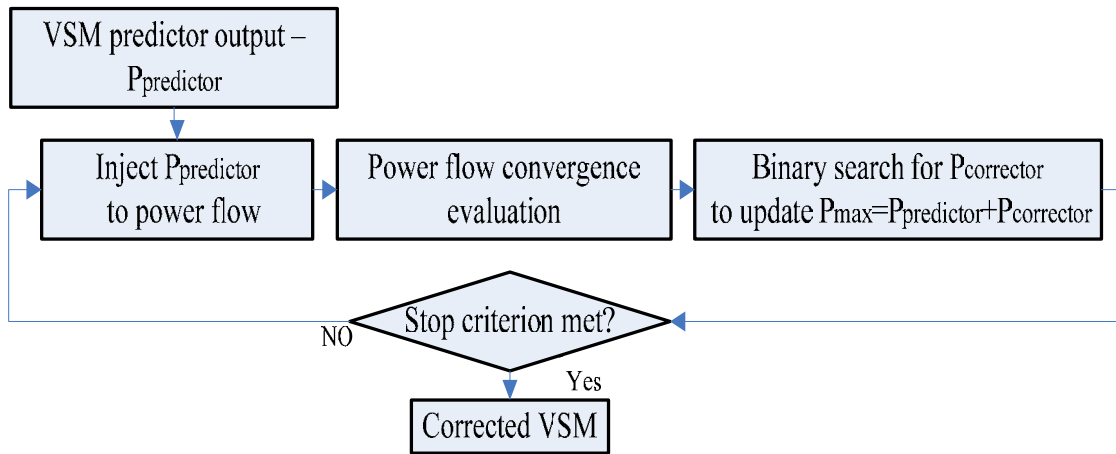


Figure 10 Flowchart of VSM correction by the corrector

2.2.6 Identification of VSM by Predictor and Corrector

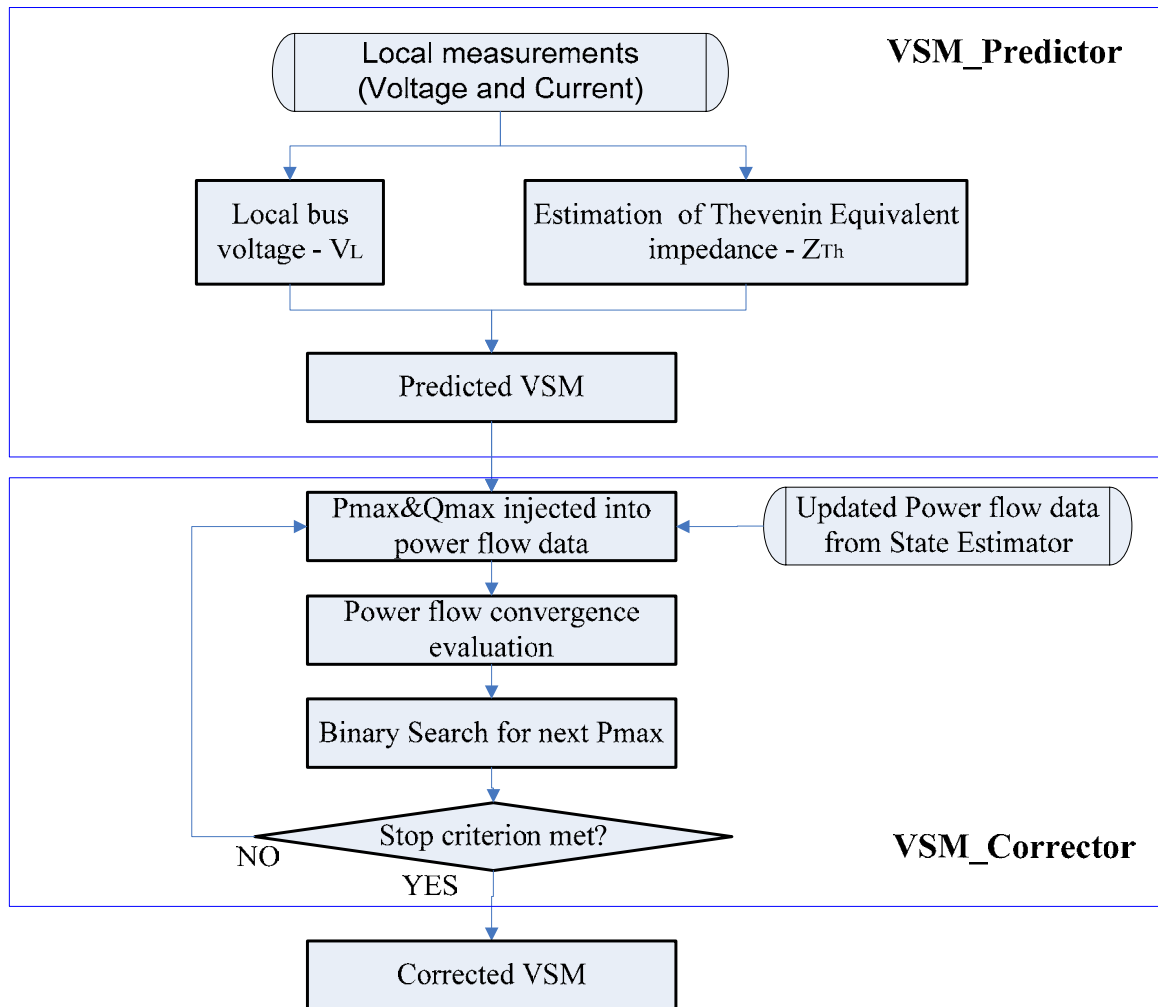


Figure 11 Identification of VSM by predictor and corrector

3. Optimal Control Strategy against Voltage Instability

3.1 Introduction

This section presents the formulation of the reactive power control problem including the voltage stability margin constraint, relay margin constraint, transmission line thermal limits, bus voltage limits, generator capacity limits, AC power flow constraints and control variable limits. Reactive power control is one of the important tasks in the operation and control of the power system. Reactive power control problem can be formulated as a non-linear constrained optimization problem. Minimization of real power loss is the objective of this reactive power optimization problem. The optimization is solved by the heuristic searching algorithm. .

3.2 Overview

The purpose of reactive power dispatch is mainly to improve the voltage profile in the system and to minimize the real power transmission loss while satisfying the unit and system constraints [29]. This goal is achieved by proper adjustment of reactive power control variables like generator bus voltage magnitudes (V_{gi}), transformer tap settings (t_i), reactive power generation of the capacitor bank (Q_{ci}). The optimal reactive power control strategy can provide an operator the optimal control actions or the optimal combination of all the settings of reactive power sources in the system.

3.3 Formulation of the Optimal Control Strategy

3.3.1 Control Objective

Reactive power control can be used to improve the system voltage profile and to minimize the real power transmission loss while satisfying system operation and stability constraints. In this project, we apply the minimization of the real power loss in the system as the objective function for the optimal control model.

3.3.2 System Constraints

3.3.2.1 Load Voltage Limit

For power quality and system security purpose, the load voltages should be maintained in a certain level which is within a specified range around their nominal values. For any load bus i :

$$V_i^{\min} \leq V_i \leq V_i^{\max} \quad (21)$$

where, V_i^{\min} and V_i^{\max} are the allowable minimum and maximum voltages, respectively.

3.3.2.2 Relay Margin Limit

According to the relay margin criteria for post-contingency stability, relay margin should be maintained within certain range to ensure system security,

$$\rho_{c\min} \leq \rho_c \quad (22)$$

where ρ_c represents the relay margin at a particular operating point and $\rho_{c\min}$ is the required margin. The formulation of relay margin can be obtained from the previous section and only voltage phasor measurements are needed to calculate the relay margin.

3.3.2.3 Voltage Stability Margin Limit

Here the voltage stability margin is given as:

$$\lambda_{c\min} \leq \lambda_c \quad (23)$$

where λ_c represents the voltage stability margin for a given operating condition, and $\lambda_{c\min}$ is required margin. The formulation of voltage stability margin and the proposed method to derive the margin can be obtained from the previous section and voltage and current phasor measurements are needed to calculate the voltage stability margin.

3.3.2.4 On Load Tap Changer (OLTC) Limit

Most of the power system loads are voltage dependent and the system voltage drop will cause a reduction in the load demand which may release the stress on the system. However, OLTCs could act within tens of seconds after contingencies to bring the load voltages back to their rated values, which consequently would cause further stress on the system.

The tap ratio of OLTC can be used to control the reactive power and voltage profile of the system,

$$T_i^{\min} \leq T_i \leq T_i^{\max} \quad (24)$$

where T_i is the tap ratio of the OLTC which is one of the three control variables in this optimal reactive power control model.

3.3.2.5 Shunt Capacitor Limit

The application of shunt capacitors increases the maximum transfer capability across power systems. The capacitor banks can be switched on or off with a discrete value. Although the SVCs can provide continuously variable susceptance, they are generally much more expensive than the capacitor banks. For practical implementation consideration, shunt capacitor banks with discrete control is applied in this optimal control problem formulation,

$$Q_{ci}^{\min} \leq Q_{ci} \leq Q_{ci}^{\max} \quad (25)$$

where Q_{ci} is the reactive power output from the shunt capacitor installed in the system which is also one of the three control variables in this optimal reactive power control model.

3.3.3 Mathematical Formulation of the Optimization

The goal of optimal reactive power dispatch is achieved by proper adjustment of reactive power control variables which includes generator terminal voltage magnitudes (VGi), transformer tap settings (Ti), reactive power generation of the capacitor bank (Qci).

The following optimization model is applied to obtain the optimal reactive power dispatch in the power system. The voltage stability margin is incorporated as one of the constraints. The relay margin is also included,

$$\begin{aligned} & \text{Min} : P_{Loss}(V_{Gi}, T_i, Q_{ci}) \\ & \text{s.t.} \end{aligned}$$

$$\text{Power Flow Constraint:} \quad 0 = g(x, y, u)$$

$$\text{Load Voltage Limit:} \quad V_i^{\min} \leq V_i \leq V_i^{\max}$$

$$\text{Generator Voltage Limit:} \quad V_{Gi}^{\min} \leq V_{Gi} \leq V_{Gi}^{\max}$$

$$\text{Line Flow Limit:} \quad -F_j^{\max} \leq F_j \leq F_j^{\max}$$

$$\begin{aligned} \text{Generation Capacity Limit:} \quad & P_{Gi}^{\min} \leq P_{Gi} \leq P_{Gi}^{\max} \\ & Q_{Gi}^{\min} \leq Q_{Gi} \leq Q_{Gi}^{\max} \end{aligned}$$

$$\text{Capacitor Capacity Limit:} \quad Q_{ci}^{\min} \leq Q_{ci} \leq Q_{ci}^{\max}$$

$$\text{OLTC Tap Ratio Limit:} \quad T_i^{\min} \leq T_i \leq T_i^{\max}$$

$$\text{Voltage Stability Margin Limit:} \quad \lambda_{c\min} \leq \lambda_c$$

$$\text{Relay Margin Limit:} \quad \rho_{c\min} \leq \rho_c$$

where g represents power balance equations; x is the vector of state variables; y is the vector of algebraic variables; u is the vector of control variables; P_{Gi} is the generator real power output; Q_{Gi} is the generator reactive power output; P_{Loss} is the real power loss in the network; F represents line flows; V_i is the load bus voltage; V_G is generator terminal voltage; Q_{ci} is reactive power output of shunt capacitors; T is OLTC tap ratio; λ is voltage stability margin (in term of P); ρ is relay margin. In this optimal reactive power control scheme, the control variable vector u is made up by Q_{ci} , T , and V_G .

3.4 Overall Framework of Optimal Control Strategy

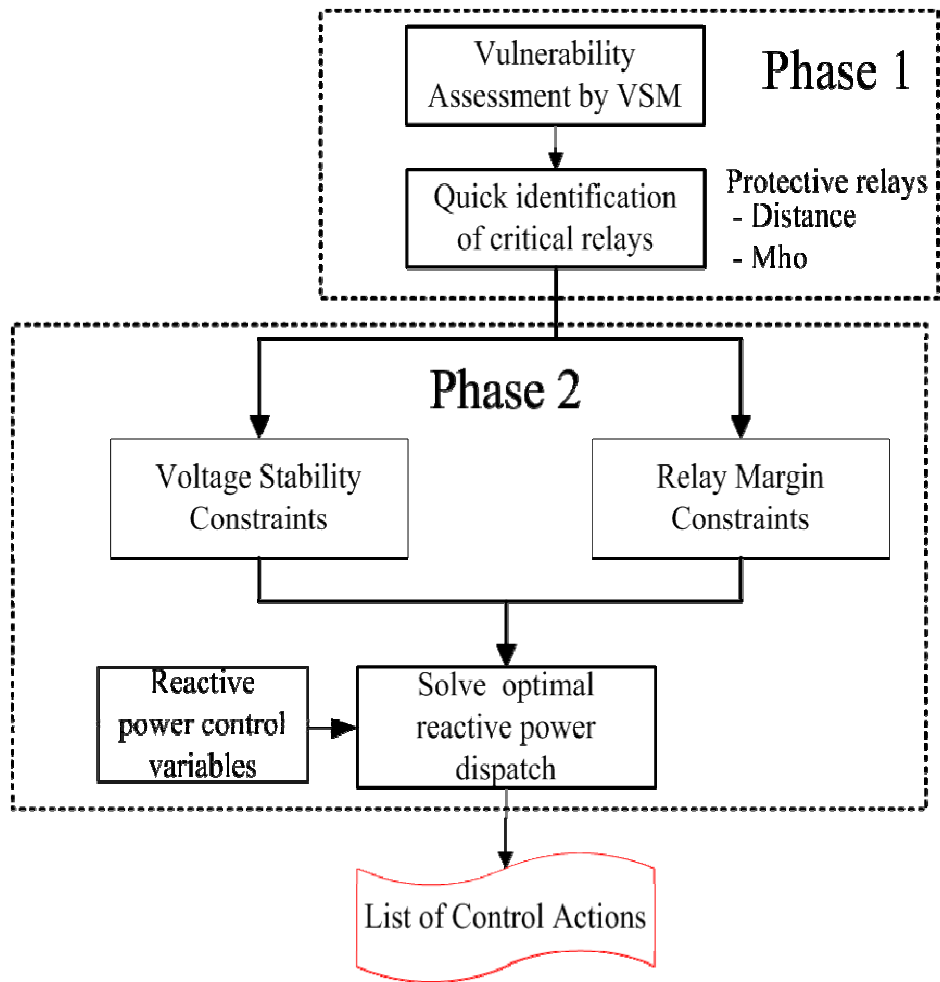


Figure 12 Framework of optimal control strategy against voltage collapse

4.1.2 Numerical Results

Three contingencies are applied to the test system: 1. tripping line *154-205* 2. tripping line *151-201* 3. tripping line *153-154_2*. For the three contingencies, Tables 1-3 tabulate the relay evaluation and ranking results based on the RSTR and RMR values.

Table 1 Relay ranking for contingency 1 in 23-bus test system

	Contingency 1: trip line 154-205				
Relay	RSTR	Relay margin	Relay ranking	RMR	Relay ranking
153-154_2	0.1079		1		1
154-153_2		0.0741	7	0.3966	8
153-154_1	0.1079		2		2
154-153_1		0.0619	5	0.3965	7
3008-154		0.0248	4	0.1122	4
154-3008		0.0668	6	0.2769	6
154-203		0.0878	8	0.2664	5
203-154		0.0243	3	0.0851	3

Table 2 Relay ranking for contingency 2 in 23-bus test system

	Contingency 2: trip line 151-201				
Relay	RSTR	Relay margin	Relay ranking	RMR	Relay ranking
153-154_2	0.0083		1		1
154-153_2		0.0498	8	0.1879	8
153-154_1	0.0083		2		2
154-153_1		0.0414	7	0.1893	9
3008-154	0.0083		3		3
154-3008		0.0295	6	0.1224	6
205-154		0.0061	4	0.0440	4
154-205		0.0110	5	0.0771	5
154-203		0.1178	10	0.2188	10
203-154		0.0755	9	0.1381	7

Table 3 Relay ranking for contingency 3 in 23-bus test system

Relay	Contingency 3: trip line 153-154_2				
	RSTR	Relay margin	Relay ranking	RMR	Relay ranking
153-154_2	0.1079		1		1
154-153_2		0.0741	7	0.3966	8
153-154_1	0.1079		2		2
154-153_1		0.0619	6	0.3965	7
205-154		0.0168	3	0.1529	4
154-205		0.0233	4	0.2050	5
154-203		0.1105	8	0.3356	6
203-154		0.0375	5	0.1313	3

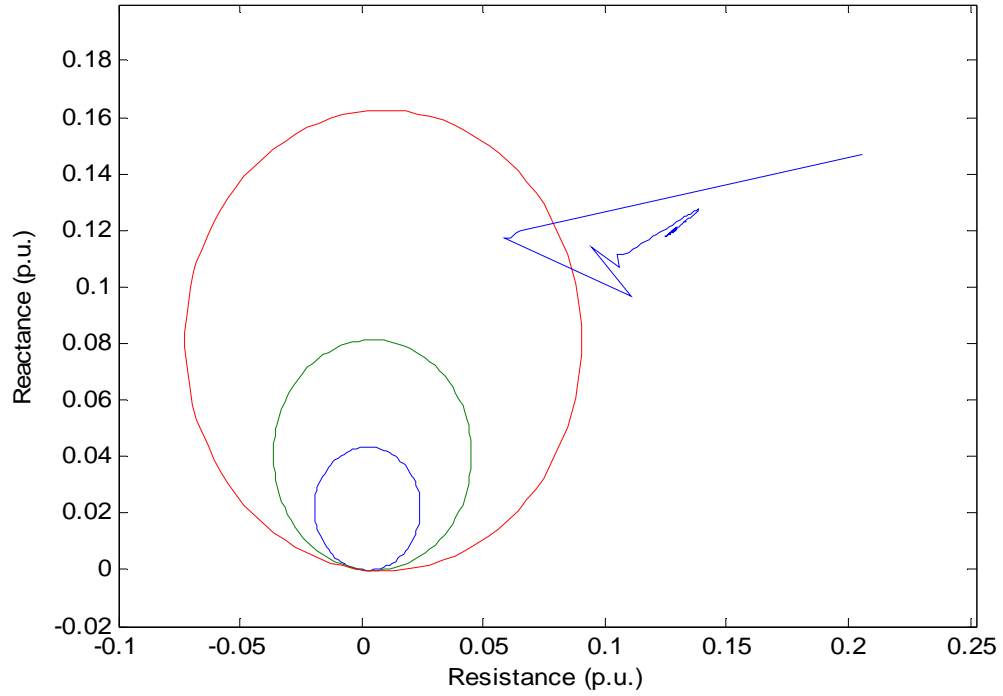


Figure 14 Impedance swing trajectory of relay 153-154_2 for contingency 1

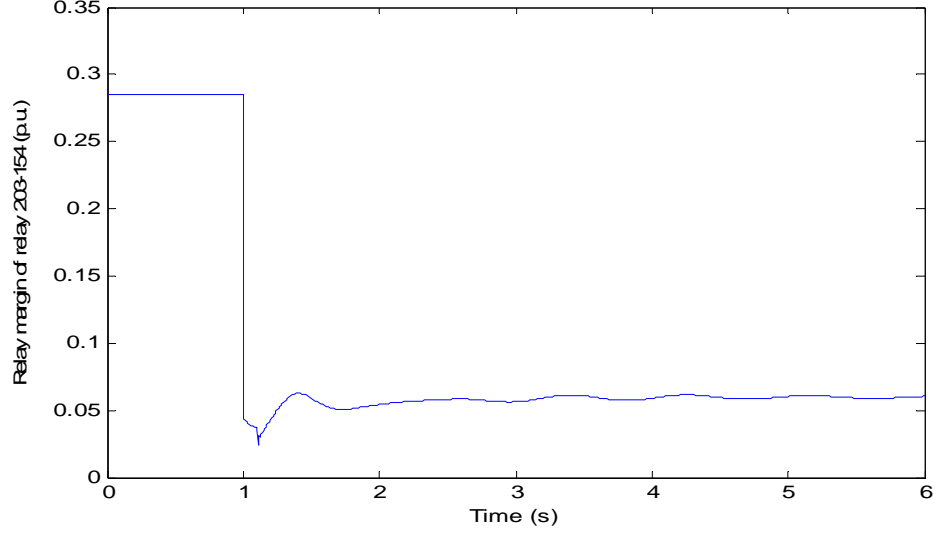


Figure 15 Relay margin trajectory of relay 203-154 for contingency 1

Based on RMR values, we can identify the relays with smaller relay margin ratios over the interested time span. Based on RSTR values, we can identify the relays which have a longer staying time within the tripping zones. From Table 1 and Table 2, we can see that the RMR based and relay margin based relay rankings are almost the same. However, from Table 3, we can see that the two variables based relay rankings are different. Therefore, we can have the conclusion that a smaller relay margin does not necessarily mean that the corresponding relay have a smaller relay margin ratio. Actually, from the single value of relay margin, we can only tell the distance of a trajectory to the tripping zone at each time instant. However, we do not know the rate of relay margin change. Figure 14 shows the impedance swing trajectory of the top 1 critical relay-153-154_2 in the relay ranking list for contingency 1. We can see that after the tripping of line 154-205 caused by the three phase fault, the system trajectory stayed in the third tripping zone of relay 153-154_2 for 10.79% of the preset time. Figure 15 shows the relay margin trajectory of relay 203-154 for contingency 1. We can see that the post-contingency relay margin is 0.0604 p.u. and its pre-contingency relay margin is 0.2853, thus the RMR is 0.2117. This satisfies the relay margin criteria for post-contingency [11].

4.1.3 Conclusions

Since power system protection at the transmission system level is based on distance relays which are sensitive to the power flow variations on a transmission line, it is important to evaluate the relay status during transmission system disturbances and identify critical relays for system stability study.

Based on the practical dynamic system security criteria for relay margin, the concept of voltage based relay margin is applied to redefine the two variables: relay margin ratio and relay staying time ratio. These two variables are calculated and relays are ranked accordingly. The critical relays are identified in the 23-bus test system with three different contingencies.

4.2 Numerical Results for VSM Calculation

The New England 39-bus test system is used to illustrate the predictor-corrector based identification of VSM. Also, the numerical test results are obtained for the optimal control incorporating the voltage stability margin and relay margin using this test system.

4.2.1 New England 39-bus Test System Description

Fig 16 shows the New England 39-bus system which consists of 46 branches, 10 generator buses, and 31 load buses.

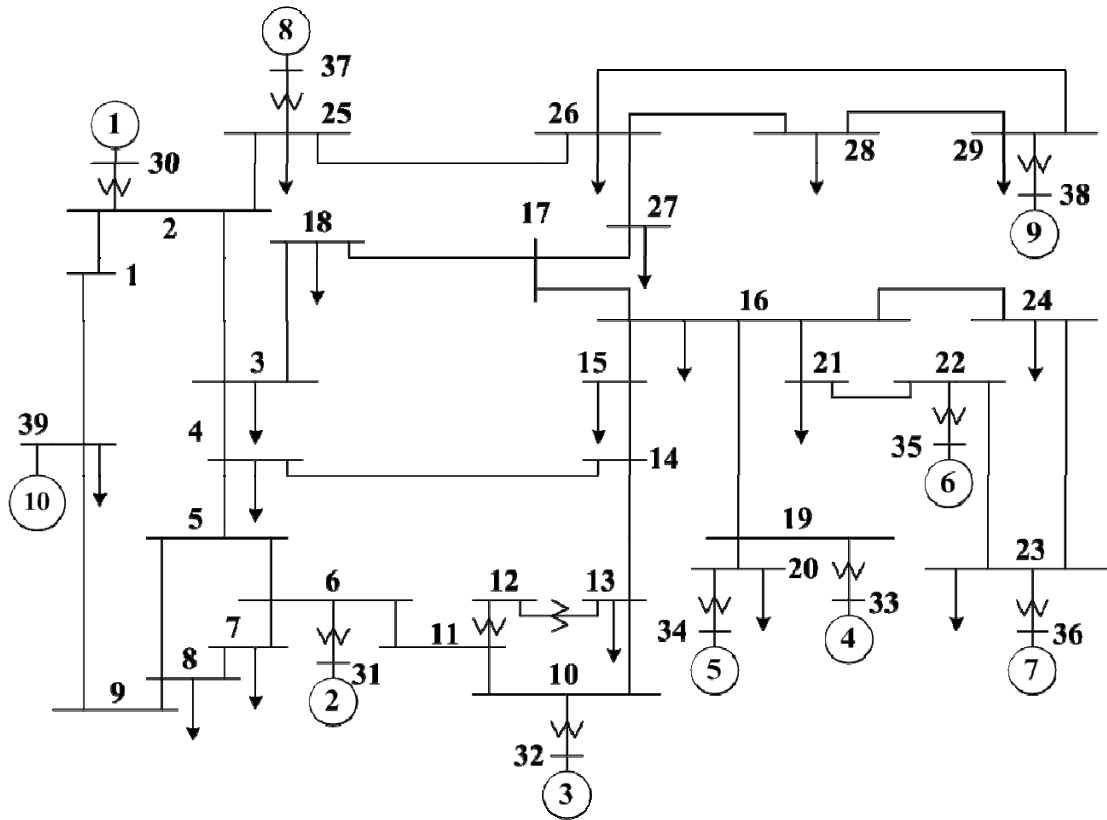


Figure 16 New England 39-bus system

4.2.2 Numerical Results

The numerical test results are provided in Table 4. Continuation power flow method is applied to compare with the predictor-corrector based method with respect to three aspects: accuracy (P_{\max}), number of iterations, and total CPU time.

Three test cases are applied to test the proposed method: base case, line 2-25 outage case and line 26-29 outage case. Table 4 shows that the results obtained by the proposed method have a good accuracy. Also, in the calculations of the three test cases, the

iteration times and calculation time needed for VSM identifications are reduced in general by about 75 percent using the predictor-corrector method.

Table 4 Numerical results for the VSM calculation

	Parameter	Pre-Cor method	CPF method
Base Case	P_{\max} (p.u.)	21.6674	21.7956
	No. of Iterations	5	19
	Total CPU time	0.4536	1.7338
Contingency Line 2-25 outage	P_{\max} (p.u.)	20.0379	21.0324
	No. of Iterations	5	22
	Total CPU time	0.3438	2.4216
Contingency Line 26-29 outage	P_{\max} (p.u.)	20.3156	21.3069
	No. of Iterations	5	20
	Total CPU time	0.3750	1.5902

Fig. 17 and Fig. 18 plot the predictor-corrector based VSM identification results. The plots show the VSM of load bus 26 when the load is increased from initial value to the voltage collapse point where power flow cannot converge.

Fig. 17 incorporates the outage of line 26-29 in the system. Fig. 18 considers the scenario of all the other loads increased by 100 percent. Without considering any contingencies or load increase, the maximum loading point for load bus 26 is at the intersection point of predictor curve and load curve which indicates the predictor is accurate at the collapse point. However, when the load is far away from the collapse point, there is a relatively large error between the predictor based VSM and the true VSM.

After applying the corrector to correct the VSM by incorporating system constraints, the corrected VSM shows a better estimation of the true VSM value. However, the corrected VSM still shows some errors compared with the true values.

Fig. 17 and Fig. 18 also indicate that different system operating scenarios may affect the VSM as expected. Therefore, it is necessary to incorporate system constraints and consider possible system scenarios for VSM identification. Through applying the VSM corrector, system constraints can be incorporated and possible system scenarios can be considered which make the VSM calculation more reliable and flexible.

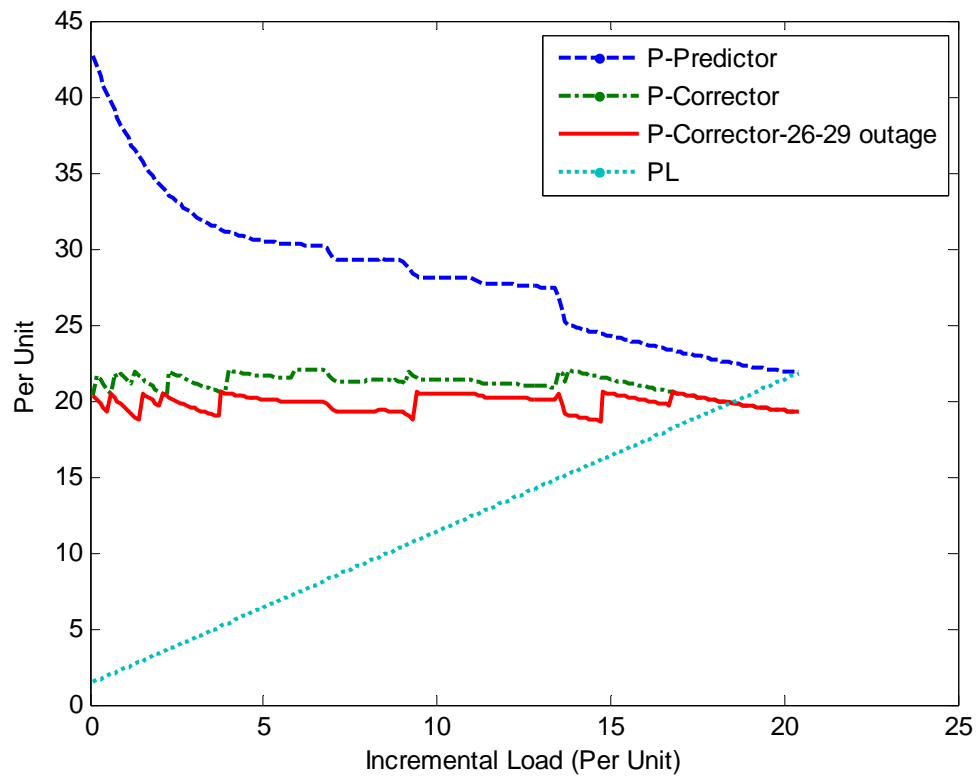


Figure 17 Predictor-corrector based VSM identification with contingency

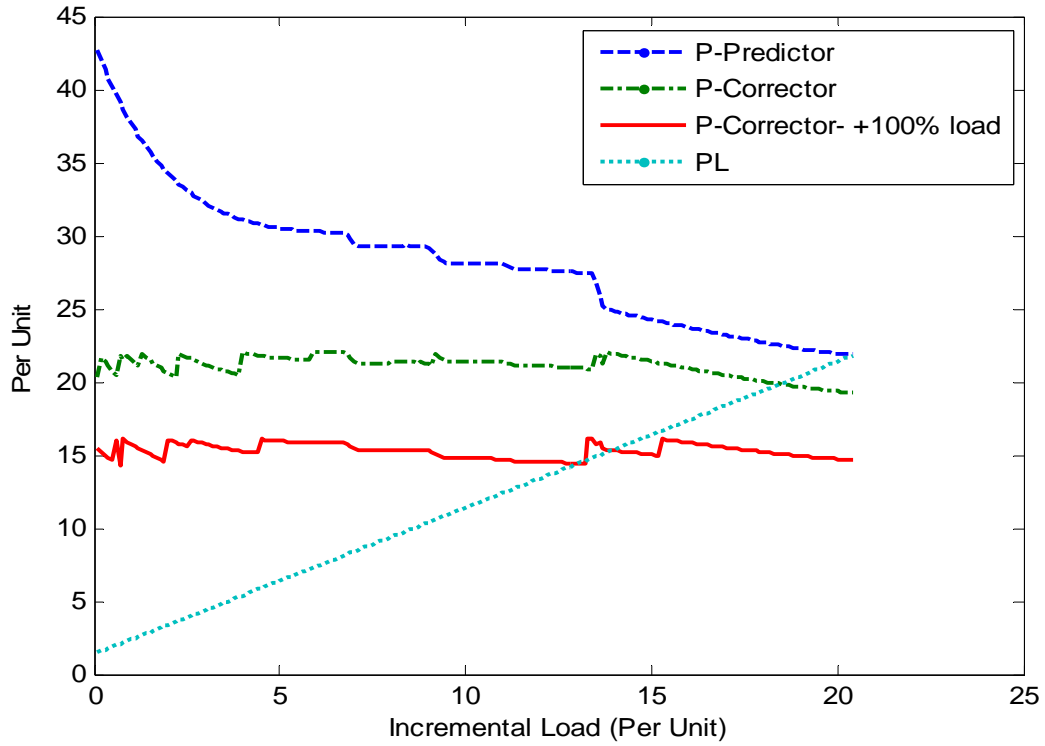


Figure 18 Predictor-corrector based VSM identification with load increase

4.2.3 Conclusions

This new VSM calculation scheme makes three contributions:

First, it formulates the VSM identification problem in a predictor-corrector framework.

Second, it provides a method to incorporate system constraints and consider possible system scenarios during VSM calculation which makes it more reliable and flexible.

Third, it shows that the new method is able to obtain the VSM with a good accuracy with reduced computational effort.

Generally, this scheme provides a new method for VSM identification which is fast, reliable and flexible.

4.3 Numerical Results for Optimal Reactive Power Control

The IEEE 39-bus system is applied to perform the numerical test for optimal reactive power control. The results show the effect of rescheduling control variables to minimize the system real power loss and its effects on the improvement of voltage stability margin, relay margin and system voltage profile. Two test cases which correspond to two contingencies are applied in the system to test the results of the optimal reactive power control effects. The two contingencies are line 2-25 outage and line 26-29 outage.

4.3.1 Numerical Results

In this optimal reactive power control problem, there is totally 18 control variables to control the reactive power in the system, which includes 10 control variables of generator terminal voltages, 4 control variables of OLTC tap ratios, 4 control variables of shunt capacitor reactive power outputs. Table 5 shows the optimal reactive power control variable settings for the base case and the line 2-25 outage case.

Through optimal reactive power control, the system voltage profile has been improved. Fig. 19 show the system voltage profile before and after the optimal control for the test case of line 2-25 outage. From Fig. 19, we can see that in order to meet the system stability constraints, the optimal control adjusted almost all the generator terminal voltage to their maximum values.

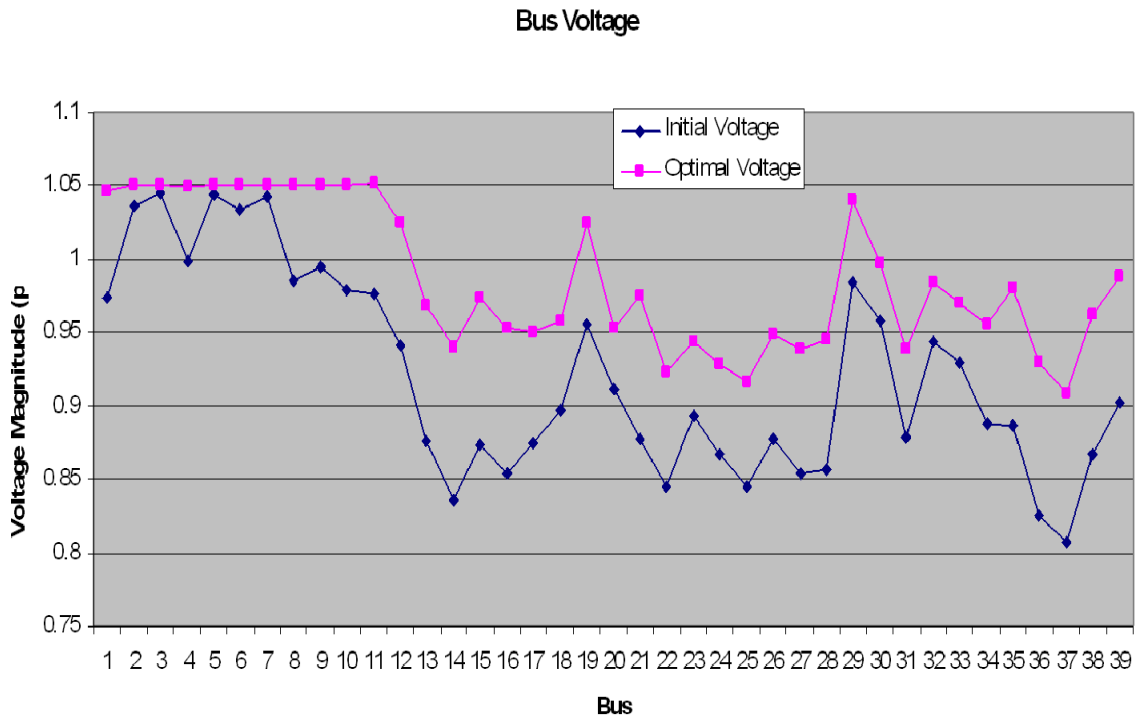


Figure 19 System voltage profile before and after optimal control (2-25 outage case)

Table 5 Optimal reactive power control variable settings

		Base case		Line 2-25 outage	
Control Variables	Variable Range	Initial settings	Optimal settings	Initial settings	Optimal settings
<i>VG1</i>	0.95 – 1.05	1.0139	1.0336	0.9737	1.0462
<i>VG2</i>	0.95 – 1.05	1.0369	1.0226	1.0357	1.0500
<i>VG3</i>	0.95 – 1.05	1.0331	1.0377	1.0459	1.0500
<i>VG4</i>	0.95 – 1.05	1.0316	1.0175	0.9980	1.0492
<i>VG5</i>	0.95 – 1.05	1.0247	0.9892	1.0438	1.0500
<i>VG6</i>	0.95 – 1.05	1.0368	1.0494	1.0335	1.0500
<i>VG7</i>	0.95 – 1.05	0.9923	1.0012	1.0431	1.0500
<i>VG8</i>	0.95 – 1.05	1.0341	1.0289	0.9852	1.0500
<i>VG9</i>	0.95 – 1.05	1.0131	1.0329	0.9944	1.0500
<i>VG10</i>	0.95 – 1.05	0.9958	1.0409	0.9796	1.0500
<i>Qc4</i>	0 – 1.5	1.3000	1.5000	1.0000	1.5000
<i>Qc8</i>	0 – 1.5	1.4000	0.8000	1.5000	1.5000
<i>Qc16</i>	0 – 1.5	0.5000	1.1000	1.1000	1.5000
<i>Qc20</i>	0 – 1.5	0.1000	0.6000	0.9000	1.4000
<i>T7</i>	0.9 – 1.1	1.0000	0.9600	0.9800	1.0200
<i>T8</i>	0.9 – 1.1	1.0600	0.9600	1.0600	1.0400
<i>T9</i>	0.9 – 1.1	1.0000	0.9600	0.9000	0.9800
<i>T15</i>	0.9 – 1.1	1.0000	1.0400	1.0200	0.9600

Figure 20 shows that after the optimal reactive power control, voltage stability margin of every load bus is increased. By existing control sources, if the VSM requirement still cannot be achieved, other control methods are needed, such as load shedding.

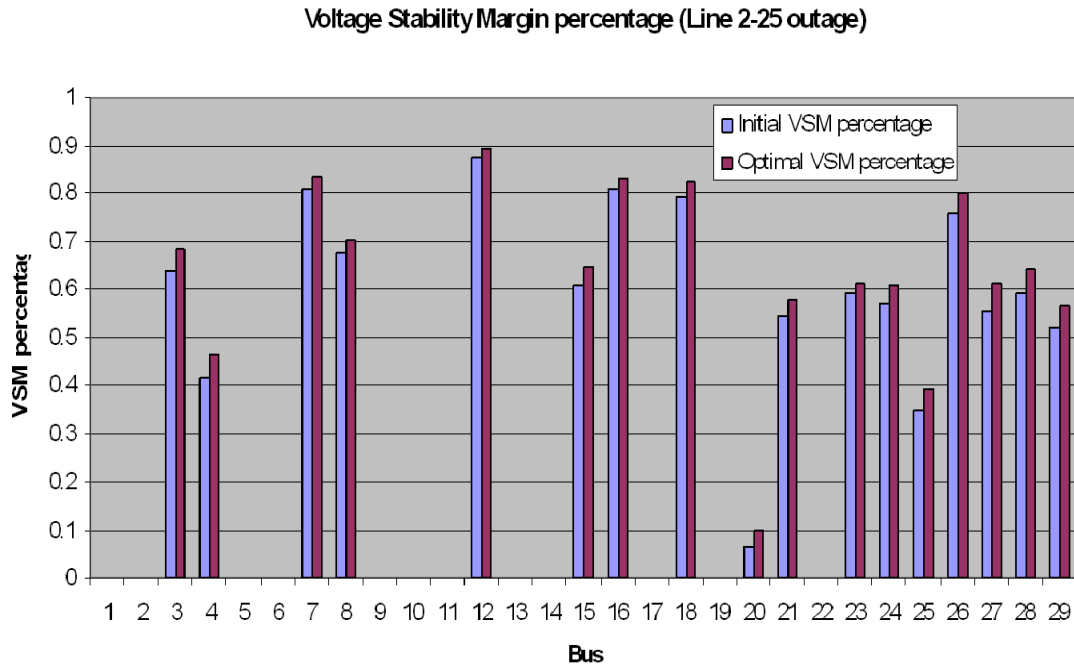


Figure 20 Voltage stability margin before and after optimal control (2-25 outage case)

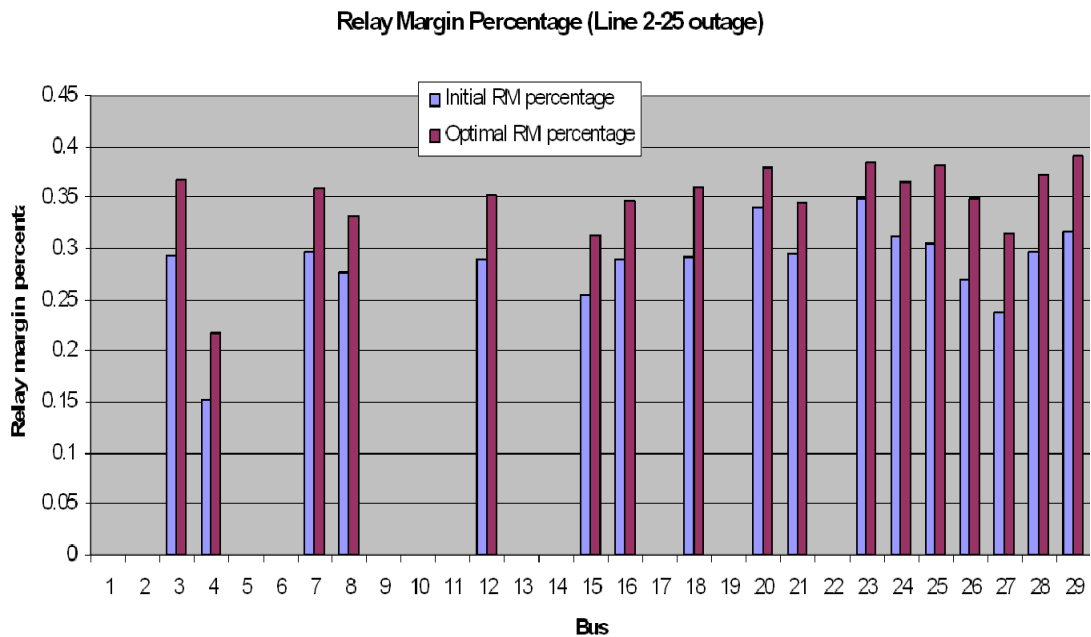


Figure 21 Relay margin before and after optimal control (2-25 outage case)

Figure 21 shows the relay margin before and after optimal control which indicates relay margins have been increased by the optimal control after the contingency. By the relay margin criterion, relay margin at bus 4 was improved by the optimal control to meet the requirement.

The following three figures show the voltage profile, voltage stability margin and relay margin before and after the optimal control which are used to further validate the effects of optimal control against voltage collapse.

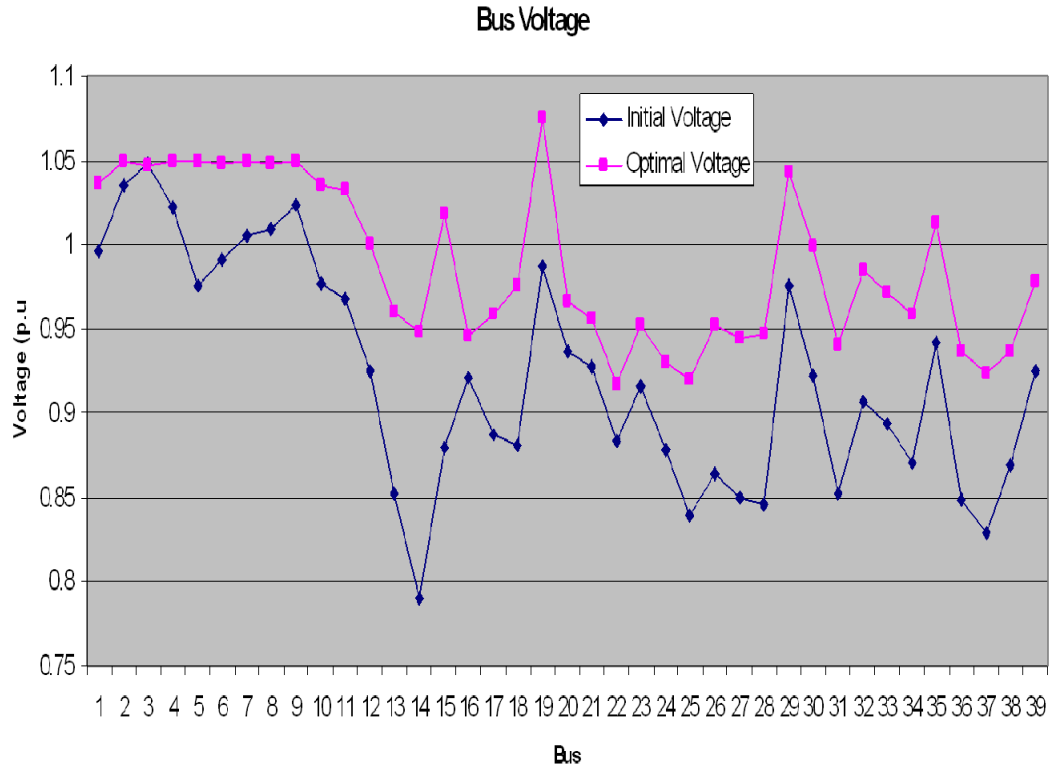


Figure 22 System voltage profile before and after optimal control (26-29 outage case)

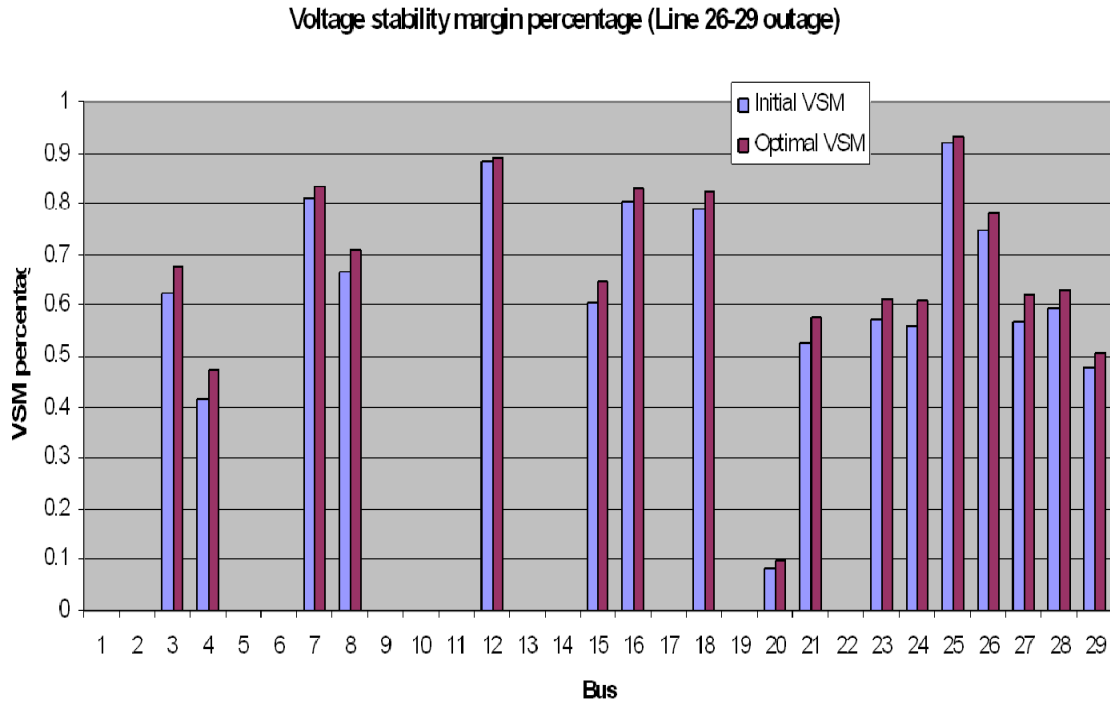


Figure 23 Voltage stability margin before and after the optimal control (26-29 outage case)

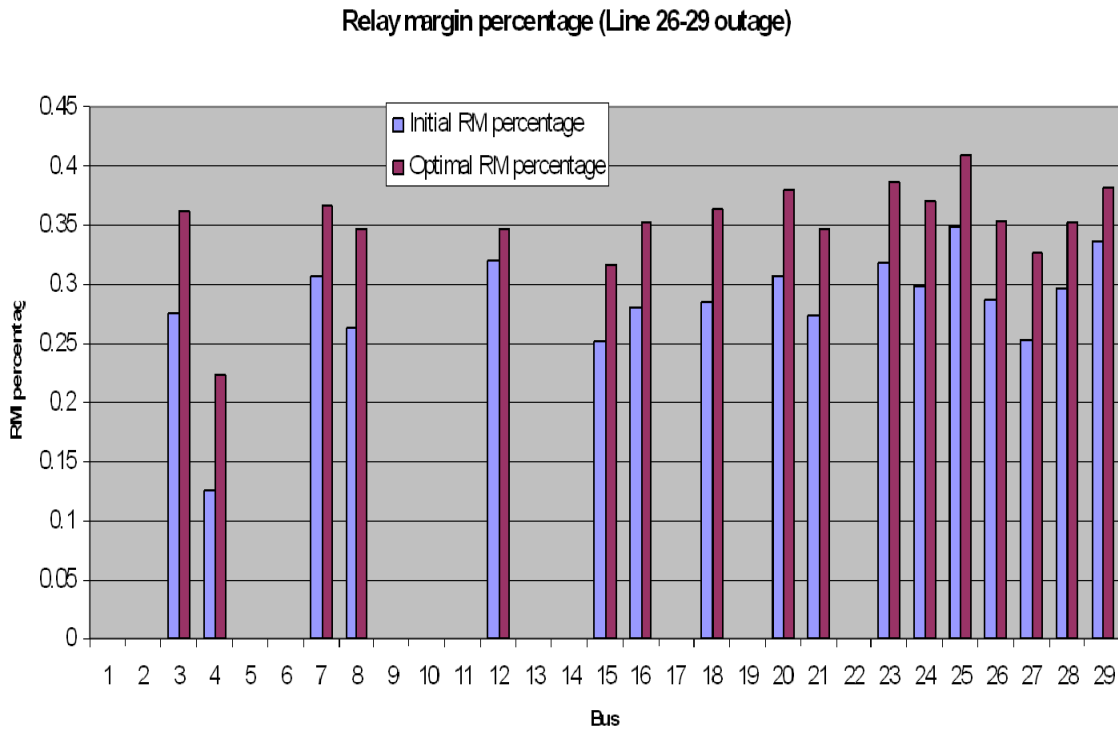


Figure 24 Relay margin before and after optimal control (26-29 outage case)

4.3.2 Conclusions

Voltage stability margin and relay margin are incorporated as constraints in the optimization model. Optimal reactive power control is proposed to maintain voltage stability and enhance relay margin. The optimal control strategy uses existing control sources to improve the system voltage stability.

The numerical results from this section show that the optimal reactive power control can effectively improve the system voltage profile after contingencies. Also, the voltage stability margin and relay margin have been improved by adjusting the control variables to the optimal settings. Two test cases with two contingencies are applied in the test system which validate that the optimal reactive power control strategy is effective to prevent voltage collapse.

4.3.3 Future Work

The power flow based relay margin calculation and critical relay identification have been used in the process of solving the optimal reactive power control problem. According to the relay margin criteria for post-contingency stability, the relay margin which violates the criteria is incorporated in the optimization model as a constraint. Through the optimal reactive power control, the relay margin has been increased after contingencies to meet the requirement of the post-contingency stability criteria.

In the next phase of research work, we will formulate a dynamic optimization model which incorporates the relay margin based on the time domain simulation as a constraint. Through the dynamic optimization, the relay margin will be improved during the interested time interval to prevent the unintended relay operation which may aggravate the system operating condition under stressful situations.

References

- [1] N. B. Bhatt, "August 14, 2003 U.S.-Canada blackout," presented at the IEEE PES General Meeting, Denver, CO, 2004.
- [2] Western Systems Coordinating Council Disturbance Rep. For the Power System Outages that Occurred on the Western Interconnection on July 2, 1996, 1424 MAST and July 3, 1996, 1403 MAST
- [3] X. Vieira et al., "The March 11th 1999 blackout: short-term measures to improve system security and overview of the reports prepared by the international experts," in Proc. CIGRÉ Session, SC 39 Workshop on Large Disturbances, Paris, France, Aug. 29, 2000.
- [4] M. Jonsson and J. E. Daalder, "An adaptive scheme to prevent undesirable distance protection operation during voltage instability," *Power Delivery, IEEE Transactions on*, vol. 18, pp. 1174-1180, 2003.
- [5] M. Larsson and D. Karlsson, "Coordinated system protection scheme against voltage collapse using heuristic search and predictive control," *Power Systems, IEEE Transactions on*, vol. 18, pp. 1001-1006, 2003.
- [6] A. G. Phadke and J. S. Thorp, *Computer Relaying for Power Systems*, 1st ed. Baldock, Hertfordshire, U.K.: Research Studies, 1988, p. 31,263.
- [7] W. A. Elmore, "System stability and out of step relaying," in *Protective Relaying Theory and Applications*. New York: Marcel Dekker, 1994, pp. 319-333.
- [8] M.A. Pai, P.W. Sauer, F. Dobraca, "A new approach to transient stability evaluation in power systems", *Proceedings of the 27th Conference on Decision and Control*, Austin, Texas, December 1988.
- [9] F. Dobraca, M.A. Pai, P.W. Sauer, "Relay margin as a tool for dynamic security analysis," *Int. J. Electr. Power Energy Syst.*, vol. 12, no.4, pp. 226-234, Oct. 1990.
- [10] www.wecc.biz/documents/library/procedures/operating/WECC_reliability_criteria_MORC.pdf
- [11] www.ieso.ca/imoweb/pubs/marketAdmin/IMO_req_0041_transmission_assessment_criteria.pdf
- [12] P. Kundur, J. Paserba, V. Ajjarapu, G. Andersson, A. Bose, C. Canizares, N. Hatziaargyriou, D. Hill, A. Stankovic, C. Taylor, T. Van Cutsem, and V. Vittal, "Definition and classification of power system stability IEEE/CIGRE joint task force on stability terms and definitions," *Power Systems, IEEE Transactions on*, vol. 19, pp. 1387-1401, 2004.
- [13] L.A.Ll. Zarate, C.A. Castro, J.L.M. Ramos and E.R. Ramos, Fast computation of voltage stability security margins using nonlinear programming techniques, *IEEE Trans Power Syst*, vol. 21, pp. 19-27, 2006.
- [14] N. Flatabø, R. Ognedal, and T. Carlsen, "Voltage stability condition in a power transmission system calculated by sensitivity methods," *IEEE Trans. Power Syst.*, vol. 5, no. 4, pp. 1286-1293, Nov. 1990.
- [15] G. K. Morison, B. Gao, and P. Kundur, "Voltage stability analysis using static and dynamic approaches," *IEEE Trans. Power Syst.*, vol. 8, no. 3, pp. 1159-1171, Aug. 1993.

- [16] T. Van Cutsem, C. Moisse, and R. Mailhot, "Determination of secure operating limits with respect to voltage collapse," *IEEE Trans. Power Syst.*, vol. 14, no. 1, pp. 327–335, Feb. 1999.
- [17] C. Cañizares, A. C. Z. Souza, and V. Quintana, "Comparison of performance indices for detection of proximity to voltage collapse," *IEEE Trans. Power Syst.*, vol. 11, no. 3, pp. 1441–1450, Aug. 1996.
- [18] V. Ajjarapu and C. Christy, "The continuation power flow: A tool for steady state voltage stability analysis," *IEEE Trans. Power Syst.*, vol. 7, no. 1, pp. 416–423, Feb. 1992.
- [19] N. Flatabø, O. Fosso, R. Ognedal, and T. Carlsen, "A method for calculation of margins to voltage instability applied on the Norwegian system for maintaining required security level," *IEEE Trans. Power Syst.*, vol. 8, no. 3, pp. 920–928, Aug. 1993.
- [20] V. Ajjarapu, P. Lin, and S. Battula, "An optimal reactive power planning strategy against voltage collapse," *IEEE Trans. Power Syst.*, vol. 9, no. 2, pp. 906–917, May 1994.
- [21] G. D. Irissari, X. Wang, and S. Mokhtari, "Maximum loadability of power system using interior point nonlinear optimization method," *IEEE Trans. Power Syst.*, vol. 12, no. 1, pp. 162–172, Feb. 1997.
- [22] A. C. Z. Souza, L. M. Honorio, G. L. Torres, and G. Lambert-Torres, "Increasing the loadability of power system through optimal-local control actions," *IEEE Trans. Power Syst.*, vol. 19, no. 1, pp. 188–194, Feb. 2004.
- [23] C. W. Taylor, *Power system voltage stability*. McGraw-Hill, New York, 1994.
- [24] P. Kundur, *Power system stability and control*, McGraw-Hill, New York, 1994.
- [25] V. Ajjarapu, "Identification of steady state voltage stability in power systems," *Int. J. Energy Syst.*, vol. 11, no. 1, pp. 43–46, 1991.
- [26] C. A. Cañizares and F. L. Alvarado, "Point of collapse and continuation methods for large AC/DC systems," *IEEE Trans. Power Syst.*, vol. 8, no. 1, pp. 1–8, Feb. 1993.
- [27] G. D. Irisarri, X. Wang, and J. Tong et al., "Maximum loadability of power systems using interior point nonlinear optimization method," *IEEE Trans. Power Syst.*, vol. 12, no. 1, pp. 162–172, Feb. 1997.
- [28] Khoi Vu, Miroslav M Begovic, Damir Novosel, Murari Mohan Saha, "Use of local Measurements to estimate voltage – stability margin " *IEEE Trans. Power syst.*, vol. 14, no. 3, pp. 1029-1035, August, 1999
- [29] R. E. Putman, F. C. Huff and J. K. Pal, "Optimal reactive power control for industrial power networks," *IEEE Trans. Power Syst.*, vol. 35, no. 3, May, 1999.

Project Publications

Hua Bai, V. Ajjarapu, “Relay Margin Trajectory Based Identification of Transmission Vulnerability for Power System Security Assessment,” Bulk Power System Dynamics and Control VII, IREP Conference, Charleston, South Carolina, August 2007.

Hua Bai, V. Ajjarapu, “Transmission System Vulnerability Assessment based on Practical Identification of Critical Relays and Contingencies,” the 2008 PES General Meeting, Pittsburgh, PA, July 2008.

Hua Bai, V. Ajjarapu, “A Novel Identification Scheme for Voltage Stability Margin,” Submitted to the IEEE Transactions on Power Systems.

Incorporating Relays in a Power System Model with Dynamic Loads for Voltage Transient and Stability Analyses

Final Project Report

Volume 2

Project Team

A.P. Sakis Meliopoulos, Georgia Institute of Technology

Information about this project

For information about this project contact:

A. P. Sakis Meliopoulos
School of Electrical and Computer Engineering
Georgia Institute of Technology
Atlanta, Georgia 30332
Phone: 404 894-2926
Fax: 404 894-4641
Email: sakis.meliopoulos@ece.gatech.edu

Power Systems Engineering Research Center

This is a project report from the Power Systems Engineering Research Center (PSERC). The Power Systems Engineering Research Center (PSERC) is a multi-university Center conducting research on challenges facing the electric power industry and educating the next generation of power engineers. More information about PSERC can be found at the Center's website: <http://www.pserc.org>.

For additional information, contact:

Power Systems Engineering Research Center
Arizona State University
577 Engineering Research Center
Box 878606
Tempe, AZ 85287-8606
Phone: 480-965-1643
Fax: 480-965-0745

Notice Concerning Copyright Material

PSERC members are given permission to copy without fee all or part of this publication for internal use if appropriate attribution is given to this document as the source material. This report is available for downloading from the PSERC website.

© 2008 Iowa State University and Georgia Institute of Technology.
All rights reserved.

Table of Contents

1. Introduction.....	1
1.1 Background.....	1
2. Voltage-Load Dynamics: System Modeling.....	2
2.1 Introduction	2
2.2 Quasi-Dynamic Quadratized Analysis	4
2.2.1 Overview of Quadratized Analysis	5
2.2.2 Quadratic Integration Method	6
2.3 Three-Phase Induction Motor Model	7
2.4 Single-Phase Induction Motor Model	13
2.5 Synchronous Generating Unit Model	16
3. Voltage-Load Dynamics: Control.....	20
3.1 Introduction	20
3.2 Problem Description	20
3.3 Mathematical Problem Formulation	21
3.4 Solution Methodology	24
4. Numerical Examples	27
4.1 Test System Definition	27
4.1.1 Test System 1 – Transmission System	27
4.1.2 Test System 2 – Distribution System	36
4.2 Simulation of Voltage Recovery	43
4.2.1 Test System 1 – Transmission System	43
4.2.2 Test System 2 – Distribution System	53
4.3 Summary.....	61
References.....	62
Project Publications	65

List of Figures

Figure 1. Possible Behavior of Voltage Recovery During and After a Disturbance	4
Figure 2. Three-Phase Induction Motor Sequence Networks	8
Figure 3. Induction Motor Input Data Form	9
Figure 4. Single-Phase Induction Motor Input Data	14
Figure 5. Single-Phase Induction Motor Physical Circuit	15
Figure 6. Equivalent Circuit of Synchronous Generator Model	18
Figure 7 Transmission Line Data.....	29
Figure 8. Transmission Line Data.....	30
Figure 9. Distribution Line Data.....	30
Figure 10. Generating Unit Substation Configuration (Unit 1)	30
Figure 11. Distribution Substation Configuration	31
Figure 12. Step-up, Three-Phase Transformer Data	32
Figure 13. Step-down, Three-Phase Transformer Data	32
Figure 14. Three-Phase Distribution Transformer Data	32
Figure 15. Load Data	33
Figure 16. Three-Phase Induction Motor Data	34
Figure 17. Motor Protection Scheme	35
Figure 18. Single-Line Diagram of Test System 2	36
Figure 19. Underground Cable Model	37
Figure 20. Mutually Coupled Distribution Line	38
Figure 21. Single-Phase Pole Transformer with Center-tapped Secondary	39
Figure 22. Secondary Bus Load.....	40
Figure 23. Single-Phase Induction Motor	41
Figure 24. Additional Three-Phase Induction Motor Data	42
Figure 25. Steady-State Analysis Results for Induction Motor 1	44
Figure 26. Steady-State Analysis Results for Induction Motor 2	44
Figure 27. Generating Unit Response after a Three-Phase Fault.....	45
Figure 28. Induction Motor Response after a Three-Phase Fault	46
Figure 29. Transmission System Response after a Three-Phase Fault	47
Figure 30. Induction Motor Response after a Three-Phase Fault with Motor Disconnection	48

List of Figures (continued)

Figure 31. Impedance Trajectory and Relay Settings of BUS03-side Relay of Line BUS03-BUS04 (faulted line)	49
Figure 32. Impedance Trajectory and Relay Settings of SLACK-side Relay of Line SLACK-BUS04	49
Figure 33. Impedance Trajectory and Relay Settings of BUS01-side Relay of Line BUS01-BUS04.....	50
Figure 34. Impedance Trajectory and Relay Settings of BUS02-side Relay of Line BUS02-BUS03.....	51
Figure 35. Impedance Trajectory and Relay Settings of BUS04-side Relay of Line BUS04-BUS05.....	51
Figure 36. Impedance Trajectory and Relay Settings of BUS04-side Relay of Line BUS04-BUS06.....	52
Figure 37. Steady-State Analysis Results for Induction Motor BUS08-M	54
Figure 38. Steady-State Analysis Results for Induction Motor BUS07-M	54
Figure 39. Steady-State Analysis Results for Induction Motor MCC-P2.....	54
Figure 40. Steady-State Analysis Results for Induction Motor MCC-P3.....	55
Figure 41. Steady-State Analysis Results for Induction Motor PAD-4.....	55
Figure 42. Generating Unit Response after a Three-Phase Fault.....	56
Figure 43. Induction Motor Response after a Three-Phase Fault	57
Figure 44. Terminal Voltages of Induction Motors at All Three Phases.....	58
Figure 45. Current Absorption of Induction Motors at All Three Phases	59
Figure 46. Current Absorption of Feeder Sections at All Three Phases	60

1. Introduction

1.1 Background

The primary motivation for this part of the project arises from the need to develop analytical tools to study and enhance power system voltage stability incorporating system dynamics (in particular load dynamics) and integrate the protection system for the purpose of studying the response of relays during voltage instabilities. Emphasis is given to detailed system modeling and in particular inclusion of distribution feeder models with distributed dynamic loads to capture voltage phenomena that may have both local and global impact on the system.

In most investigations after blackouts two observations emerged: (a) voltage transients and/or lack of reactive power support was a contributing factor and (b) relay unwanted operations have contributed to spreading the disturbance and impact on the system. These observations are related. During voltage transients and/or voltage instabilities flow of high currents are experienced in an un-faulted system together with depressed voltages that may be recovering slowly. These phenomena can cause operations of over-current relays or distance relays in the form of load encroachment. It is important to fully understand these phenomena and to (a) determine the conditions that make these phenomena manifest themselves and damage the system and (b) develop mitigation methods to alleviate the impact on the system.

It is important to recognize that the best way to study these phenomena is by developing integrated models of the power systems, the dynamics of the load and the protective system. The work of this project focused on this approach. An integrated model was developed and the phenomena were studied using this model as well as techniques for mitigating the effects of these transients. The report presents the methodology and preliminary results.

2. Voltage-Load Dynamics: System Modeling

2.1 Introduction

It is well-known that protection performance and voltage stability (voltage recovery) after a disturbance in electric power systems is affected or delayed by load dynamics (such as the dynamics of induction motors, etc.), especially when not enough fast reacting reactive resources (dynamic VAR sources) exist [1]-[9]. This phenomenon has caused serious problems on specific systems and it is typically studied either using static load flow techniques or with full scale transient simulations. In addition, in case of generating unit transient oscillations after the successful clearance of a fault, voltages may dip or collapse near the center of oscillation. During periods of low voltage motors decelerate and when the disturbance is removed, the voltage tries to recover but the recovery is affected by the acceleration of the motor loads and in general the dynamics of the load. The end result may be sluggish voltage recovery and in extreme cases prolonged voltage dips and subsequent motor tripping before voltage recovery or prolonged higher currents and possible tripping of circuits. Therefore, both of these phenomena may trigger secondary effects such as motor tripping and other undesired relay operations. It is therefore important for this project to use realistic load models that capture the dynamics of the load and its effect on voltage stability.

Most off-line studies are mainly based on traditional load flow analysis that does not take into account the dynamics of the load. The proper way to analyze these phenomena is to use dynamic simulation techniques that take into consideration the load dynamics. These approaches are relatively few and depend on assumed data for the dynamic behavior of the electric load. Real-time tools are almost exclusively based on traditional load flow models and they are not capable of capturing the dynamic nature of voltage recovery phenomena. This practice leads to discrepancies between the analytical models and the real behavior of the system.

The issue of load modeling and the effects of dynamic loads on voltage phenomena have been studied to a significant extent in literature [1]-[18]. In [1] the issues of voltage dips in 3-phase systems after symmetric or asymmetric faults and the accurate modeling of voltage recovery are addressed. In [2], [3] the voltage recovery phenomena and the effect of induction motor loads are studied from a practical point of view, based on actual events from utility experience. References [4] and [5] study the voltage recovery of wind turbines after short-circuits. The issue of mitigating the delayed voltage recovery using fast VAR resources is addressed in [6]-[8]. The impact of induction motor loads on voltage phenomena has also been studied on a more general research basis. Reference [9] addresses the topic of voltage oscillatory instability caused by induction motors, in particular in isolated power systems, while [10] refers to the impact of induction motor loads in the system loadability margins and in the damping of inter-area oscillations. Finally, references [11]-[20] are indicative of current research approaches and issues in induction motor load modeling in power systems.

This work focuses on modeling and simulation of voltage recovery phenomena taking into consideration the key dynamic characteristics of the load. The approach is based on an advanced load flow modeling for the electric network, which is assumed to

operate at quasi-steady state, coupled with quasi-dynamic models of generating units, loads (motors, etc.) and other voltage controlled devices such as SVCs. The quasi-dynamic models explicitly represent the electromechanical oscillations of generators and dynamic loads (mainly motors) while neglect the electrical transients. This allows a more realistic yet simple representation of load dynamics. While the methodology is capable of handling various classes of electric loads, this work focuses on induction motor loads, which represents the majority of dynamic electric loads. Emphasis is also given in utilizing a unified model for representing induction motors of different designs.

The induction motor nonlinearities depend on the slip and cause singularities as the slip approaches zero. To avoid numerical problems, the proposed solution method is based on quadratization of the induction motor model [19]-[20]. This model is interfaced with the quadratized power flow model to provide a robust solution method for a system with induction motors. In addition, this model is a more realistic representation of a power system with moderate increase of the complexity of the power flow equations [20]. The system modeling is based on full three-phase models of all the elements, allowing therefore consideration of system asymmetries and unbalanced operating conditions. Furthermore the methodology makes use of an advanced numerical integration scheme with improved numerical stability properties, which provides a means of overcoming possible numerical problems [21]-[22].

The problem of transient voltage sags during disturbances and voltage recovery after the disturbance has been removed is quite well known. The importance of the problem has been well identified and has been detected as a contributing factor to many recent blackouts. Its significance is increasing especially in modern restructured power systems that may frequently operate close to their limits under heavy loading conditions. Furthermore, the increased number of voltage-sensitive loads and the requirements for improved power system reliability and power quality are imposing more strict criteria for the voltage recovery after severe disturbances. It is well known that slow voltage recovery phenomena have secondary effects such as operation of protective relays, electric load disruption, motor stalling, etc. Many sensitive loads may have stricter settings of protective equipment and therefore will trip faster in the presence of slow voltage recovery resulting in loss of load with severe economic consequences. A typical situation of voltage recovery following a disturbance is illustrated in Figure 1. Note there is a fault during which the voltage collapses to a certain value. When the fault clears, the voltage recovers quickly to another level and then slowly will build up to the normal voltage. The last period of slow recovery is mostly affected by the load dynamics and especially induction motor behavior.

The objective of the work is to present a method that can be used to study voltage recovery events after a disturbance and their effects on the protection system. More specifically the problem is stated as follows: Assume a power system with dynamic loads such as induction motors. A fault occurs at some place in the system and it is cleared by the protection devices after some period of time. The objective is to study the voltage recovery after the disturbance has been cleared at the buses where dynamic or other sensitive loads are connected and also determine how these loads affect the recovery process. The solution to this problem provides the voltages and currents at any point of

the system including the location of protective relays. Therefore the solution can be used to determine the response of the relays during the recovery period, if any.

A new method has been developed for the solution of this problem. The method is based on the quadratized power flow and includes dynamic models of generating units and electric loads. It provides a high fidelity response of the integrated system during the disturbance and after the disturbance has been cleared as well as the response of the relays if any. We have named the method “Quasi-Dynamic Quadratized Analysis”. This method is described next.

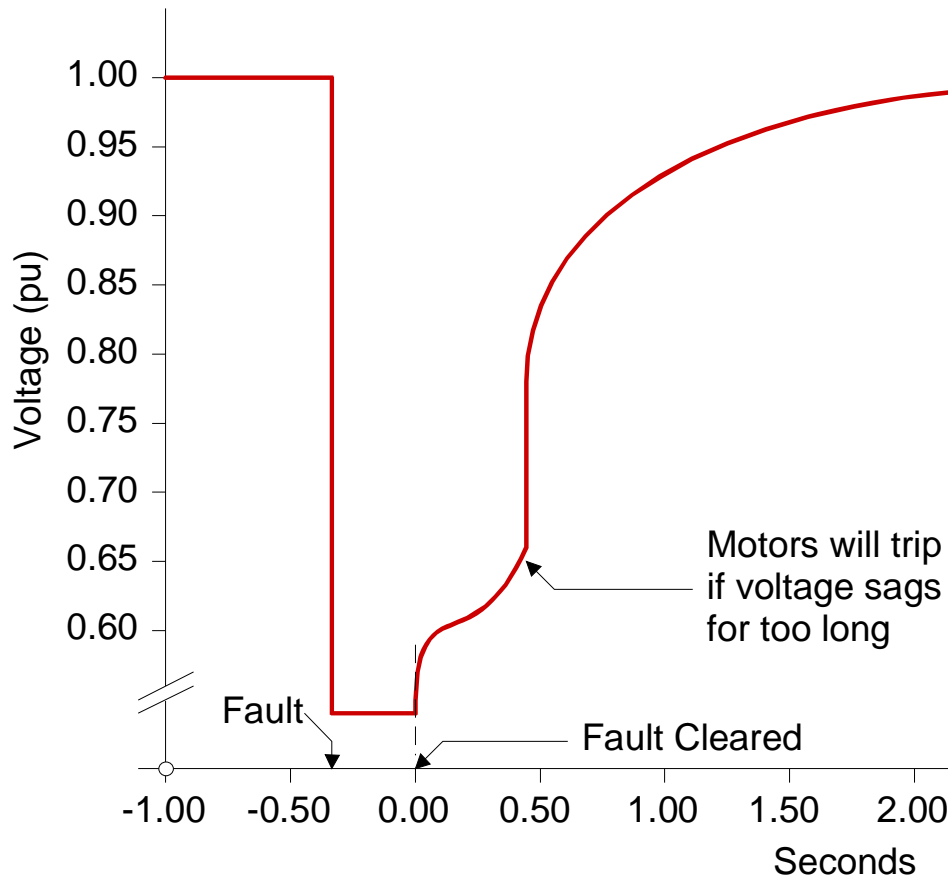


Figure 1. Possible Behavior of Voltage Recovery During and After a Disturbance

2.2 Quasi-Dynamic Quadratized Analysis

The developed method models explicitly the mechanical dynamics of the rotating equipment and loads of the systems and assumes that the electrical transients are fast and decay quickly. The voltages and currents are affected by the location of the rotating electrical machinery of the system. The details of the methodology are described in the subsequent paragraphs that provide the models and the solution algorithm.

2.2.1 Overview of Quadratized Analysis

The proposed system modeling is based on a quadratized power system model. The basic idea is to have a set of equations, most of which in our case are the power flow equations, of degree no greater than two, i.e. have a set of linear or quadratic equations. This can be achieved without making any approximations, so the power system model is an exact model. Since this way the problem is transformed into a quadratic problem, the advantages of problems of this type can be exploited.

The first step in expressing the power system equations in quadratic form is to avoid the trigonometric nonlinearities. This can be achieved by utilizing rectangular coordinates instead of the traditionally used polar coordinates for expressing the voltage and current phasors. Therefore, the system states are not the voltage magnitudes and angles, but instead the real and imaginary parts of the voltage phasors. This results in a set of polynomial equations. If the degree of nonlinearity of these equations is more than two, then quadratization of the equations can be achieved by introducing additional state variables. It is important to note that the quadratization is performed without any approximations, and the resulting quadratic model is an exact model.

The system modeling is performed on the device level, i.e. a set of quadratic equations is used to represent the model of each device. A generalized component model is used, representing every device, which consists of the current equations of each device, which relate the current through the device to the states of the device, along with additional internal equations that model the operation of the device. If a device model contains dynamical equations, then these equations are discretized using some implicit numerical integration rule. An improved numerical integration scheme has been employed in this approach that is described in the next section.

The general form of the model, for any component k , at each time step, is as in (2.1)

$$\begin{bmatrix} i^k \\ 0 \end{bmatrix} = Y^k x^k + \begin{bmatrix} x^{kT} F_1^k x^k \\ x^{kT} F_2^k x \\ \vdots \end{bmatrix} - b^k. \quad (2.1)$$

where i^k is the current through the component, x^k is the vector of the component states and b^k the driving vector for each component, which may contain past history terms, as well, in the case of dynamical models. Matrix Y^k models the linear part of the component and matrices F_i^k the nonlinear (quadratic) part. This model can refer to a passive component of the system (no dynamical equations) or a dynamic component of the system, i.e. a component that is described with algebraic and differential equations. The form (2.1) results from (a) the quadratization of the equations and (b) the integration of the differential equations. The integration of the differential equations is described in the next section. Two examples of this modeling approach are given in subsequent paragraphs (induction motor and synchronous generator).

Application of the connectivity constraints (Kirchoff's current law) at each bus yields a set of quadratized equations for the whole system:

$$\begin{bmatrix} 0 \\ 0 \end{bmatrix} = Y \cdot X + \begin{bmatrix} X^T F_1 X \\ X^T F_2 X \\ \vdots \end{bmatrix} - b = G(X), \quad (2.2)$$

where

- X : system state vector,
- Y : linear term coefficient matrix (admittance matrix),
- F_i : quadratic term coefficient matrix,
- b : driving vector.

The solution to the quadratic equations is obtained using the Newton-Raphson iterative method:

$$X^\nu = X^{\nu-1} - J(X^{\nu-1})^{-1} \cdot G(X^{\nu-1}) \quad (2.3)$$

where

- ν : iteration step,
- $J(X^{\nu-1})$: Jacobian matrix at iteration $\nu - 1$.

The iterative procedure terminates when the norm of the equations is less than a defined tolerance. This iterative procedure is repeated at each time step. If the system exhibits no dynamical behavior (i.e. is completely static), the analysis is equivalent to the load flow analysis and the solution of the above system of equations provides the steady state solution of the system.

2.2.2 Quadratic Integration Method

A new numerical integration scheme is employed for the solution of the dynamical equations. It relies on a collocation-based implicit Runge-Kutta method (Lobatto family) and is A-stable and order 4 accurate. The method is based on the following two innovations: (a) the nonlinear model equations (differential or differential-algebraic) are reformulated to a fully equivalent system of linear differential and quadratic algebraic equations, by introducing additional state variables, as described in the previous section, and (b) the system model equations are integrated assuming that the system states vary quadratically within a time step (quadratic integration).

Assuming the general nonlinear, non-autonomous dynamical system:

$$\dot{x} = f(t, x), \quad (2.4)$$

the algebraic equations at each integration step of length h , resulting from the quadratic integration method, are:

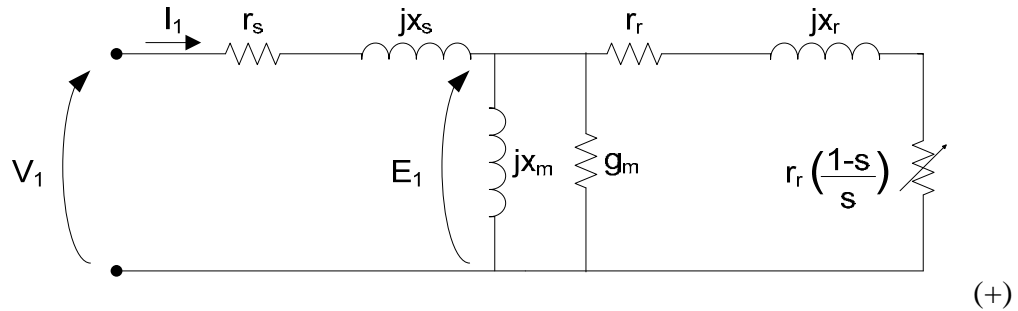
$$\begin{aligned}
x_m - \frac{h}{3} f(t_m, x_m) + \frac{h}{24} f(t, x(t)) &= x(t-h) + \frac{5h}{24} f(t-h, x(t-h)) \\
x(t) - \frac{2h}{3} f(t_m, x_m) - \frac{h}{6} f(t, x(t)) &= x(t-h) + \frac{h}{6} f(t-h, x(t-h))
\end{aligned} \tag{2.5}$$

The above equations are put in the matrix form of equation (2.1).

2.3 Three-Phase Induction Motor Model

Typically induction motors are represented in power system studies as constant power loads. Although this is a valid representation for steady-state operation under certain conditions, induction motors do not always operate under constant power, especially when large deviations of voltage occur. In reality induction motors in steady-state operate at a point where the electro-mechanical torque of the motor equals the mechanical torque of the electric load. As the voltage at the terminals of the induction motor changes, the operating point will change. Here, we present an induction motor model that can more accurately describe the motor behavior. The model is in quadratic form, that is, it consists of equations that are at most quadratic [19]-[22], and can be readily integrated into the power flow model. In addition, the model can be used to determine the operation of the system at a specific instant of time assuming that the speed of the induction motor is fixed (for example, after a disturbance). The reactive power absorption of the induction motors is different at different slip values and therefore they affect the voltage profile of the system. This behavior cannot be captured by a simple, static, constant power load model.

A quadratic, three-phase induction machine model has been developed [22], as an extension of a similar single-phase equivalent model [19]-[21]. This was done as part of a previous PSERC project, S-24 and is briefly presented in this section. The model is based on the typical steady state sequence circuits of the induction motor, shown in Figure 2. Note that induction motors have in general little or no asymmetry, so their representation with sequence networks is valid and accurate. The model input data include typical motor nominal (nameplate) data, plus electrical parameters, and mechanical load data. The user interface of the model is presented in Figure 3 and shows the model implementation details. The model supports two mechanical loading modes: (a) torque equilibrium, and (b) constant slip. In the torque equilibrium mode, the mechanical torque can be either constant, or depend linearly or quadratically on the mechanical speed.



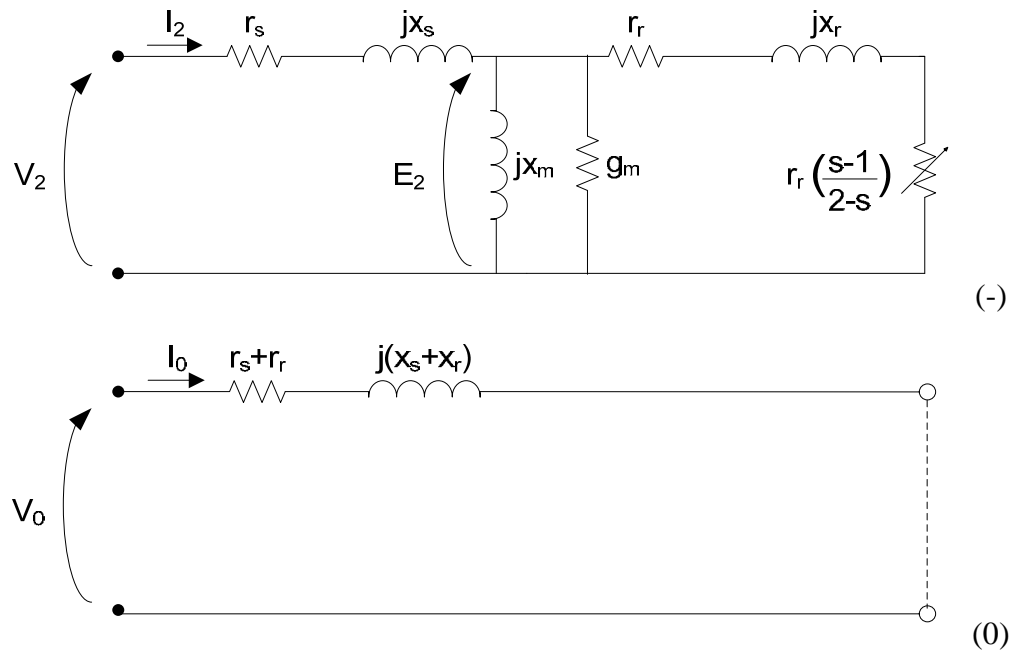


Figure 2. Three-Phase Induction Motor Sequence Networks

Copy Print Help

Three Phase Induction Motor Cancel Accept

Induction Motor

Electrical Parameters

Stator Resistance (pu) 0.01

Stator Reactance (pu) 0.06

Magnetizing Susceptance (pu) -0.286

Core Conductance (pu) 0.0

Rotor Resistance (pu) 0.02

Rotor Reactance (pu) 0.06

Estimate Parameters from Measurements

* All impedances in PU on the Motor MVA rating

Update Electrical

Update Nominal

Nominal Data

Power Rating (MVA) 10.0

Voltage Rating (kV) 13.8

Frequency Rating (Hz) 60.0

Nominal Power (MW) 1.0

Nominal Mech. Speed (RPM) 1765.0

Number of Poles 4

Power Factor 0.92382

Stator Connection ☐ Wye ☒ Delta

Wye Connection ☐ Grounded ☒ Ungrounded

Max Mechanical Torque 37.44PU

@ Slip (%) 16.75%

View Torque - Slip Curve

☐ Slip-dependent Rotor Parameters

Rotor Resistance (pu) = 0.02 + 0.02 * Slip + 0.01 * Slip²

Rotor Reactance (pu) = 0.06 + 0.04 * Slip (Slip not in %)

☒ In Service

☐ Out of Service

Bus Name MOTOR

Circuit Number 1

Mechanical Load Data

☐ Constant Torque 1.0 (pu)

☐ Constant Slip 2.0 (%)

☒ Speed Dependent Torque

PU Constant Torque (a) 1.0

PU Proportional Torque (b) 0.0

PU Quadratic Torque (c) 0.0

$T_{load} = a + b\omega + c\omega^2$

Inertia Constant H (sec) (on motor MVA rating) 0.5

Convert Convert

Moment of Inertia J (kg.m²) 281.44773

Program WinMGS-F - Form IGS_M404

Figure 3. Induction Motor Input Data Form

Circuit analysis yields the following equations:

$$\begin{aligned}
 \tilde{I}_{abc} &= T^{-1} \tilde{I}_{120} \\
 0 &= \tilde{V}_{abc} - T^{-1} \tilde{V}_{120} \\
 0 &= \tilde{I}_1 + (g_s + jb_s)(\tilde{E}_1 - \tilde{V}_1) \\
 0 &= \tilde{I}_2 + (g_s + jb_s)(\tilde{E}_2 - \tilde{V}_2) \\
 0 &= \tilde{I}_0 - (g_0 + jb_0)\tilde{V}_0 \\
 0 &= (g_m + jb_m)\tilde{E}_1 + \tilde{E}_1 \frac{s}{r_r + jx_r s} - (g_s + jb_s)(\tilde{V}_1 - \tilde{E}_1) \\
 0 &= (g_m + jb_m)\tilde{E}_2 + \tilde{E}_2 \frac{2-s}{r_r + jx_r(2-s)} - (g_s + jb_s)(\tilde{V}_2 - \tilde{E}_2)
 \end{aligned} \tag{2.6}$$

where:

$$T^{-1} = \begin{bmatrix} 1 & 1 & 1 \\ e^{j240^\circ} & e^{j120^\circ} & 1 \\ e^{j120^\circ} & e^{j240^\circ} & 1 \end{bmatrix},$$

with $e^{j120^\circ} = -0.5 + j\sqrt{3}/2$, and $e^{j240^\circ} = -0.5 - j\sqrt{3}/2$

$$g_s + jb_s = \frac{1}{r_s + jx_s},$$

$$g_m + jb_m = \frac{1}{r_m + jx_m},$$

$$g_0 + jb_0 = \frac{1}{r_s + r_r + jx_s + jx_r} \text{ for grounded Y, and 0 otherwise.}$$

An additional equation links the electrical state variables to the mechanical torque. This equation is derived by equating the mechanical power (torque times mechanical frequency) to the power consumed by the variable resistors in the positive and negative circuits of Figure 2.

$$0 = \left| \frac{\tilde{E}_1}{r_r + jx_r s} \right|^2 sr_r - \left| \frac{\tilde{E}_2}{r_r + jx_r (2-s)} \right|^2 (2-s)r_r - T_{em} \omega_s \quad (2.7)$$

where:

s_n : induction machine slip,

T_{em} : electromechanical motor torque,

ω_s : synchronous mechanical speed.

Two steady state operating modes are defined from the above equations:

(a) *Constant Slip Model (Linear)*:

$$\begin{aligned} \tilde{I}_{abc} &= T^{-1} \tilde{I}_{120} \\ 0 &= \tilde{V}_{abc} - T^{-1} \tilde{V}_{120} \\ 0 &= \tilde{I}_1 + (g_s + jb_s)(\tilde{E}_1 - \tilde{V}_1) \\ 0 &= \tilde{I}_2 + (g_s + jb_s)(\tilde{E}_2 - \tilde{V}_2) \\ 0 &= \tilde{I}_0 - (g_0 + jb_0)\tilde{V}_0 \\ 0 &= (g_m + jb_m)\tilde{E}_1 + \tilde{E}_1 \frac{s}{r_r + jx_r s} - (g_s + jb_s)(\tilde{V}_1 - \tilde{E}_1) \\ 0 &= (g_m + jb_m)\tilde{E}_2 + \tilde{E}_2 \frac{2-s}{r_r + jx_r (2-s)} - (g_s + jb_s)(\tilde{V}_2 - \tilde{E}_2) \end{aligned} \quad (2.8)$$

In the constant slip mode the motor operates at constant speed. The value of the slip is known from the operating speed and therefore the model is linear. If a neutral exists at the stator side (wye connection) the neutral voltage, \tilde{V}_n , is added as state, along with the equation $\tilde{I}_n = \tilde{I}_A + \tilde{I}_B + \tilde{I}_C = 3\tilde{I}_0$.

(b) *Torque Equilibrium Model (Nonlinear-Quadratic):*

$$\begin{aligned}
\tilde{I}_{abc} &= T^{-1} \tilde{I}_{120} \\
0 &= \tilde{V}_{abc} - T^{-1} \tilde{V}_{120} \\
0 &= \tilde{I}_1 + (g_s + jb_s)(\tilde{E}_1 - \tilde{V}_1) \\
0 &= \tilde{I}_2 + (g_s + jb_s)(\tilde{E}_2 - \tilde{V}_2) \\
0 &= \tilde{I}_0 - (g_0 + jb_0)\tilde{V}_0 \\
0 &= -T_{em}\omega_s + U_1sr_r - U_2(2-s)r_r \\
0 &= -(g_s + jb_s)\tilde{V}_1 + (g_s + g_m + j(b_s + b_m))\tilde{E}_1 + \tilde{W}_1s \\
0 &= -(g_s + jb_s)\tilde{V}_2 + (g_s + g_m + j(b_s + b_m))\tilde{E}_2 + \tilde{W}_2(2-s) \\
0 &= r_r\tilde{Y}_1 + jx_rs\tilde{Y}_1 - 1 \\
0 &= r_r\tilde{Y}_2 + jx_r(2-s)\tilde{Y}_2 - 1 \\
0 &= \tilde{W}_1 - \tilde{Y}_1\tilde{E}_1 \\
0 &= \tilde{W}_2 - \tilde{Y}_2\tilde{E}_2 \\
0 &= \tilde{W}_1\tilde{W}_1^* - U_1 \\
0 &= \tilde{W}_2\tilde{W}_2^* - U_2
\end{aligned} \tag{2.9}$$

If the mechanical torque is not constant, but depends on the speed (slip), equation (2.10) is also added completing the general model.

$$0 = T_m - a - b\omega_s - c\omega_s^2 + (b\omega_s + 2\omega_s^2)s - \omega_s^2s^2 \tag{2.10}$$

In the torque equilibrium model the motor electromechanical torque T_{em} is equal to the mechanical load torque, T_m . The slip is not a known constant and thus it becomes part of the state vector. Note that this model is nonlinear. Note also that the state vector and the equations are given in compact complex format. They are to be expanded in real and imaginary parts to get the actual real form of the model. Note also that the last equation is real. As in the previous mode, if a neutral exists at the stator side (wye-connection) the neutral voltage, \tilde{V}_n , is added as state, along with the equation $\tilde{I}_n = \tilde{I}_A + \tilde{I}_B + \tilde{I}_C = 3\tilde{I}_0$.

In order to capture the essential dynamic behavior of induction motor loads the model described in the previous section is augmented by the dynamical equation (2.11) describing the rotor motion:

$$J \cdot \frac{d\omega_m}{dt} = T_{em} - T_m, \tag{2.11}$$

where

J : rotor-load moment of inertia,

ω_m : rotor mechanical speed,

T_{em} : electrical motor torque,

T_m : mechanical load torque,

and equation (8) relating the speed and slip:

$$0 = \omega_m - s\omega_s - \omega_s. \quad (2.12)$$

The above transient (hybrid) model can capture the effects of the motor in the voltage profile of the power system. The electrical transients in the motor are neglected, as they do not have significant effect in the network solution, especially for the time scales of interest, which are very long compared to the time scales of the electrical transients. Phasor representation is therefore used for the electrical quantities. The elimination of stator electrical transients makes it possible to interface the dynamic motor model with the static network model (quasi steady state network model) yielding an integrated hybrid model.

The model described above is based on the standard equivalent circuit of an induction machine. This model is in general capable of representing a wide variety of motors; however, there are several motor types that cannot be adequately represented with this model, for example motors with double cage or deep bar rotors. For proper modeling of such motors a slightly modified equivalent circuit has been used [25]–[29]. Here, a generalized model is used that assumes that the rotor parameters are not constant, but depend on the slip (speed) of the motor [23]. A quadratic dependence is assumed for the rotor resistance and a linear dependence for the rotor reactance:

$$\begin{aligned} r_r(s) &= \alpha + \beta \cdot s + \gamma \cdot s^2 \\ x_r(s) &= \delta + \varepsilon \cdot s \end{aligned} \quad (2.13)$$

where s is the operating slip. These equations are included in the motor model. Note that in the constant slip operating mode the model is not significantly affected, since the slip is known and thus the rotor impedance is simply computed for this slip value. In the constant torque mode, however, the rotor parameters become part of the state vector after the inclusion of equations (2.13). The values of the resistance reduce as the speed increases, while the reactance may have some very small variation with speed. In fact the reactance value changes slightly and remains mainly constant, as it is also linearly related to the stator reactance which we assume constant. A similar change could also be assumed for the stator reactance, to make the model more precise.

A model with slip dependent rotor parameters can adequately represent, in a unified way, motors of every type and every NEMA design (A, B, C or D), including motors with double cage, or deep bar rotors. Designs A and D can be accurately represented using constant parameter models; for designs B and C the slip-depended model is used for more realistic representation.

2.4 Single-Phase Induction Motor Model

Single-phase induction motors are very common in residential and commercial load areas (representing a substantial part of the electric load) and have been identified to have major contribution to many voltage related problems, especially when they operate as air-conditioning compressors. A comprehensive single-phase induction motor model was developed as part of this project to allow modeling of such conditions. The model input data include typical motor nominal (nameplate) data, plus electrical parameters, and mechanical load data. The model supports four mechanical loading modes, in steady state: (a) Constant torque, (b) Constant power, (c) Constant slip, and (d) Speed-dependent torque. For dynamic analysis the constant electric power and constant slip modes have no meaning and therefore only the constant torque or slip dependent torque modes are used. The model also supports the options of including a running and a starting capacitor. The model incorporates four starting methods: (a) Split Phase, (b) Capacitor Start, (c) Permanent Split Capacitor, and (d) Capacitor Start, Capacitor Run. The input data form is illustrated in Figure 4.

Copy Print Help

Single or Two Phase Induction Motor

Cancel Accept

Single Phase Induction Motor

First Node
NEWBUS A

Second Node
NEWBUS N

Main Winding
Auxiliary Winding

☒ Split-Phase Motor

☐ Capacitor-Start Motor

☐ Permanent-Split-Capacitor Motor

☐ Capacitor-Start, Capacitor-Run Motor

Setpoint Operating Speed: % of n_{syn}

Electrical Parameters

Main Winding

Main Winding Resistance (Ohms)

Main Winding Self Inductance (mH) Ohms

Main and Rotor Winding Mutual Inductance (mH) Ohms

Auxiliary Winding

Auxiliary Winding Resistance (Ohms)

Auxiliary Winding Self Inductance (mH) Ohms

Auxiliary and Rotor Winding Mutual Inductance (mH) Ohms

Rotor Windings

Rotor Winding Resistance (Ohms)

Rotor Winding Self Inductance (mH) Ohms

Nominal Data

Power Rating (kVA)	500
Voltage Rating (kV)	0.230
Frequency Rating (Hz)	60.0
Number of Poles	4
Core Losses (W)	100
Rotational Losses (W)	40
Nominal Mech. Speed (RPM)	1765.0
Nominal Power (kW)	10.0
Nominal Power Factor	0.92

Max Mechanical Torque

Blip (%)

View: Nominal Blip - Torque Curve

Capacitor Values

Starting Capacitor (uF) Running Capacitor (uF)

☒ In Service ☐ Out of Service

Bus Name

Circuit Number

Mechanical Load Data

Inertia Constant H (sec) (on motor kVA rating) Moment of Inertia J (kg.m²)

☒ Constant Torque (pu)

☐ Constant Power (pu)

☐ Constant Blip (%)

☐ Speed Dependent Torque

PU Constant Torque (a)

PU Proportional Torque (b)

PU Quadratic Torque (c)

$T_{load} = a + b\omega + c\omega^2$

Program WINMDS.F - Form IDS_M31-1

Figure 4. Single-Phase Induction Motor Input Data

The compact model is based on the revolving field theory of a single phase induction motor. The physical circuit is presented in Figure 5, showing the case of both main and auxiliary windings and starting and running capacitors. The equations for simpler cases are simply derived by removing the elements (and thus equations) that are not present in each case.

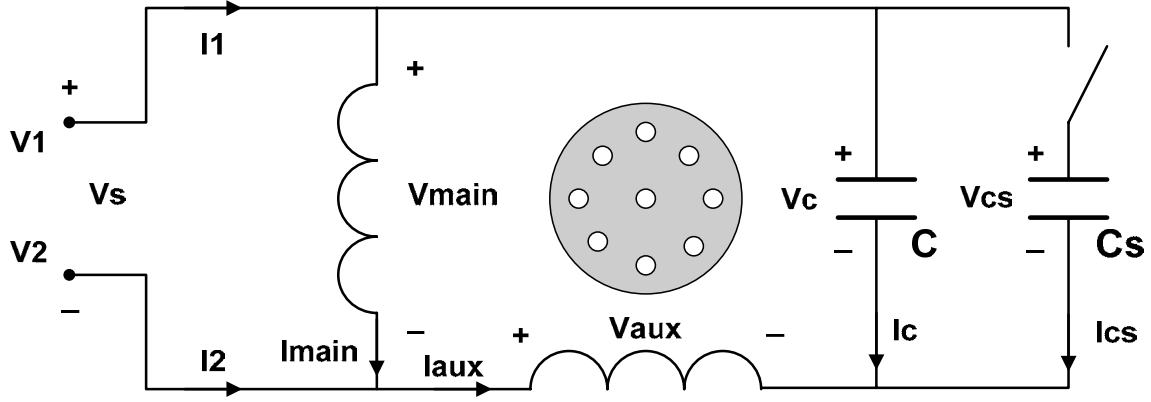


Figure 5. Single-Phase Induction Motor Physical Circuit

Circuit analysis yields the following equations, for the full case:

$$\begin{aligned}
 \tilde{I}_1 &= \tilde{I}_{main} + \tilde{I}_C + \tilde{I}_{CS} \\
 \tilde{I}_2 &= -\tilde{I}_{main} - \tilde{I}_C - \tilde{I}_{CS} \\
 \tilde{V}_S &= \tilde{V}_1 - \tilde{V}_2 \\
 \tilde{V}_{main} &= \tilde{V}_S \\
 \tilde{V}_C &= \tilde{V}_S \\
 \tilde{V}_{CS} &= \tilde{V}_S \\
 \tilde{I}_C &= \frac{\tilde{V}_C}{j\omega_e C} \\
 \tilde{I}_{CS} &= \frac{\tilde{V}_{CS}}{j\omega_e C_S} \\
 \tilde{I}_C + \tilde{I}_{CS} + \tilde{I}_{aux} &= 0 \\
 \tilde{V}_{main} &= \tilde{I}_{main} R_{main} + j\omega_e \tilde{\lambda}_{main} \\
 \tilde{V}_{aux} &= \tilde{I}_{aux} R_{aux} + j\omega_e \tilde{\lambda}_{aux} \\
 \tilde{\lambda}_{main} &= [L_{main} - jL_{main,r}^2 (\tilde{K}^+ + \tilde{K}^-)] \cdot \tilde{I}_{main} + L_{main,r} L_{aux,r} (\tilde{K}^+ - \tilde{K}^-) \tilde{I}_{aux} \\
 \tilde{\lambda}_{aux} &= -L_{main,r} L_{aux,r} (\tilde{K}^+ - \tilde{K}^-) \tilde{I}_{main} + [L_{aux} - jL_{aux,r}^2 (\tilde{K}^+ + \tilde{K}^-)] \tilde{I}_{aux} \\
 \tilde{I}_{r1}^+ &= \frac{-js\omega_e [L_{main,r} \tilde{I}_{main} + jL_{aux,r} \tilde{I}_{aux}]}{2(R_r + js\omega_e L_r)} \\
 \tilde{I}_{r1}^- &= \frac{-j(2-s)\omega_e [L_{main,r} \tilde{I}_{main} - jL_{aux,r} \tilde{I}_{aux}]}{2(R_r + j(2-s)\omega_e L_r)}
 \end{aligned} \tag{2.14}$$

$$\begin{aligned}\tilde{I}_{r2}^+ &= -j\tilde{I}_{r1}^+ \\ \tilde{I}_{r2}^- &= j\tilde{I}_{r1}^-\end{aligned}$$

where

$$\tilde{K}^+ = \frac{s\omega_e}{2(R_r + js\omega_e L_r)}, \quad (2.15)$$

$$\tilde{K}^- = \frac{(2-s)\omega_e}{2(R_r + j(2-s)\omega_e L_r)}, \quad (2.16)$$

ω_e is the synchronous electrical angular velocity, in electrical rad/sec,
and the slip, s , is related to the angular velocity and mechanical speed as:

$$s = \frac{\omega_{sm} - \omega_m}{\omega_{sm}} = \frac{n_s - n}{n_s}, \quad (2.17)$$

where

ω_{sm} : synchronous mechanical speed in rad/s,

ω_m : motor mechanical speed in rad/s,

n_s : synchronous mechanical speed in rpm,

n : motor mechanical speed in rpm.

An additional equation links the electrical state variables to the electrical torque produced by the motor.

$$T_e = \left(\frac{\text{poles}}{2} \right) \cdot \text{Re} \left\{ L_{main,r}^2 \tilde{I}_{main} \tilde{I}_{main}^* + L_{aux,r}^2 \tilde{I}_{aux} \tilde{I}_{aux}^* \left(\tilde{K}^+ - \tilde{K}^- \right)^* + jL_{main,r} L_{aux,r} \left(\tilde{I}_{main}^* \tilde{I}_{aux} - \tilde{I}_{main} \tilde{I}_{aux}^* \right) \left(\tilde{K}^+ + \tilde{K}^- \right)^* \right\} \quad (2.18)$$

2.5 Synchronous Generating Unit Model

A single axis generator model is used in this work. The unit is electrically described as a source (controlled by its subsystems) behind an equivalent impedance, as illustrated in the equivalent circuit of Figure 6. The rotor mechanical dynamics are the only dynamics included in the model. The internal sources provide a set of balanced three phase voltages, described with the state variables E , δ . The dynamic model is based on a quasi-steady-state model that assumes that the generator is operating under sinusoidal steady state conditions as far as the electrical system is concerned. Only the rotor mechanical system dynamics are assumed, therefore the steady-state equations described in the previous section also hold, with the augmentation of the system with the swing equation of the rotor rotational movement. This equation defines the mechanical rotational speed $\omega(t)$ as well as the internal voltage angle $\delta(t)$ which is now a time varying quantity. The internal voltage magnitude $E(t)$ is specified by the excitation

system, or may have constant value. Therefore the model compact equations are as follows:

$$\begin{aligned}
\tilde{I}_a &= (g + jb)(\tilde{V}_a - \tilde{V}_n - \tilde{E}_a) \\
\tilde{I}_b &= (g + jb)(\tilde{V}_b - \tilde{V}_n - \tilde{E}_b) \\
\tilde{I}_c &= (g + jb)(\tilde{V}_c - \tilde{V}_n - \tilde{E}_c) \\
\tilde{I}_n &= (g + jb)(-\tilde{V}_a - \tilde{V}_b - \tilde{V}_c + 3\tilde{V}_n) \\
\frac{d\delta(t)}{dt} &= \omega(t) - \omega_s \\
J \frac{d\omega(t)}{dt} &= T_m(t) - T_e(t) - D(\omega(t) - \omega_s) \\
0 &= P_e(t) + \text{Re}\{\tilde{E}_a \tilde{I}_a^* + \tilde{E}_b \tilde{I}_b^* + \tilde{E}_c \tilde{I}_c^*\} \\
0 &= T_e(t)\omega(t) - P_e(t) \\
0 &= E(t) - KE_f(t)
\end{aligned} \tag{2.19}$$

where:

$$g = -\frac{R}{R^2 + \omega^2 L^2},$$

$$b = -\frac{\omega L}{R^2 + \omega^2 L^2},$$

J is the moment of inertia of the generator,

D is a damping coefficient,

ω_s is the synchronous speed, and

K is a constant of proportionality.

Furthermore,

$$\tilde{E} = E(t)e^{j\delta(t)} = E(t)\cos\delta(t) + jE(t)\sin\delta(t)$$

$$\tilde{E}_a = Ee^{j\delta}$$

$$\tilde{E}_b = Ee^{j(\delta - \frac{2\pi}{3})}$$

$$\tilde{E}_c = Ee^{j(\delta - \frac{4\pi}{3})}$$

The state vector is:

$$x = [V_{ar} \ V_{ai} \ V_{br} \ V_{bi} \ V_{cr} \ V_{ci} \ V_{nr} \ V_{ni} \ \delta(t) \ \omega(t) \ P_e(t) \ T_e(t) \ E(t)]$$

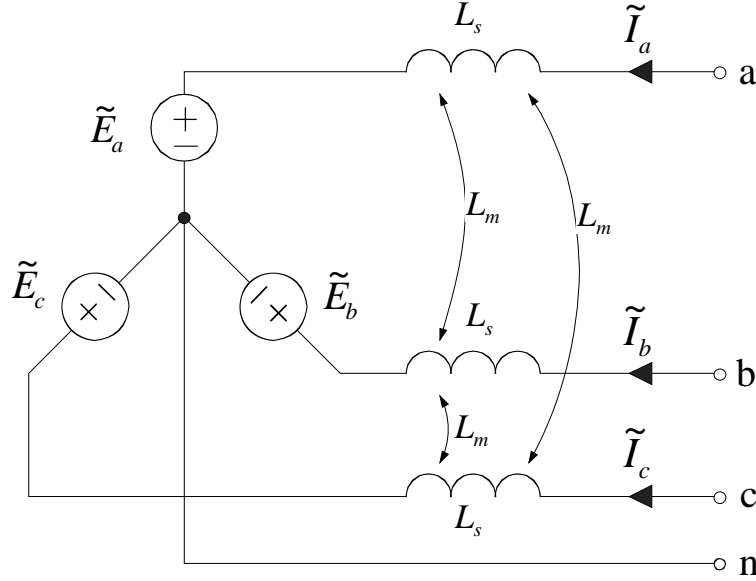


Figure 6. Equivalent Circuit of Synchronous Generator Model

Generic exciter and prime-mover models have been developed as briefly illustrated by block diagrams in Figures 7 and 8.

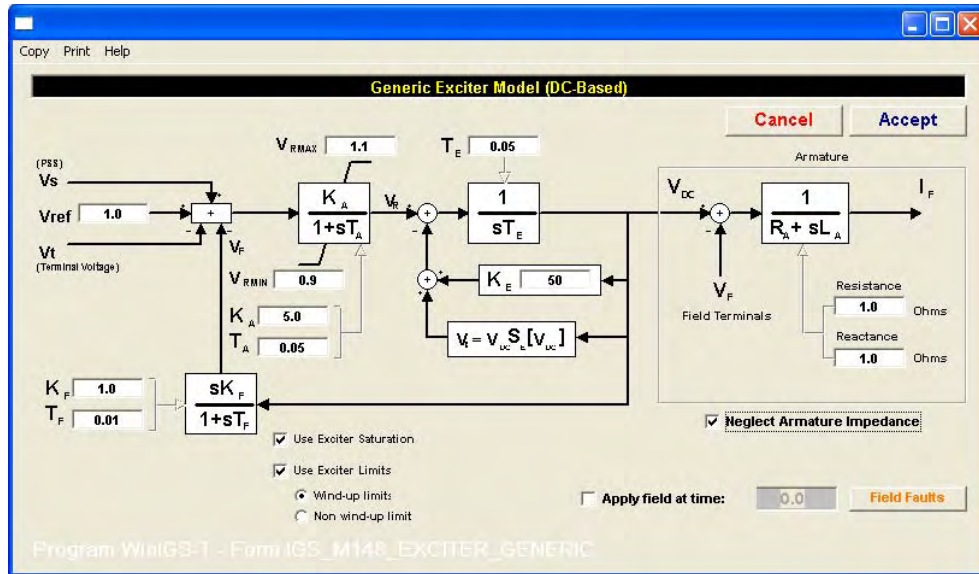


Figure 7. Generic Exciter Model

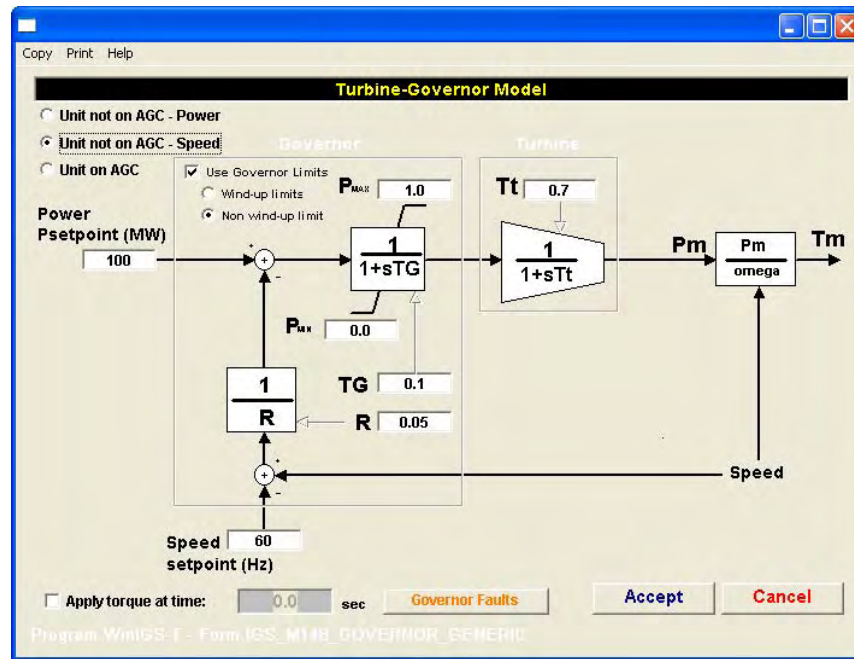


Figure 8. Generic Prime-Mover Model

3. Voltage-Load Dynamics: Control

3.1 Introduction

Once the voltage recovery phenomena are modeled and studied the topic of mitigation of such phenomena is addressed. Installation and operation of dynamic VAR devices provides the means of locally controlling the voltage in real time, during transients, and thus alleviating or even eliminating such problems. The focus of this part of the report is the optimal operation of installed VAR resources for speeding up the transient voltage recovery and minimizing the impact of these transients.

The overall problem is stated as follows: Assume a power system with static and dynamic loads, generating units with specific VAR control capabilities and other VAR control devices that is subject to a wide variety of exogenous disturbances. For a specific disturbance the protective system will respond and will take the system through specific switching operations. During this period the system will experience transients that may include voltage recovery transients and possible voltage instability. For this sequence of events, the needed control for the dynamic VAR sources is determined to ensure that the system will not experience any voltage instabilities (operational problem).

This project briefly addresses this topic on a theoretical basis. The problem is formulated as an optimal control problem that determines the minimum control effort that provides the desired system behavior, based on specific operational criteria. Such criteria are associated with the rate of recovery and the minimum time to recovery. Direct transcription methods are used to create a discrete numerical approximation of the continuous optimal control problem, using an implicit Runge-Kutta discretization scheme. The mathematical problem formulation is presented considering a power system quasi-steady state dynamic model, operational path constraints and specific objective functions. The end result provides an insight of the optimal operation and control of reactive support resources, under such transient phenomena.

3.2 Problem Description

A typical simulation scenario can be described as follows. Assume an electric power system operating under normal steady state conditions. The system is subject to a wide variety of exogenous disturbances, like e.g. short circuits. When such a disturbance takes place the system moves from its normal operating state, to the faulted state. For a specific disturbance the protective system will respond and will take the system through specific switching operations, moving it from the faulted state to the post fault state. During this period the system will experience transients that may include voltage recovery transients and possible voltage instability. For this sequence of events, the needed control, via specific controlling devices, needs to be determined to ensure that the system will not experience any instability and will promptly return to acceptable operating conditions.

More specifically a typical scenario consists of the following phases:

- 1) Pre-fault phase: The system is operating at steady state condition.

2) During-fault phase: When a fault (or a disturbance in general) takes place the system enters a transient operating condition. Typically the during-fault phase is characterized by severely abnormal operating conditions, like e.g. very low voltage levels or significant frequency excursions.

3) Post-fault phase: This is the most important and interesting phase of the analysis. The fault is cleared by the protective system (or in general the disturbance is removed). This is in general associated with a change in the system configuration, which may now move to a new acceptable or unacceptable steady state or even become unstable, based on the control action applied to the system. The final operating condition at the end of the fault period is the initial conditions of the post fault system.

Voltage recovery following short circuits in electric power systems is one such phenomenon. Short circuits of various types (three-phase, two-phase, two-phase to ground, single phase to ground) are common events in electric transmission or distribution systems. Such faults can cause significant voltage dips in their vicinity. They are usually cleared by the operation of protective circuit breakers and possibly the isolation of the fault location from the rest of the system (e.g. removal of faulted line). However, voltage built-up after such a fault may be slow and even exhibit a strong oscillatory behavior, depending on the dynamic characteristics of the system, and in particular synchronous generating units and dynamic loads, like e.g. motor loads. Such slow voltage recovery can result in system-wide problems, like voltage instability and voltage collapse or local problems in particular weak system areas. That is, the system as a whole may recover and appear to reach an acceptable new steady state, however, specific load areas of the system may continue experiencing unacceptable operating conditions. This might result from the fact that slow voltage recovery may have other secondary effects and result in undesired protective relay operation like tripping of sensitive loads.

Voltage behavior in a power system is mainly controlled via the synchronous generating units, or via reactive support devices (VAr devices) like switched capacitors deployed throughout the system. However, generators cannot provide local support, while capacitors have to be switched on and off mechanically and thus cannot provide continuous and fast, real time response. They are, thus, mainly used for controlling the voltage based on steady state criteria, rather than during transients. They are also passive elements, and their control ability depends on the system voltage at their locations. Therefore, during faults that result in significant voltage dips their response might not be considerable.

Therefore, dynamic VAr sources, in the form of FACTS devices, are the only practical way of locally controlling the voltage. Such devices use power electronic technology to control the reactive power they inject into the system. This allows fast response times and thus practically real time control of the system, in the form of continuous, rather than discrete control action.

3.3 Mathematical Problem Formulation

An electric power system can be modeled as a set of nonlinear differential-algebraic equations (DAEs) of the general form:

$$\begin{aligned}\dot{x}(t) &= f(x(t), y(t), u(t), p, t) \\ 0 &= g(x(t), y(t), u(t), p, t)\end{aligned}\tag{3.1}$$

where

$x(t)$ are the dynamical system states;

$y(t)$ are the algebraic states;

$u(t)$ are the system control variables;

p is the system parameter vector;

f is the vector function of the dynamic system equations;

g is the vector function of the algebraic system equations.

The number of dynamical states is n_x , of algebraic states n_y , and of control variables n_u . The number of differential equations is n_f and of algebraic equations n_g . For implementation purposes it is convenient, and possible for most of the power system applications, to convert the function f to a set of linear equations and move all the nonlinearities to the algebraic equations, g . Furthermore, g is assumed to be a set of at most quadratic equations. This can be, in general, achieved by introducing some additional algebraic state variables to quadratize the model, without any approximations, as also explained earlier in the report. Functions f and g , in general, also contain switching functions representing elements that are switched on an off or change their operating mode, or modifications in the system configuration during different stages of the analysis and during the various scenarios under study. Changes in f and g define different phases of the problem, so within a single phase the system dynamics are considered unmodified.

The control vector can contain any available control of interest, like e.g. generator controls, load controls (if available) both continuous and discrete. In our case, as described in the previous section, the control variables are the desired reactive power injections from existing dynamic VAr sources of interest. This is a continuous control, in the form of a trajectory of reactive power injection during the during-fault and post-fault phases of the analysis. During the pre-fault phase the control input is some specific reference value that keeps the system operating under the desired steady state conditions.

The problem is to define the optimal (minimum effort) control trajectory for dynamic VAr source injections that satisfies specific recovery criteria, associated with the rate of recovery. The approach presented in [30]-[31] is followed. Specifically, the control functions $u(t)$ are to be chosen to minimize the objective function

$$J = \phi[x(t_F), y(t_F), t_F]\tag{3.2}$$

subject to the state equations (3.1) and the boundary conditions

$$\psi[x(t_F), y(t_F), p, t_F] = 0\tag{3.3}$$

where the initial conditions $x(t_I) = x_I$ and $y(t_I) = y_I$ are given at the fixed initial time t_I and the final time t_F is free. The modified objective function of the problem is defined as

$$\hat{J} = [\varphi + v^T \psi]_{t_F} - \int_{t_I}^{t_F} \{ \mu^T(t) g + \lambda^T(t) [\dot{x}(t) - f] \} dt. \quad (3.4)$$

Vector v is the vector of Lagrange multipliers for the discrete constraints, while vectors $\lambda(t)$ and $\mu(t)$ are the multipliers for the continuous constraints, referred to as adjoint or costate variables. The necessary conditions for a constraint optimum are obtained by setting the first variation $\delta \hat{J} = 0$. The system Hamiltonian is defined as, assuming that the differential-algebraic equation (DAE) system (3.1) is of index one.

$$H = \lambda^T f + \mu^T g \quad (3.5)$$

and the auxiliary function

$$\Phi = \varphi + v^T \psi \quad (3.6)$$

The resulting necessary conditions are:

$$\begin{bmatrix} \dot{\lambda} & \dot{\mu} \end{bmatrix} = \begin{bmatrix} -H_x^T & -H_y^T \end{bmatrix}, \text{ (adjoint equations)} \quad (3.7)$$

$$0 = H_u^T, \quad \text{(control equations)} \quad (3.8)$$

$$\begin{aligned} \lambda(t_F) &= \Phi_x^T \Big|_{t=t_F}, \\ \mu(t_F) &= \Phi_y^T \Big|_{t=t_F}, \\ 0 &= (\Phi_y + H) \Big|_{t=t_F}, \quad \text{(transversality conditions)} \\ 0 &= \lambda(t_I), \\ 0 &= \mu(t_I). \end{aligned} \quad (3.9)$$

Equations (3.1), (3.5) and (3.8) comprise a DAE system with boundary conditions at both t_I and t_F provided by (3.3) and (3.9). Altogether they form a two-point boundary value problem.

Furthermore, additional equality or inequality path constraints can be imposed, within each phase, of the general form

$$h_l \leq h(x(t), y(t), u(t), p, t) \leq h_u, \quad (3.10)$$

as well as simple bounds on the state and control variables, representing, e.g., upper and lower limits of specific device outputs.

$$\begin{aligned} x_l &\leq x(t) \leq x_u \\ y_l &\leq y(t) \leq y_u \\ u_l &\leq u(t) \leq u_u \end{aligned} \quad (3.11)$$

3.4 Solution Methodology

Direct transcription is used to convert the infinite dimensional, continuous time, optimal control problem to an approximate, finite dimensional, discrete, nonlinear programming (NLP) problem. Assume a single phase of the problem, like e.g. the post fault phase. The phase duration is divided into M intervals.

$$t_I = t_0 < t_1 < \dots < t_M = t_F$$

The number of grid points is $N = M + 1$. The values of the state and control variables are treated as a set of NLP variables. The differential equations are replaced by a finite set of discretized equations, at each grid point, based on some numerical integration scheme. For the trapezoidal scheme the NLP variables are

$$X^T = [x_1^T \quad y_1^T \quad u_1^T \quad \dots \quad x_M^T \quad y_M^T \quad u_M^T],$$

and the discretization equations are

$$x_k = x_{k-1} + \frac{h_k}{2}(f_k + f_{k-1}) \quad (3.12)$$

or

$$0 = \left[x_k - \frac{h_k}{2} f_k \right] + \left[-x_{k-1} - \frac{h_k}{2} f_{k-1} \right] \quad (3.13)$$

where the subscripts k and $k-1$ denote the values at the current time t_k and the previous time $t_{k-1} = t_k - h$ respectively, and h_k is the discretization step at grid point k . Usually the step is constant, however, this notation also accommodates the case where the step is variable. The stepsize can be defined as:

$$h_k = \tau_k(t_F - t_I) = \tau_k \Delta t \quad (3.14)$$

with $0 < t_k < 1$.

Therefore, $x_k = x(t_k)$, $y_k = y(t_k)$, $u_k = u(t_k)$, $f_k = f(x_k, y_k, u_k, p, t_k)$, and similarly at $k-1$. For the Hermite-Simpson discretization (also referred to as quadratic integration scheme for conciseness) the NLP variables are

$$X^T = [x_1^T \quad y_1^T \quad u_1^T \quad x_{2m}^T \quad y_{2m}^T \quad u_{2m}^T \quad x_2^T \quad y_2^T \quad u_2^T \quad \dots \quad x_{Mn}^T \quad y_{Mn}^T \quad u_{Mn}^T \quad x_M^T \quad y_M^T \quad u_M^T]$$

and the discretization equations are

$$\begin{aligned} x_m - \frac{h}{3} f_m + \frac{h}{24} f_k &= x_{k-1} + \frac{5h}{24} f_{k-1} \\ x_k - \frac{2h}{3} f_m + \frac{h}{6} f_k &= x_{k-1} + \frac{h}{6} f_{k-1} \end{aligned} \quad (3.15)$$

or

$$\begin{aligned}
0 &= \frac{h}{24} f_k + \left[x_m - \frac{h}{3} f_m \right] + \left[-x_{k-1} - \frac{5h}{24} f_{k-1} \right] \\
0 &= \left[x_k + \frac{h}{6} f_k \right] - \frac{2h}{3} f_m + \left[-x_{k-1} - \frac{h}{6} f_{k-1} \right]
\end{aligned} \tag{3.16}$$

The subscript m denotes the midpoint of the segment with endpoints $k-1$ and k . All the algebraic equations are enforced at the grid points and appended to the algebraized differential equations. This means that the following equations, (3.17) and (3.18), are appended for the trapezoidal and quadratic discretization schemes respectively, as derived from (3.1), (3.10) and (3.11).

$$\begin{aligned}
0 &= g(x_k, y_k, u_k, p, t_k) \\
h_l &\leq h(x_k, y_k, u_k, p, t_k) \leq h_u \\
x_l &\leq x_k \leq x_u \\
y_l &\leq y_k \leq y_u \\
u_l &\leq u_k \leq u_u
\end{aligned} \tag{3.17}$$

$$\begin{aligned}
0 &= g(x_k, y_k, u_k, p, t_k) \\
h_l &\leq h(x_k, y_k, u_k, p, t_k) \leq h_u \\
x_l &\leq x_k \leq x_u \\
y_l &\leq y_k \leq y_u \\
u_l &\leq u_k \leq u_u \\
0 &= g(x_m, y_m, u_m, p, t_m) \\
h_l &\leq h(x_m, y_m, u_m, p, t_m) \leq h_u \\
x_l &\leq x_m \leq x_u \\
y_l &\leq y_m \leq y_u \\
u_l &\leq u_m \leq u_u
\end{aligned} \tag{3.18}$$

Inequality constraints are treated by the introduction of slack variables that convert them to equality constraints.

Therefore, the resulting equality constraint NLP problem is to choose the decision variables X , as defined earlier, to minimize the objective function

$$F(X) = \phi(x_M, y_M), \tag{3.19}$$

as derived from (3.2), subject to the constraints

$$c(X) = 0, \tag{3.20}$$

which in this case are defined by equations (3.13) and (3.17) or (3.16) and (3.18) for $k=1$ to $M=N-1$, depending on the discretization scheme. It is assumed that the provided initial condition, referring to the first grid point (at t_0) are consistent with all the algebraic constraints.

The form of (3.19), though it appears simplistic and restrictive, is quite general and can also accommodate objective functions or constraints defined via quadrature forms. This can be done by introducing additional dynamical states and casting the optimization problem in Mayer form [3.11]. So, for example, for an objective function defined as

$$J = \int_{t_I}^{t_F} w(x(t), y(t), u(t), p, t) dt \quad (3.21)$$

an additional dynamic state variable, $\zeta(t)$, can be introduced along with the differential equation

$$\dot{\zeta} = w(x(t), y(t), u(t), p, t) \quad (3.22)$$

and the initial condition $\zeta(t_I) = 0$.

In this case, the objective function simply becomes

$$J = \zeta(t_F) = \phi(x_M, y_M). \quad (3.23)$$

The Lagrangian of the NLP is given by

$$L(X, \xi) = F(X) - \xi^T c(X) = \phi(x_M, y_M) - \sum_{k=1}^M \xi_k^T c_k(X). \quad (3.24)$$

The necessary conditions for this problem are

$$\frac{\partial L}{\partial \xi_k} = 0 = c(X), \quad (3.25)$$

The solution of the defined NLP problem is obtained via Newton's method.

The solution provides the control signals for the system to mitigate the voltage recovery transients. The method will be demonstrated with examples in the next section.

4. Numerical Examples

4.1 Test System Definition

Two test systems have been utilized to demonstrate the methodology the dynamic simulation of voltage recovery and mitigation of voltage transients. The first system is a small transmission system with little representation of distribution parts that operates under near-balanced conditions and presents very little asymmetry. The second system is an extension of the first to include a more detailed modeling of distribution feeders connected to the bulk power system. The distribution parts are asymmetric and operate under unbalanced conditions. The two test systems are described next.

4.1.1 Test System 1 – Transmission System

The first test system is illustrated in Figure 9.

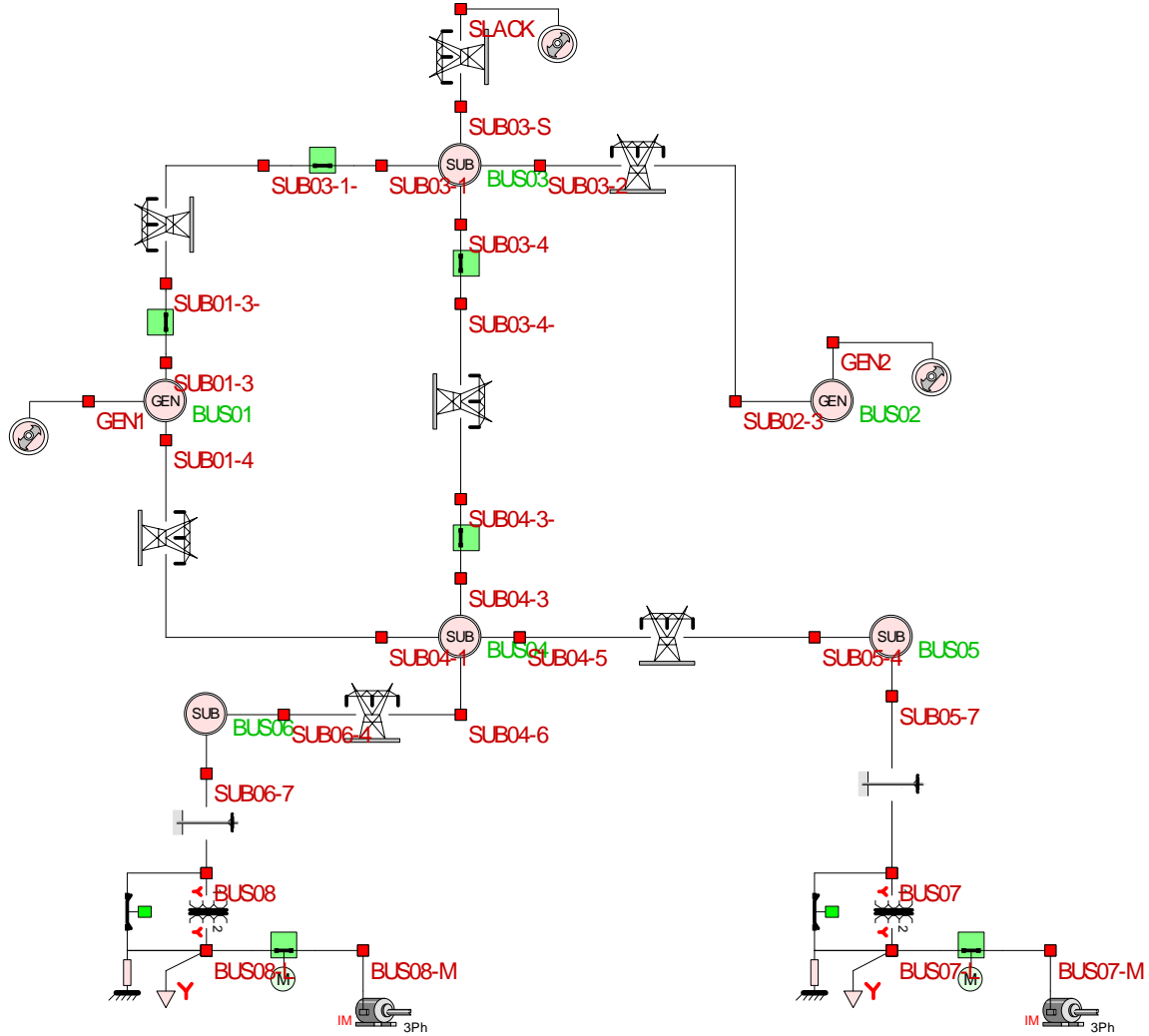


Figure 9. Single-Line Diagram of Test System 1

The system consists of two generating units and a third generator (acting as slack unit in steady state) representing the equivalent external network, where the system is connected to, via a transmission line. There are two generating substations (buses 1 and 2), equipped with step-up transformers, two transmission substations (buses 3 and 4), two distribution substations (buses 5 and 6), with step down transformers, seven transmission lines and two distribution lines in the system. Loads are connected to the system at the ends of the distribution lines via transformers. Portion of the load is represented as constant impedance load and another portion as induction motor loads. Motor 1 has a fan-type mechanical loading, while motor 2 drives a constant torque mechanical load. The generating units operate at 12 kV. The transmission system operates at 115 kV. The small distribution feeders operate at 25 kV and 13.8 kV. The system data for all the system components are presented in Figures 10 through 21.

Synchronous Generator Model - Generating Unit 1

Machine Identifier: 1, Circuit Number: 1, Machine Status: ☒ In Service, ☐ Out of Service, Power Bus: GEN1

Controls: ☒ PV Control, ☐ PQ Control, ☐ Slack, Nominal Voltage (kV): 12.0, Voltage Setpoint (pu): 1.0, Voltage Regulated Bus: GEN1

Other Parameters: Per Unit Inertia Constant: 1.9

	Output Power	Minimum Power	Maximum Power	
Real	6.0	0.0	10.0	MW
Reactive	0.0	-5.0	5.0	MVar

Reactive Power Allocation Factor: 1.0

Source Impedance	Ohms	PU	Base
Positive Sequence	Resistance: 0.14400, Reactance: 1.44000	0.01, 0.1	10.0 MVA, 12.000 kV
Negative Sequence	Resistance: 0.14400, Reactance: 1.44000	0.01, 0.1	6.481 kA
Zero Sequence	Resistance: 0.14400, Reactance: 1.44000	0.01, 0.1	14.400 Ohms

Buttons: Update Ohms, Update PU

Synchronous Generator Model - Generating Unit 2

Machine Identifier: 2, Circuit Number: 1, Machine Status: ☒ In Service, ☐ Out of Service, Power Bus: GEN2

Controls: ☒ PV Control, ☐ PQ Control, ☐ Slack, Nominal Voltage (kV): 12.0, Voltage Setpoint (pu): 1.00, Voltage Regulated Bus: GEN2

Other Parameters: Per Unit Inertia Constant: 3.5

	Output Power	Minimum Power	Maximum Power	
Real	5.0	0.0	10.0	MW
Reactive	0.0	-7.0	7.0	MVar

Reactive Power Allocation Factor: 1.0

Source Impedance	Ohms	PU	Base
Positive Sequence	Resistance: 0.14400, Reactance: 1.44000	0.01, 0.1	10.0 MVA, 12.000 kV
Negative Sequence	Resistance: 0.14400, Reactance: 1.44000	0.01, 0.1	6.481 kA
Zero Sequence	Resistance: 0.14400, Reactance: 1.44000	0.01, 0.1	14.400 Ohms

Buttons: Update Ohms, Update PU

Synchronous Generator Model - SLACK GENERATOR (EQUIVALENT NETWORK)

Machine Identifier: 3, Circuit Number: 1, Machine Status: ☒ In Service, ☐ Out of Service, Power Bus: SLACK

Controls: ☐ PV Control, ☐ PQ Control, ☒ Slack, Nominal Voltage (kV): 115.0, Voltage Setpoint (pu): 1.0, Voltage Regulated Bus: SLACK

Other Parameters: Per Unit Inertia Constant: 30.0

	Output Power	Minimum Power	Maximum Power	
Real	50.0	0.0	100.0	MW
Reactive	0.0	-50.0	50.0	MVar

Reactive Power Allocation Factor: 1.0

Source Impedance	Ohms	PU	Base
Positive Sequence	Resistance: 0.014399, Reactance: 0.14399	0.00010888, 0.0010888	100.0 MVA, 115.000 kV
Negative Sequence	Resistance: 0.014399, Reactance: 0.11399	0.00010888, 0.0010888	6.562 kA
Zero Sequence	Resistance: 0.014399, Reactance: 0.14399	0.00010888, 0.0010888	132.250 Ohms

Buttons: Update Ohms, Update PU

Figure 10. Generating Unit Data

3-Phase Overhead Transmission Line

TRANSMISSION LINE BUS 03 TO SLACK

Phase Conductors

TypeACSR

SizeJOREE

Shields/Neutrals

TypeHS

Size5/16HS

Tower/Pole

Type103A

Circuit Number1

Structure NameJellow Jacket

Tower/Pole Ground Impedance (Ohms)

R = 25.0

X = 0.0

Get From GIS

Line Length (miles)30.0

Line Span Length (miles)0.1

Soil Resistivity (Ohm-Meters)100.0

Bus Name, Side 1SUB03-S

Bus Name, Side 2SLACK

Failure & Repair Rates

Failure Rate (per year)1.0

Repair Rate (per year)1.0

Insulated Shields

Transposed Phases

Transposed Shields

Read GPS Coordinates

Operating Voltage (kV)115.0

Insulation Levels (kV)

FOW (Front of Wave)100.0

BIL (Basic Insulation Level)100.0

AC (AC Withstand)100.0

GA POWER WOOD POLE H-FRAME

53.5 feet

3-Phase Overhead Transmission Line

TRANSMISSION LINE BUS 01 TO BUS 03

Phase Conductors

TypeACSR

SizeJOREE

Shields/Neutrals

TypeHS

Size5/16HS

Tower/Pole

TypeAGC-H-115

Circuit Number1

Structure NameJellow Jacket

Tower/Pole Ground Impedance (Ohms)

R = 25.0

X = 0.0

Get From GIS

Line Length (miles)8.0

Line Span Length (miles)0.1

Soil Resistivity (Ohm-Meters)100.0

Bus Name, Side 1SUB01-3-

Bus Name, Side 2SUB03-1-

Failure & Repair Rates

Failure Rate (per year)1.0

Repair Rate (per year)1.0

Insulated Shields

Transposed Phases

Transposed Shields

Read GPS Coordinates

Operating Voltage (kV)115.0

Insulation Levels (kV)

FOW (Front of Wave)100.0

BIL (Basic Insulation Level)100.0

AC (AC Withstand)100.0

AGC 115 kV H-Frame

67.8 feet

3-Phase Overhead Transmission Line

TRANSMISSION LINE BUS 03 TO BUS 02

Phase Conductors

TypeACSR

SizeJOREE

Shields/Neutrals

TypeHS

Size5/16HS

Tower/Pole

TypeAGC-H-115

Circuit Number1

Structure NameJellow Jacket

Tower/Pole Ground Impedance (Ohms)

R = 25.0

X = 0.0

Get From GIS

Line Length (miles)12.0

Line Span Length (miles)0.1

Soil Resistivity (Ohm-Meters)100.0

Bus Name, Side 1SUB03-2

Bus Name, Side 2SUB02-3

Failure & Repair Rates

Failure Rate (per year)1.0

Repair Rate (per year)1.0

Insulated Shields

Transposed Phases

Transposed Shields

Read GPS Coordinates

Operating Voltage (kV)115.0

Insulation Levels (kV)

FOW (Front of Wave)100.0

BIL (Basic Insulation Level)100.0

AC (AC Withstand)100.0

AGC 115 kV H-Frame

67.8 feet

3-Phase Overhead Transmission Line

TRANSMISSION LINE BUS 01 TO BUS 04

Phase Conductors

TypeACSR

SizeSPARROW

Shields/Neutrals

TypeN/A

Size

Tower/Pole

TypeKONDOS115

Circuit Number1

Structure NameJellow Jacket

Tower/Pole Ground Impedance (Ohms)

R = 25.0

X = 0.0

Get From GIS

Line Length (miles)2.0

Line Span Length (miles)0.1

Soil Resistivity (Ohm-Meters)100.0

Bus Name, Side 1SUB01-4

Bus Name, Side 2SUB04-1

Failure & Repair Rates

Failure Rate (per year)1.0

Repair Rate (per year)1.0

Insulated Shields

Transposed Phases

Transposed Shields

Read GPS Coordinates

Operating Voltage (kV)115.0

Insulation Levels (kV)

FOW (Front of Wave)100.0

BIL (Basic Insulation Level)100.0

AC (AC Withstand)100.0

PSE, 115 kV Line without shield

60.3 feet

3-Phase Overhead Transmission Line

TRANSMISSION LINE BUS 03 TO BUS 04

Phase Conductors

TypeACSR

SizeJOREE

Shields/Neutrals

TypeHS

Size5/16HS

Tower/Pole

TypeAGC-H-115

Circuit Number1

Structure NameJellow Jacket

Tower/Pole Ground Impedance (Ohms)

R = 25.0

X = 0.0

Get From GIS

Line Length (miles)6.0

Line Span Length (miles)0.1

Soil Resistivity (Ohm-Meters)100.0

Bus Name, Side 1SUB03-4-

Bus Name, Side 2SUB04-3-

Failure & Repair Rates

Failure Rate (per year)1.0

Repair Rate (per year)1.0

Insulated Shields

Transposed Phases

Transposed Shields

Read GPS Coordinates

Operating Voltage (kV)115.0

Insulation Levels (kV)

FOW (Front of Wave)100.0

BIL (Basic Insulation Level)100.0

AC (AC Withstand)100.0

AGC 115 kV H-Frame

67.8 feet

3-Phase Overhead Transmission Line

TRANSMISSION LINE BUS 04 TO BUS 05

Phase Conductors

TypeACSR

SizeSPARROW

Shields/Neutrals

TypeHS

Size5/16HS

Tower/Pole

Type101A

Circuit Number1

Structure NameJellow Jacket

Tower/Pole Ground Impedance (Ohms)

R = 25.0

X = 0.0

Get From GIS

Line Length (miles)22.0

Line Span Length (miles)0.1

Soil Resistivity (Ohm-Meters)100.0

Bus Name, Side 1SUB04-5

Bus Name, Side 2SUB05-4

Failure & Repair Rates

Failure Rate (per year)1.0

Repair Rate (per year)1.0

Insulated Shields

Transposed Phases

Transposed Shields

Read GPS Coordinates

Operating Voltage (kV)115.0

Insulation Levels (kV)

FOW (Front of Wave)100.0

BIL (Basic Insulation Level)100.0

AC (AC Withstand)100.0

GA Power H-Frame Wood Pole TC

67.8 feet

Figure 7 Transmission Line Data

Copy Print Help

3-Phase Overhead Transmission Line

TRANSMISSION LINE BUS 04 TO BUS 06

Accept Cancel

Phase Conductors
Type: ACSR
Size: SPARROW

Shields/Neutrals
Type: HS
Size: 5/16HS

Tower/Pole
Type: 101A
Circuit Number: 1
Structure Name: Jellow Jacket

Tower/Pole Ground Impedance (Ohms)
R = 25.0 X = 0.0

Get From GIS
Line Length (miles): 12.0
Line Span Length (miles): 0.1
Soil Resistivity (Ohm-Meters): 100.0

Bus Name, Side 1: SUB06-4
Circuit Number: 1
Bus Name, Side 2: SUB04-6

Failure & Repair Rates
Failure Rate (per year): 1.0
Repair Rate (per year): 1.0

☐ Insulated Shields
☐ Transposed Phases
☐ Transposed Shields
☐ Read GPS Coordinates

Operating Voltage (kV): 115.0
Insulation Levels (kV):
FOW (Front of Wave): 100.0
BIL (Basic Insulation Level): 100.0
AC (AC Withstand): 100.0

GA. Power H-Frame Wood Pole TC

67.8 feet

28.0

N1

B1

A1

C1

WebbDoc 7 - Form: 1007, M102 - Copyright © A. R. MacIntyre 1986-2007

Figure 8. Transmission Line Data

Copy Print Help

3-Phase Overhead Transmission Line

DISTRIBUTION LINE BUS 06 TO BUS 08

Accept Cancel

Phase Conductors
Type: ACSR
Size: JOREE

Shields/Neutrals
Type: HS
Size: 5/16HS

Tower/Pole
Type: AGC-DP-25
Circuit Number: 1
Structure Name: Jellow Jacket

Tower/Pole Ground Impedance (Ohms)
R = 25.0 X = 0.0

Get From GIS
Line Length (miles): 2.0
Line Span Length (miles): 0.1
Soil Resistivity (Ohm-Meters): 100.0

Bus Name, Side 1: SUB06-7
Circuit Number: 1
Bus Name, Side 2: BUS08

Failure & Repair Rates
Failure Rate (per year): 1.0
Repair Rate (per year): 1.0

☐ Insulated Shields
☐ Transposed Phases
☐ Transposed Shields
☐ Read GPS Coordinates

Operating Voltage (kV): 25.0
Insulation Levels (kV):
FOW (Front of Wave): 100.0
BIL (Basic Insulation Level): 100.0
AC (AC Withstand): 100.0

AGC 25 kV Distribution Pole

40.0 feet

6.0

B1

A1

C1

N1

WebbDoc 7 - Form: 1007, M102 - Copyright © A. R. MacIntyre 1986-2007

Copy Print Help

3-Phase Overhead Transmission Line

DISTRIBUTION LINE BUS 05 TO BUS 07

Accept Cancel

Phase Conductors
Type: ACSR
Size: JOREE

Shields/Neutrals
Type: HS
Size: 5/16HS

Tower/Pole
Type: AGC-DP-13
Circuit Number: 1
Structure Name: Jellow Jacket

Tower/Pole Ground Impedance (Ohms)
R = 25.0 X = 0.0

Get From GIS
Line Length (miles): 3.0
Line Span Length (miles): 0.1
Soil Resistivity (Ohm-Meters): 100.0

Bus Name, Side 1: SUB05-7
Circuit Number: 1
Bus Name, Side 2: BUS07

Failure & Repair Rates
Failure Rate (per year): 1.0
Repair Rate (per year): 1.0

☐ Insulated Shields
☐ Transposed Phases
☐ Transposed Shields
☐ Read GPS Coordinates

Operating Voltage (kV): 13.8
Insulation Levels (kV):
FOW (Front of Wave): 100.0
BIL (Basic Insulation Level): 100.0
AC (AC Withstand): 100.0

AGC 13.8 kV Distribution Pole

38.0 feet

6.0

B1

A1

C1

N1

WebbDoc 7 - Form: 1007, M102 - Copyright © A. R. MacIntyre 1986-2007

Figure 9. Distribution Line Data

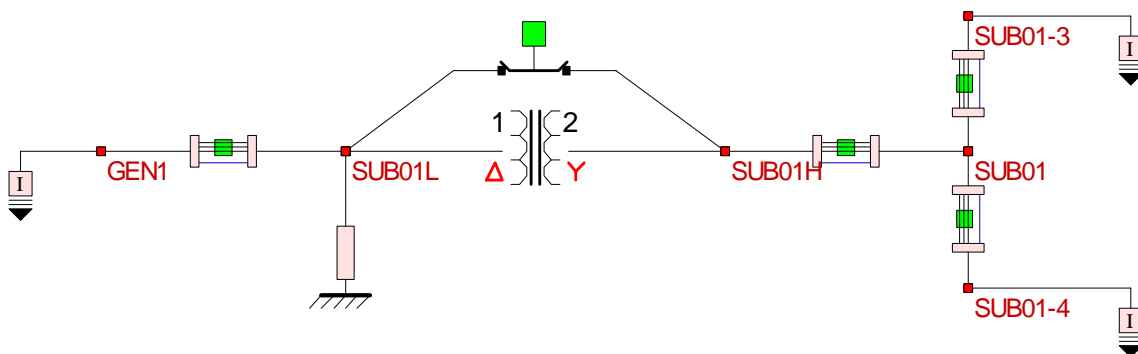
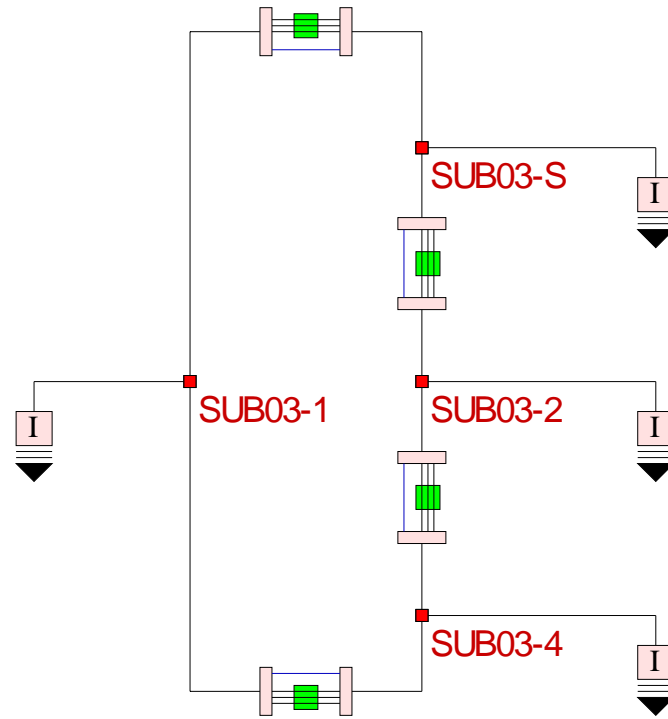
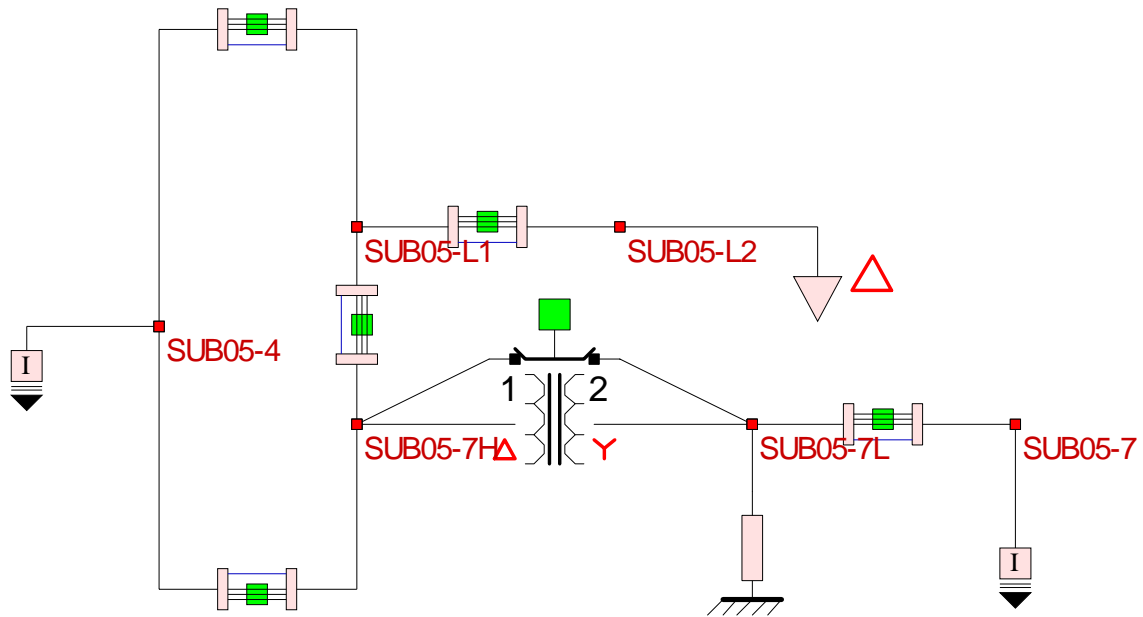


Figure 10. Generating Unit Substation Configuration (Unit 1)



(a)



(b)

Figure 11. Distribution Substation Configuration
(a) Bus 3, (b) Bus 5

3-Phase Transformer Cancel Accept

GEN01 STEP-UP TRANSFORMER

Side 1 Bus

SUB01L

12.0 kV

☒ Delta ☐ Wye

Side 2 Bus

SUB01H

115.0 kV

☐ Delta ☒ Wye

Phase Connection ☒ Standard ☐ Alternate

Transformer Rating (MVA)	100.0	Tap Setting (pu)	1.0
Winding Resistance (pu)	0.01	Minimum (pu)	1.0
Leakage Reactance (pu)	0.1	Maximum (pu)	1.0
Nominal Core Loss (pu)	0.005	Number of Taps	1
Nominal Magnetizing Current (pu)	0.005	Circuit Number	1

3-Phase Transformer Cancel Accept

GEN02 STEP-UP TRANSFORMER

Side 1 Bus

SUB02L

12.0 kV

☒ Delta ☐ Wye

Side 2 Bus

SUB02H

115.0 kV

☐ Delta ☒ Wye

Phase Connection ☒ Standard ☐ Alternate

Transformer Rating (MVA)	100.0	Tap Setting (pu)	1.0
Winding Resistance (pu)	0.01	Minimum (pu)	1.0
Leakage Reactance (pu)	0.1	Maximum (pu)	1.0
Nominal Core Loss (pu)	0.005	Number of Taps	1
Nominal Magnetizing Current (pu)	0.005	Circuit Number	1

Figure 12. Step-up, Three-Phase Transformer Data

3-Phase Transformer Cancel Accept

Transformer BUS06

Side 1 Bus

SUB06-7H

115.0 kV

☒ Delta ☐ Wye

Side 2 Bus

SUB06-7L

25.0 kV

☐ Delta ☒ Wye

Phase Connection ☒ Standard ☐ Alternate

Transformer Rating (MVA)	5.0	Tap Setting (pu)	1.0
Winding Resistance (pu)	0.01	Minimum (pu)	1.0
Leakage Reactance (pu)	0.1	Maximum (pu)	1.0
Nominal Core Loss (pu)	0.005	Number of Taps	1
Nominal Magnetizing Current (pu)	0.005	Circuit Number	1

3-Phase Transformer Cancel Accept

Transformer BUS05

Side 1 Bus

SUB05-7H

115.0 kV

☒ Delta ☐ Wye

Side 2 Bus

SUB05-7L

13.8 kV

☐ Delta ☒ Wye

Phase Connection ☒ Standard ☐ Alternate

Transformer Rating (MVA)	3.0	Tap Setting (pu)	1.0
Winding Resistance (pu)	0.01	Minimum (pu)	1.0
Leakage Reactance (pu)	0.1	Maximum (pu)	1.0
Nominal Core Loss (pu)	0.005	Number of Taps	1
Nominal Magnetizing Current (pu)	0.005	Circuit Number	1

Figure 13. Step-down, Three-Phase Transformer Data

3-Phase Transformer Cancel Accept

Transformer BUS08

Side 1 Bus

BUS08

25.0 kV

☐ Delta ☒ Wye

Side 2 Bus

BUS08-L

0.48 kV

☐ Delta ☒ Wye

Phase Connection ☒ Standard ☐ Alternate

Transformer Rating (MVA)	2.0	Tap Setting (pu)	1.0
Winding Resistance (pu)	0.01	Minimum (pu)	1.0
Leakage Reactance (pu)	0.1	Maximum (pu)	1.0
Nominal Core Loss (pu)	0.005	Number of Taps	1
Nominal Magnetizing Current (pu)	0.005	Circuit Number	1

3-Phase Transformer Cancel Accept

Transformer BUS07

Side 1 Bus

BUS07

13.8 kV

☐ Delta ☒ Wye

Side 2 Bus

BUS07-L

0.48 kV

☐ Delta ☒ Wye

Phase Connection ☒ Standard ☐ Alternate

Transformer Rating (MVA)	1.0	Tap Setting (pu)	1.0
Winding Resistance (pu)	0.01	Minimum (pu)	1.0
Leakage Reactance (pu)	0.1	Maximum (pu)	1.0
Nominal Core Loss (pu)	0.005	Number of Taps	1
Nominal Magnetizing Current (pu)	0.005	Circuit Number	1

Figure 14. Three-Phase Distribution Transformer Data

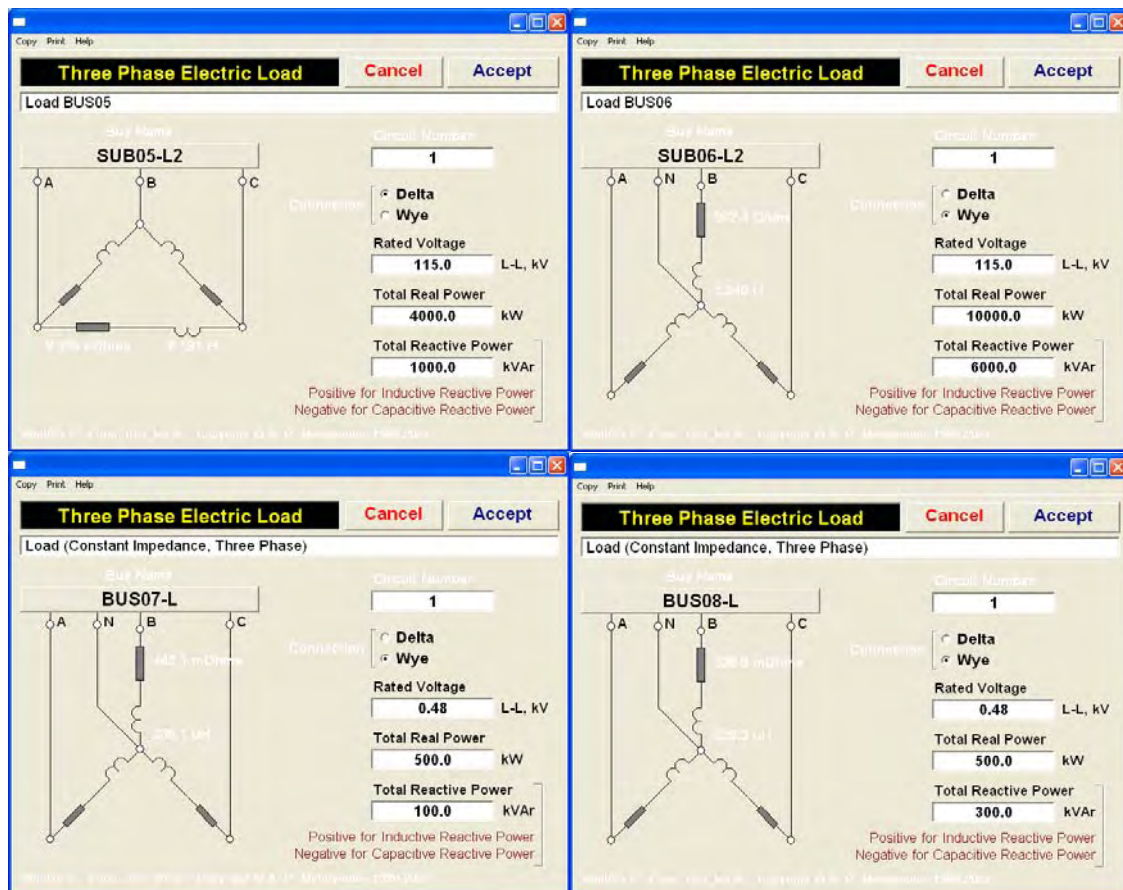


Figure 15. Load Data

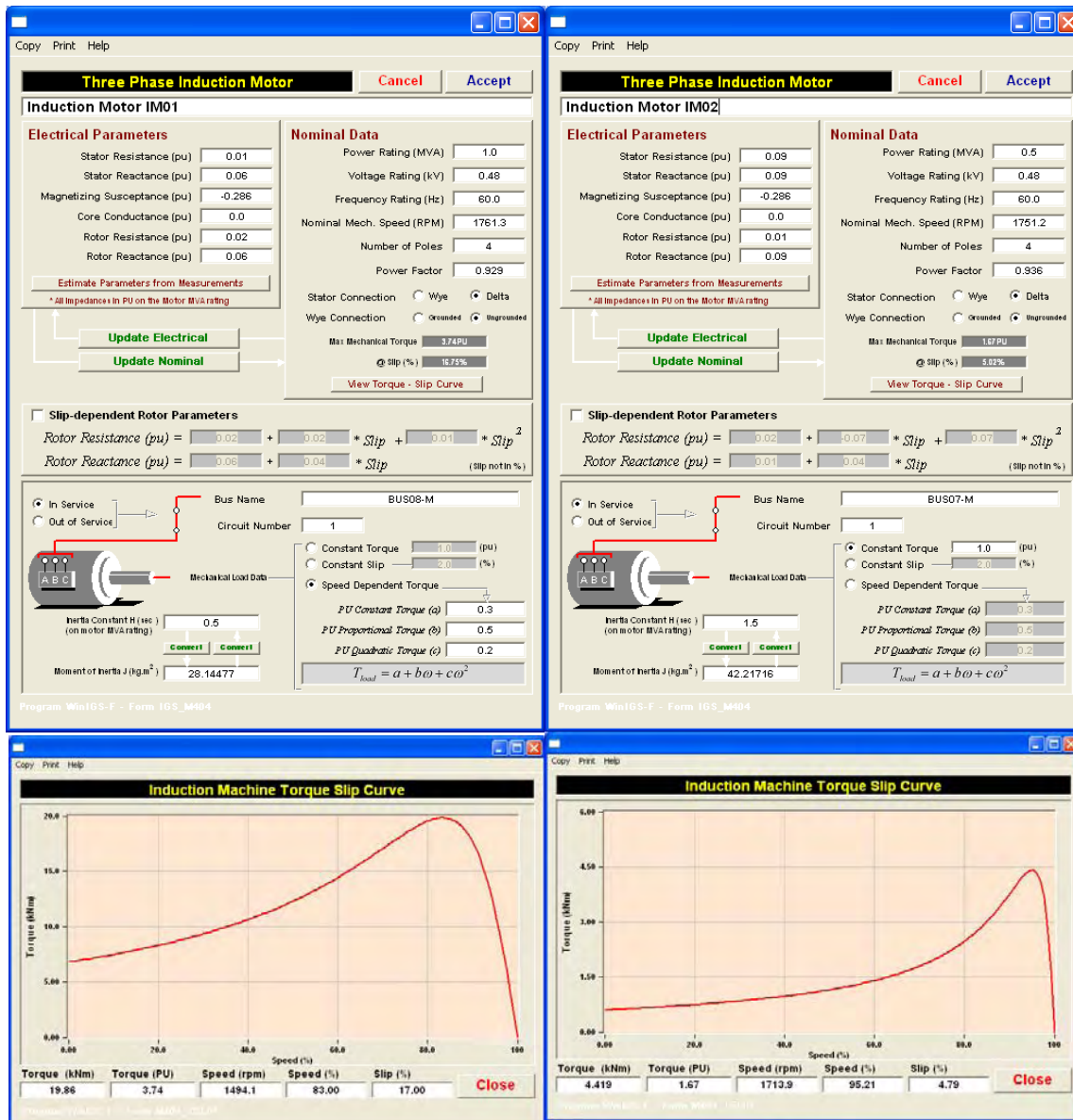


Figure 16. Three-Phase Induction Motor Data


Copy Print Help

Three-Phase Motor Breaker Model Cancel Accept

Three Phase Motor Breaker

Bus 1 Circuit Number Bus 2

BUS08-L **1** **BUS08-M**



Voltage Rating **0.48** kV

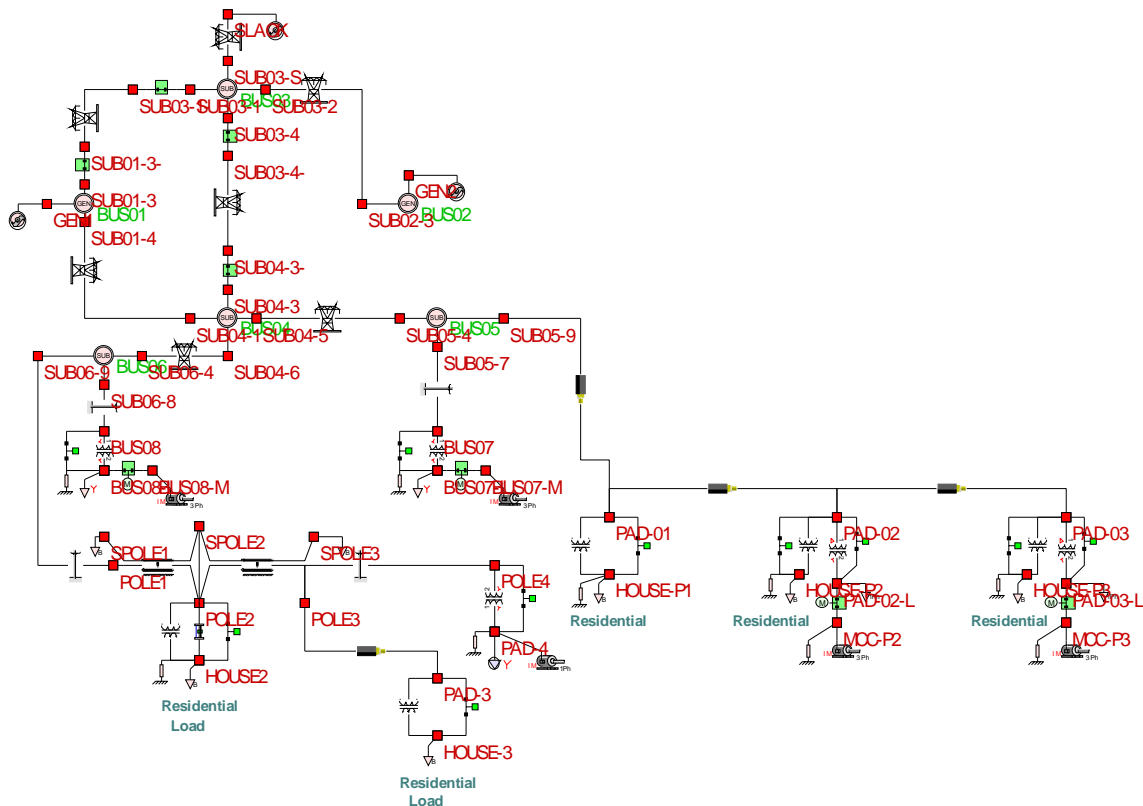
☐ Smooth Opening

Breaker Initial Status

- ☐ Open
 - Closing Criteria
 - Voltage above: p.u.
 - for: seconds
 - Reopening Criteria
 - Voltage below: p.u.
 - for: seconds
- ☒ Closed
 - Opening Criteria
 - Voltage below: p.u.
 - for: seconds
 - Reclosing Criteria
 - Voltage above: p.u.
 - for: seconds

WMS-Q - Form 165_M411 - Copyright © A. P. Mellgren & Co. 1999-2007

Figure 17. Motor Protection Scheme



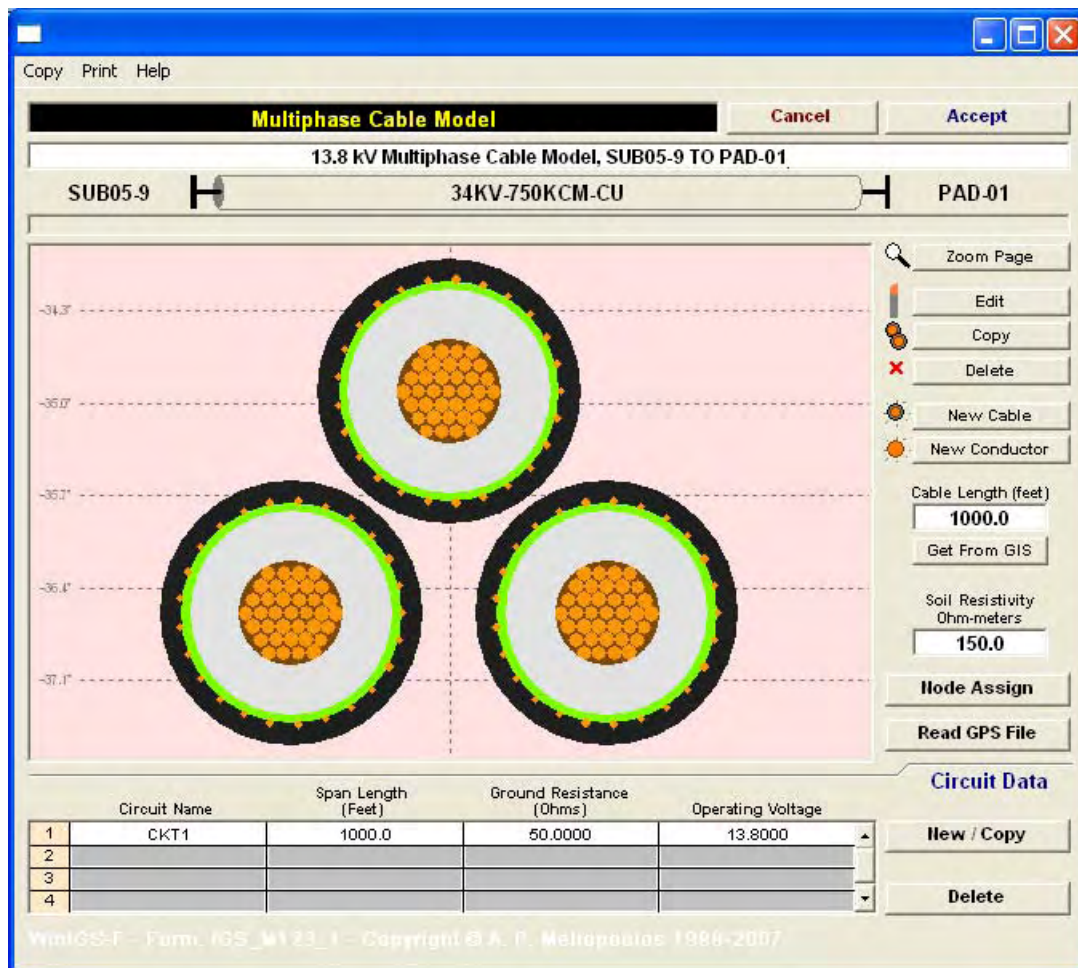


Figure 19. Underground Cable Model

Copy Print Help

Mutually Coupled Multiphase Lines

Distribution Line with secondary 240 V circuit, POLE1 TO POLE2

X Offset (ft):

Conductors								Copy	Edit	Delete
	FromNode	ToNode	Circuit	Cond	Size	Sub	Sep			
1	POLE1_A	POLE2_A	CKT1	AAC	ASTER	1	0			
2	POLE1_B	POLE2_B	CKT1	AAC	ASTER	1	0			
3	POLE1_C	POLE2_C	CKT1	AAC	ASTER	1	0			
4	POLE1_N	POLE2_N	CKT1	AAC	PANSY	1	0			
5	SPOLE1_L1	SPOLE2_L1	CKT2	COPPER	1/0	1	0			
6	SPOLE1_L2	SPOLE2_L2	CKT2	COPPER	1/0	1	0			
7	SPOLE1_NN	SPOLE2_NN	CKT2	COPPER	1/0	1	0			

Circuits										Copy	Edit	Delete
	Name	Span	Gr-R	Gr-X	OpV(kV)	FOW(kV)	BIL(kV)	AC(kV)	rPI			
1	CKT1	0.05	25.0	0.0	25.0	1450.0	1135.0	525.0	1.0			
2	CKT2	0.05	25.0	0.0	0.24	1.2	1.0	0.55	1.0			

Line Length (miles)
 Soil Resistivity (ohm-meters)
 Circuit Number

WinIGS-E - Form: IGS_M109 - Copyright © A. P. Meliopoulos 1988-2007

Figure 20. Mutually Coupled Distribution Line

Copy Print Help

Single Phase Transformer/Centertapped Secondary Accept

Title Transformer with Secondary Centertap (Single Phase) Cancel

Transformer Rating (kVA)	37.5
Side 1 kV Rating	7.96
Side 2 kV Rating	0.24
Series Resistance (pu)	0.005
Series Reactance (pu)	0.035

Side 1	Terminal Names	Side 2
PAD-01_B		HOUSE-P1_L1
		HOUSE-P1_NN
PAD-01_N		HOUSE-P1_L2

1
Circuit Number

Figure 21. Single-Phase Pole Transformer with Center-tapped Secondary

Copy Print Help

Balanced Load at Secondary Bus

Cancel

Accept

Load (Constant Impedance, Secondary Bus, Balanced)

Secondary Bus Name

HOUSE-P1/S

Circuit Number

1

L1

NN

L2

R = 864.0 mOhms

L = 763.9 uH

Rated Voltage (L1 to L2)

0.240

kV

Total Real Power

30.0

kW

Total Reactive Power *

10.0

KVAR

* Positive for Inductive, Negative for Capacitive Reactive Power

Figure 22. Secondary Bus Load

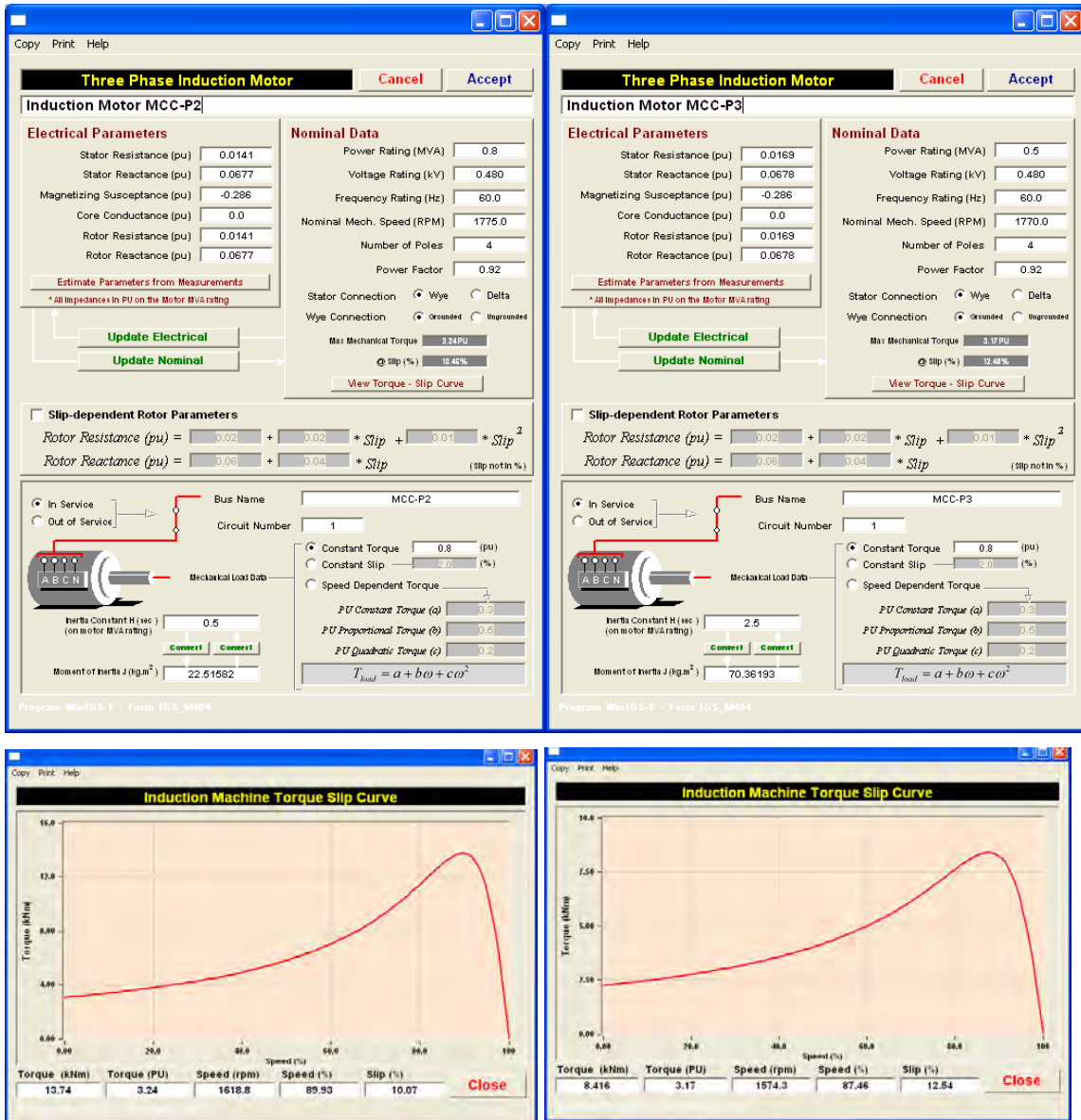


Figure 24. Additional Three-Phase Induction Motor Data

4.2 Simulation of Voltage Recovery

Results with the proposed methodology applied to the two test systems are presented in this section.

4.2.1 Test System 1 – Transmission System

The steady-state operating conditions of the two induction motors are shown in Figures 29 and 30. The system operates under steady state conditions when a three phase fault occurs on the transmission line between buses 3 and 4, very close to bus 4. The fault is cleared by the protection system after 200 ms (12 cycles) by opening the two circuit breakers at the two ends of the line and removing the faulted line. The system response during the pre-fault, fault and post-fault periods, for a total time of two seconds is shown in Figures 31 through 34. Figure 31 shows the response of each generating unit in terms of frequency, angle and power output. Figure 32 illustrates the behavior of the induction motor loads in terms of terminal voltage, speed, current and absorbed power. The important issue in the system behavior is the slow voltage recovery at the terminals of the second induction motor. While the system, as a whole, remains stable and the voltage recovers quickly at the terminals of the first motor, the voltage in fact never recovers to an acceptable value at the terminals of the second motor and this leads to the motor slowdown and eventually stalling. The transmission system response is illustrated in Figure 33 in terms of bus voltages and line currents for all the transmission buses and lines. Figure 33 illustrates the fact that the currents on the lines SLACK-BUS03, BUS01-BUS03, and BUS02-BUS03 remain much higher than the steady-state loading values for the whole transient period, even after the fault is cleared. In particular, the loading of all the system lines at steady-state ranges from 20 up to 60 Amps. The currents of the three lines mentioned above are 31, 14 and 22 Amps respectively. During the transient phase these currents reach values up to 567, 507, and 230 Amps respectively, i.e. 10 to 35 times their steady-state value. Such high values, above 300 Amps may last for 50 to 100 ms and can possibly trigger overcurrent relay settings for line protection.

When a motor protection scheme is applied to the motors, that disconnects the motor when the terminal voltage drops below 0.80 pu for more than 25 cycles of the fundamental, the second motor is disconnected from the at about 0.2 seconds after the fault is cleared and the rest of the system recovers again to an acceptable operating state, as illustrated in Figure 34. Notice that in this case the voltage at the bus where motor 2 is connected recovers to a value close to 0.9 p.u. This means that disconnection of the motor has a beneficial effect of the rest of the loads connected to the same bus.

Finally, Figures 35 through Figures 36 show the impedance trajectory as seen by one of the two impedance relays protecting each transmission line of the system. The relay settings are also shown in the figures. Notice that except for the relay at the BUS03-side of the faulted line, which trips, the relays of the lines connecting the equivalent rest of the system (slack bus) and generating unit one also trigger the second protection zone, but do not trip eventually. However, this depends significantly on the delay settings of each relay and the situation could have been different if the settings were different.

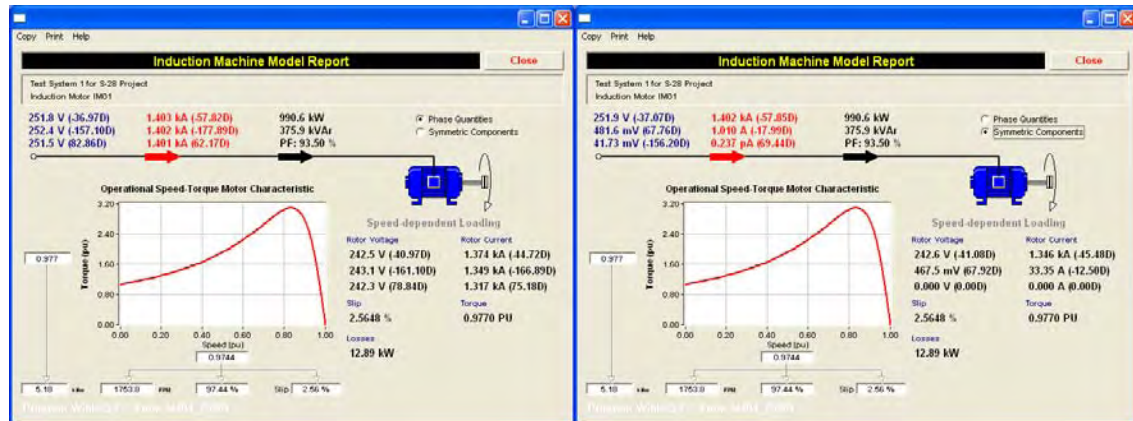


Figure 25. Steady-State Analysis Results for Induction Motor 1

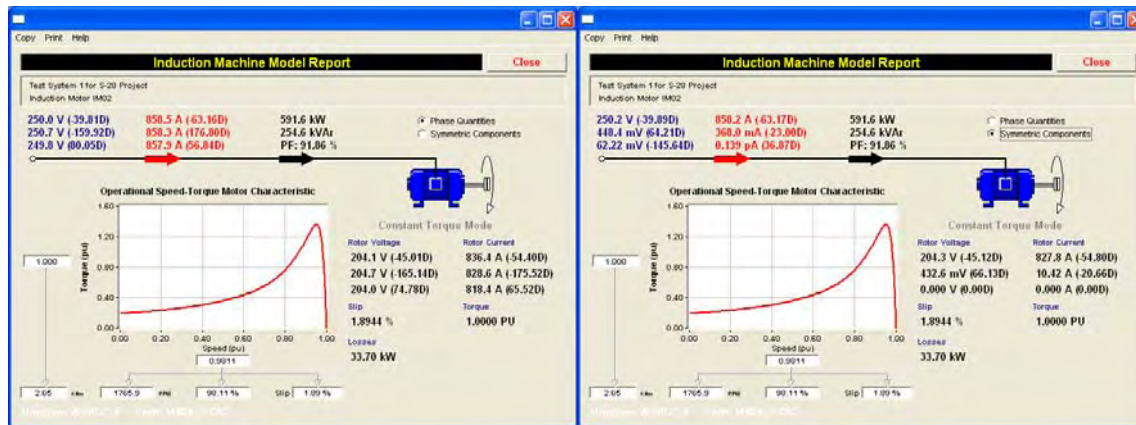


Figure 26. Steady-State Analysis Results for Induction Motor 2

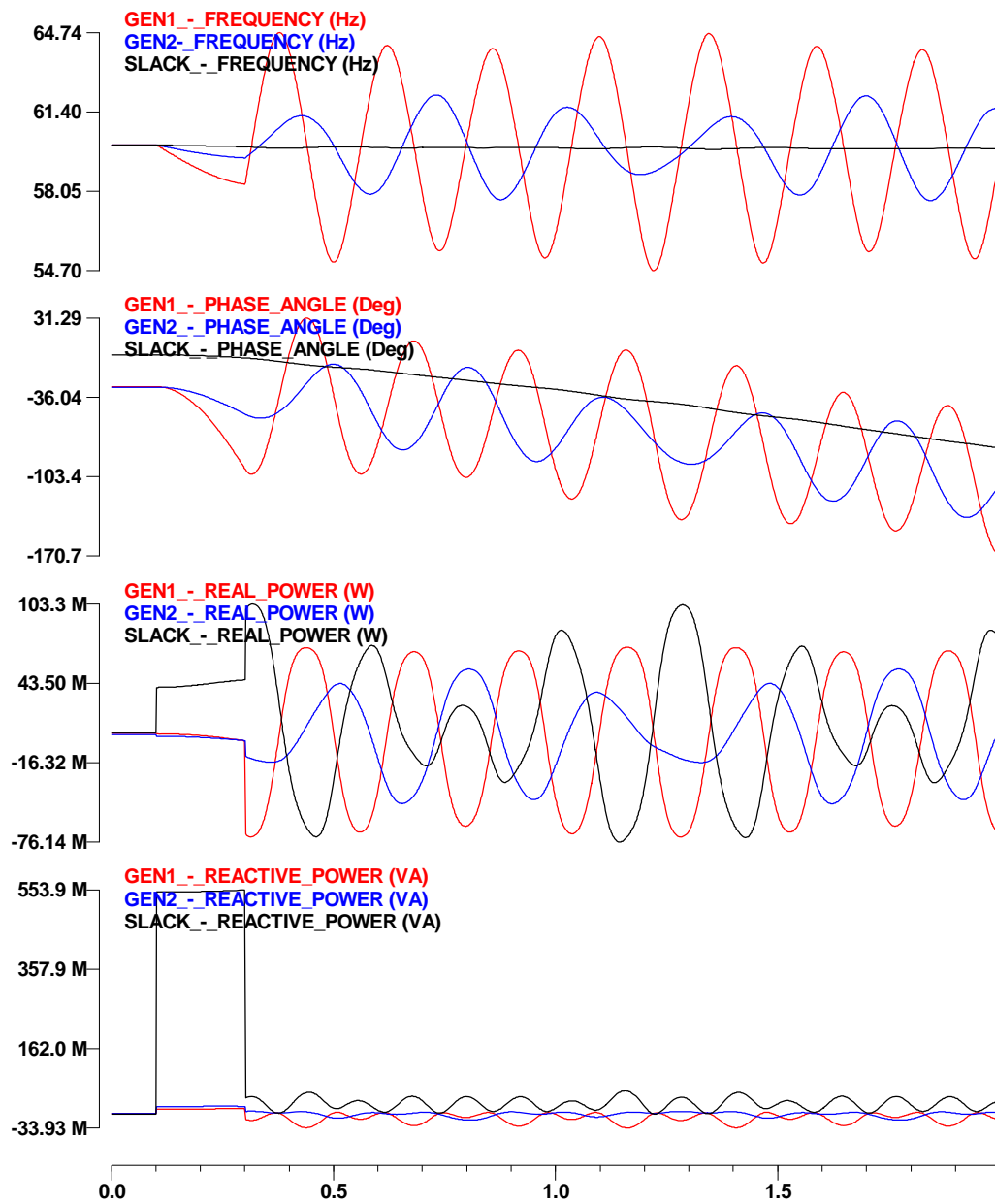


Figure 27. Generating Unit Response after a Three-Phase Fault

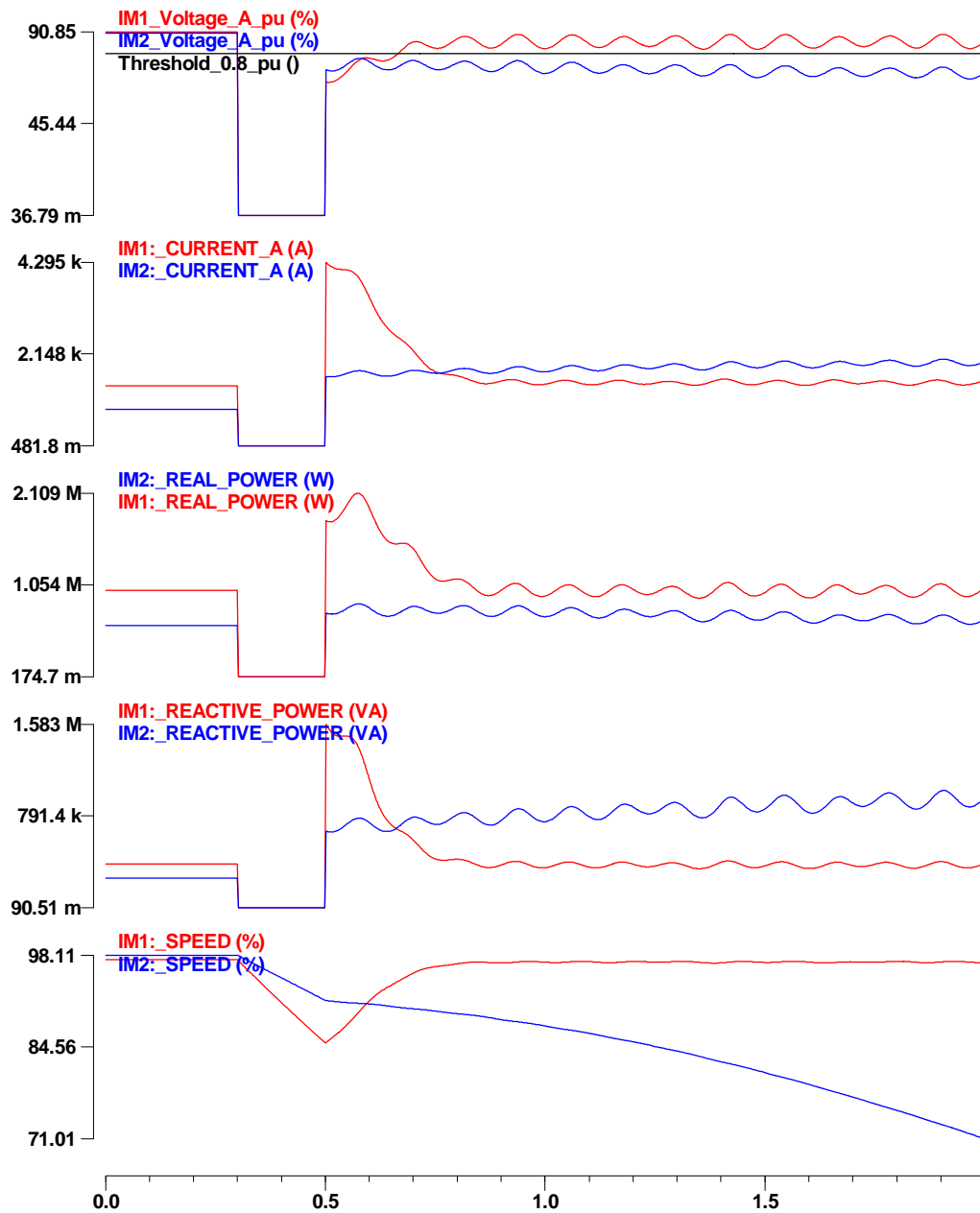


Figure 28. Induction Motor Response after a Three-Phase Fault

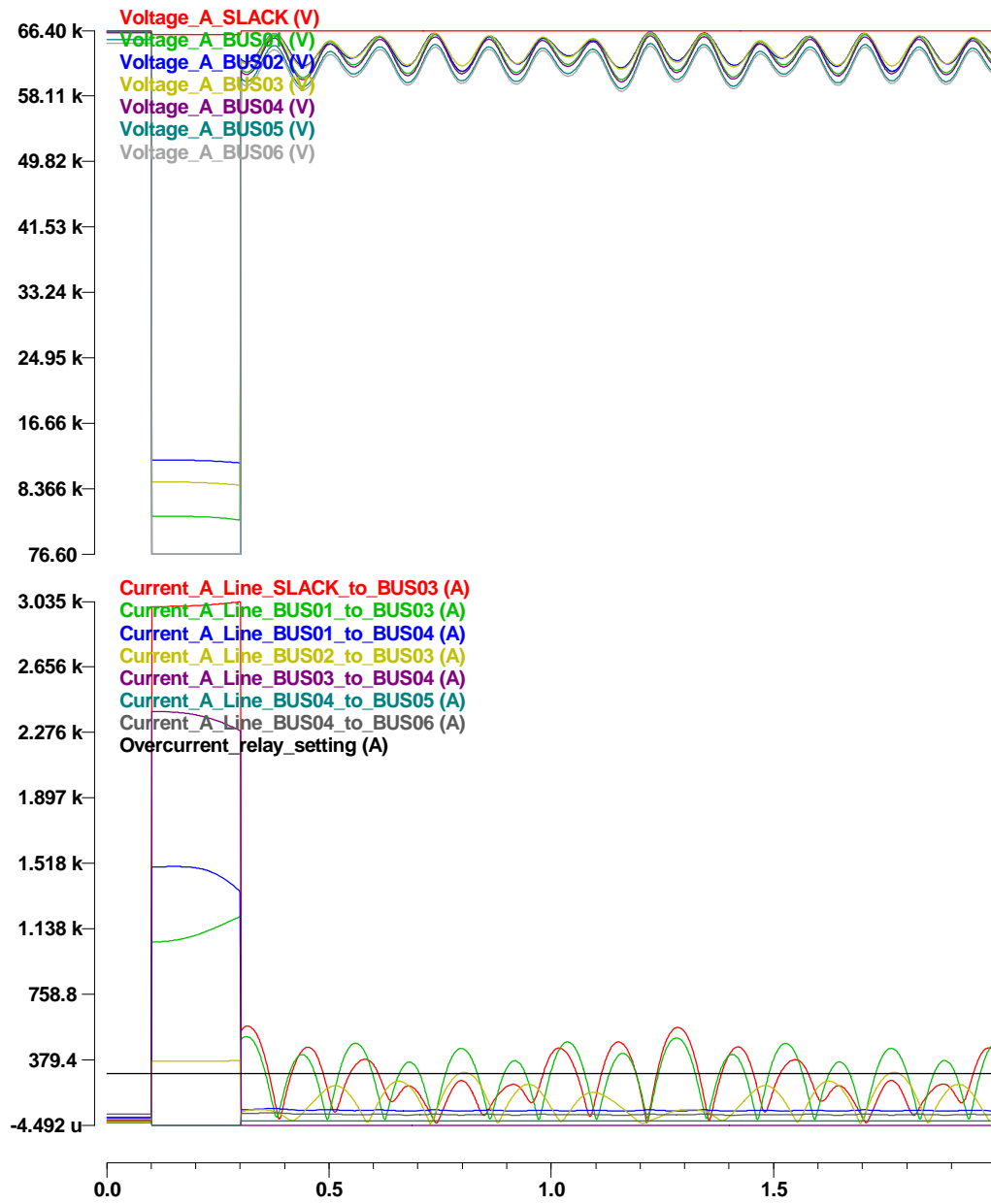


Figure 29. Transmission System Response after a Three-Phase Fault

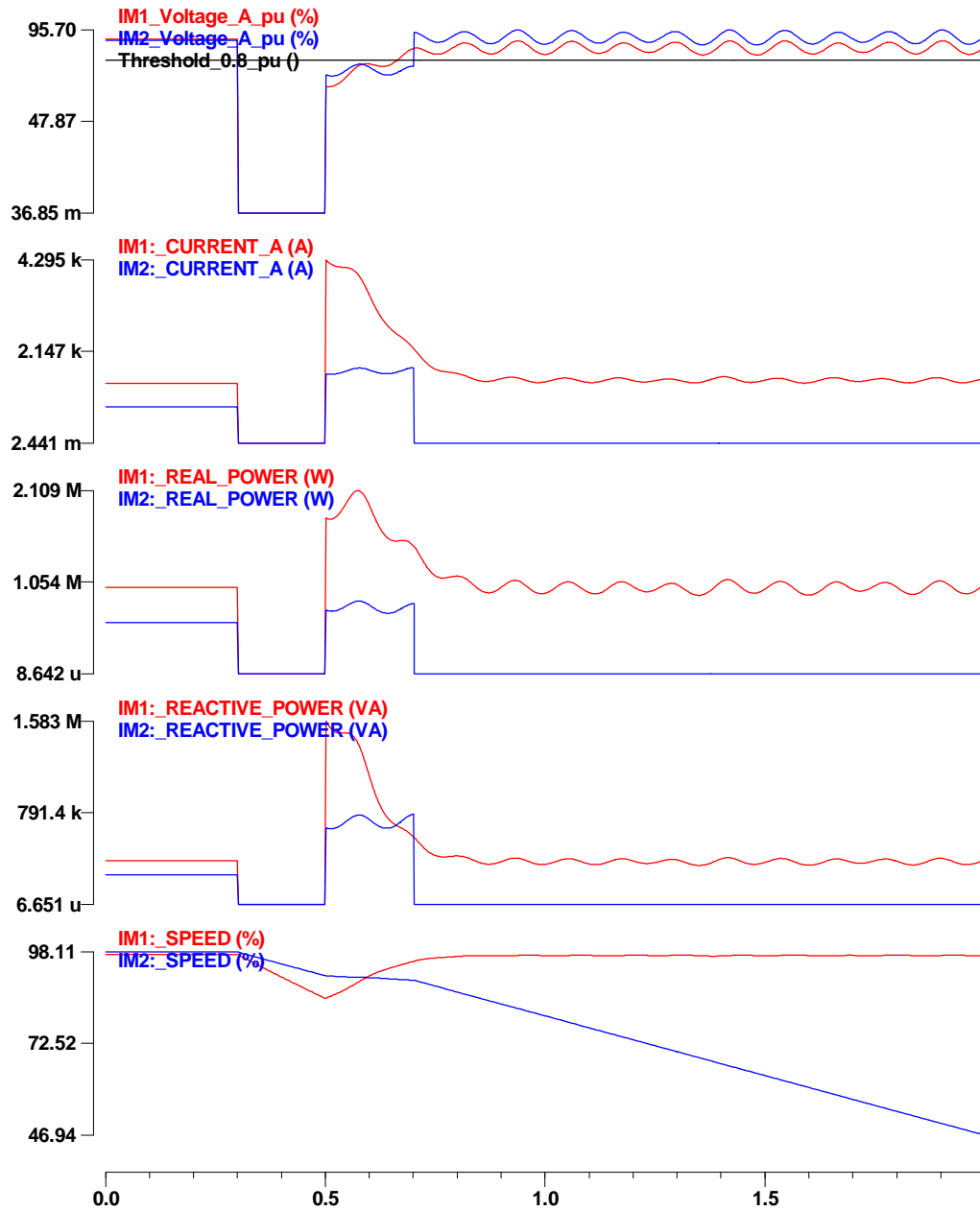


Figure 30. Induction Motor Response after a Three-Phase Fault with Motor Disconnection

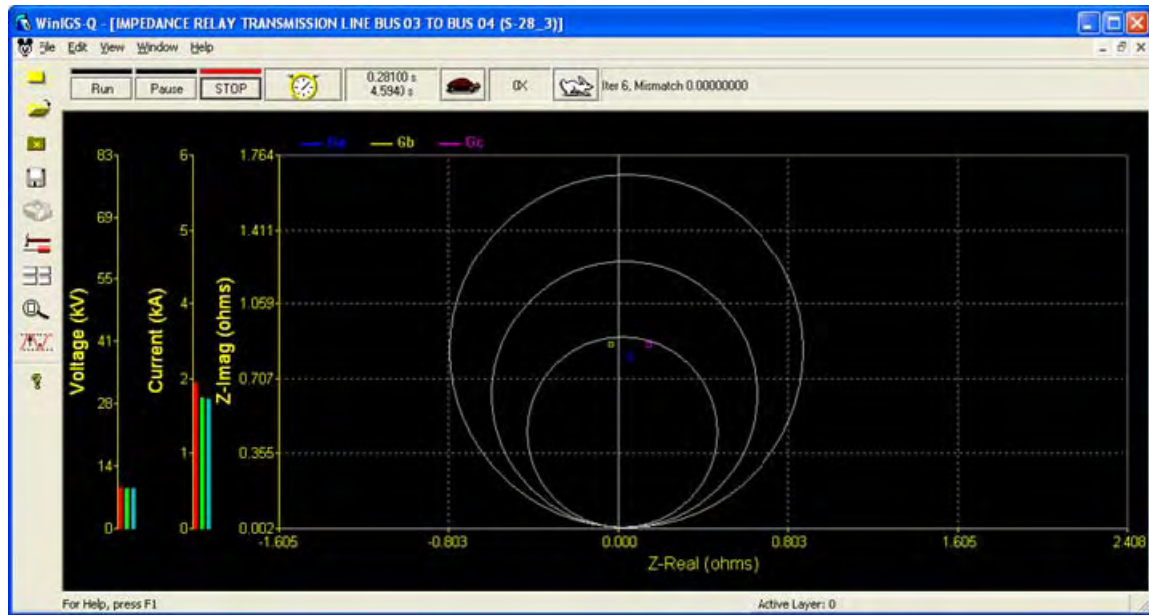


Figure 31. Impedance Trajectory and Relay Settings of BUS03-side Relay of Line BUS03-BUS04 (faulted line)



Figure 32. Impedance Trajectory and Relay Settings of SLACK-side Relay of Line SLACK-BUS04

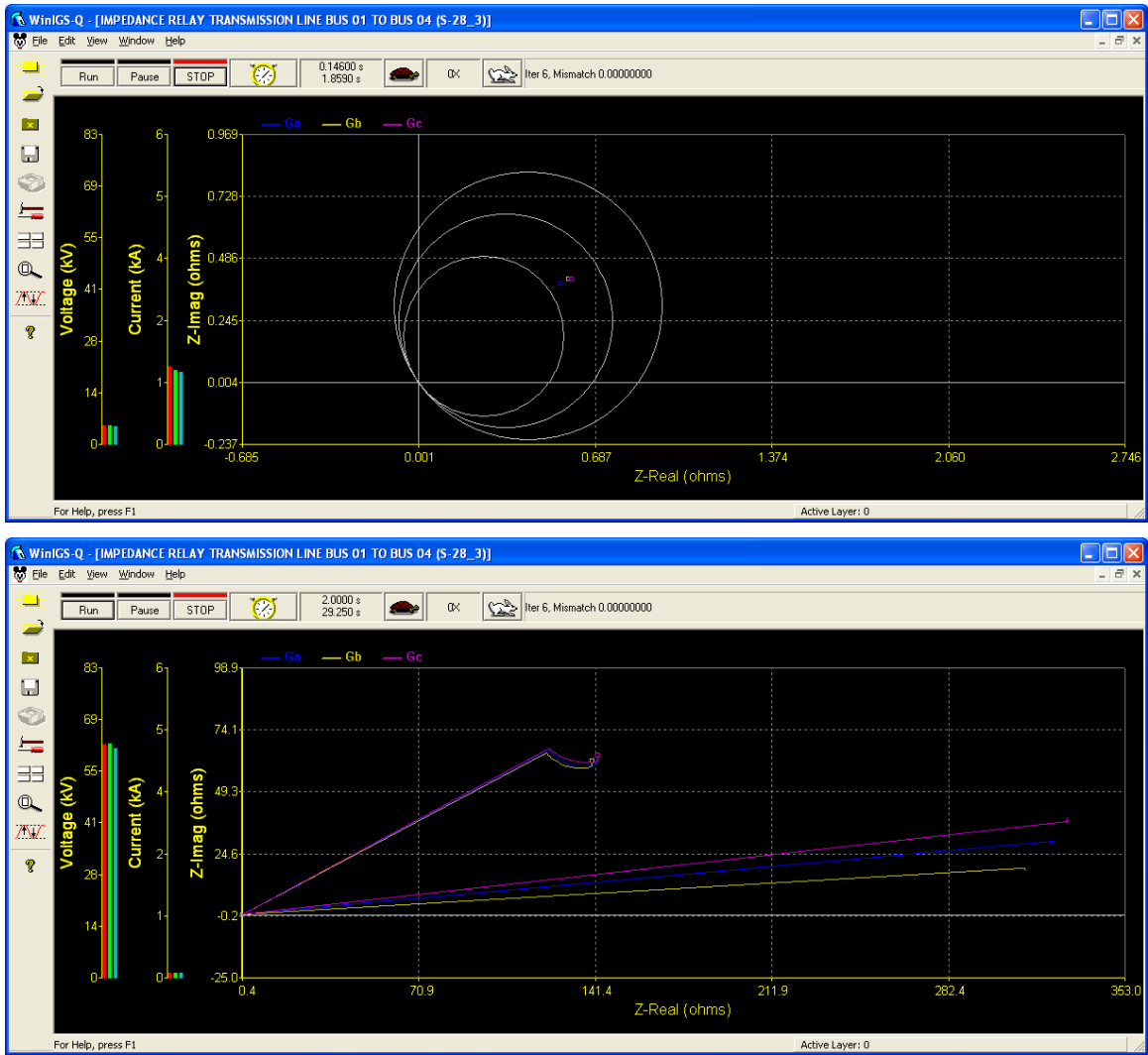


Figure 33. Impedance Trajectory and Relay Settings of BUS01-side Relay of Line BUS01-BUS04



Figure 34. Impedance Trajectory and Relay Settings of BUS02-side Relay of Line BUS02-BUS03

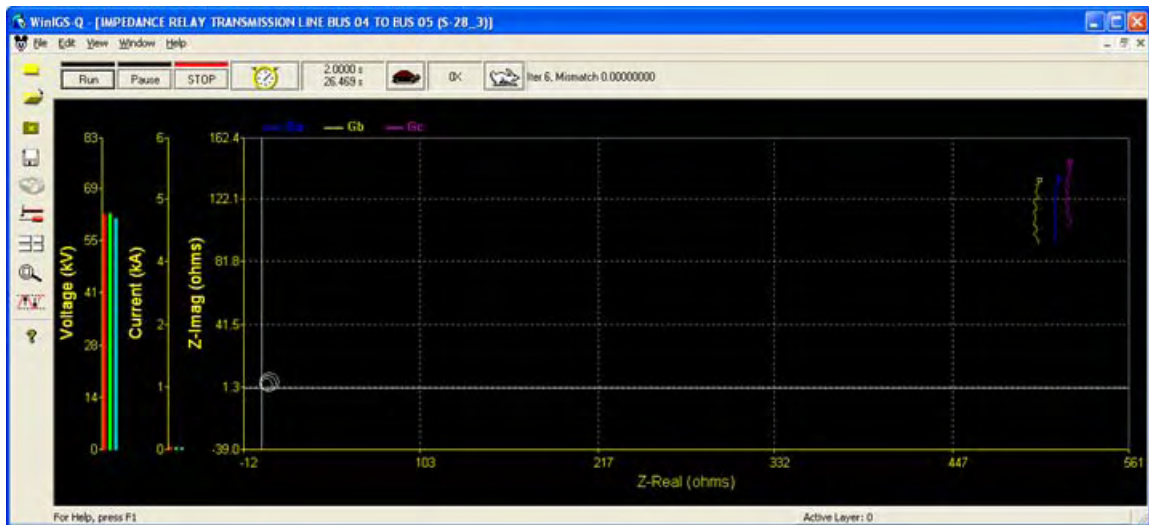


Figure 35. Impedance Trajectory and Relay Settings of BUS04-side Relay of Line BUS04-BUS05



Figure 36. Impedance Trajectory and Relay Settings of BUS04-side Relay of Line BUS04-BUS06

4.2.2 Test System 2 – Distribution System

The steady-state operating conditions of the five induction motors are shown in Figures 41 through 50.

The system operates under steady state conditions when a three phase fault occurs on the transmission line between buses 3 and 4, very close to bus 4. The fault is cleared by the protection system after 200 ms (12 cycles) by opening the two circuit breakers at the two ends of the line and removing the faulted line. The system response during the pre-fault, fault and post-fault periods, for a total time of one second is shown in Figures 46 through 50.

Figure 46 shows the response of each generating unit in terms of frequency, angle and power output. Figure 47 illustrates the behavior of the induction motor loads in terms of terminal voltage, speed, current and absorbed power. The important issue in the system behavior is the slow voltage recovery at the terminals of the second induction motor. While the system, as a whole, remains stable and the voltage recovers quickly at the terminals of motors MCC-P3, PAD-4, and BUS08-M, the voltage in fact never recovers to an acceptable value at the terminals of the motors BUS07-M and MCC-P2 and this leads to the motors' slowdown and eventually stalling. When a motor protection scheme is applied to the motors, that disconnects the motor when the terminal voltage drops below 0.80 pu for more than 25 and 30 cycles of the fundamental for the two stalling motors respectively, motors BUS07-M and MCC-P2 get disconnected from the network at about 0.6 and 0.8 seconds after the fault is cleared and the rest of the system recovers again to an acceptable operating state with voltages way above 0.8 p.u., as illustrated in Figure 47. Finally, Figures 48 through 50 illustrate the imbalances that exist among the three system phases, due to the system asymmetries and the existence of single-phase loads. Notice there is a significant voltage imbalance on phase B, compared to the other two phases, at the induction motor voltage, while there is significant imbalance of phase A at the feeder currents.

The behavior of the single-phase induction motor is similar to the one of the three-phase motors, however, since this motor is smaller and has smaller inertia constant is decelerates faster, reaching a much slower speed, but it also accelerates much faster when the fault is cleared and thus does not significantly affect the recovery process.

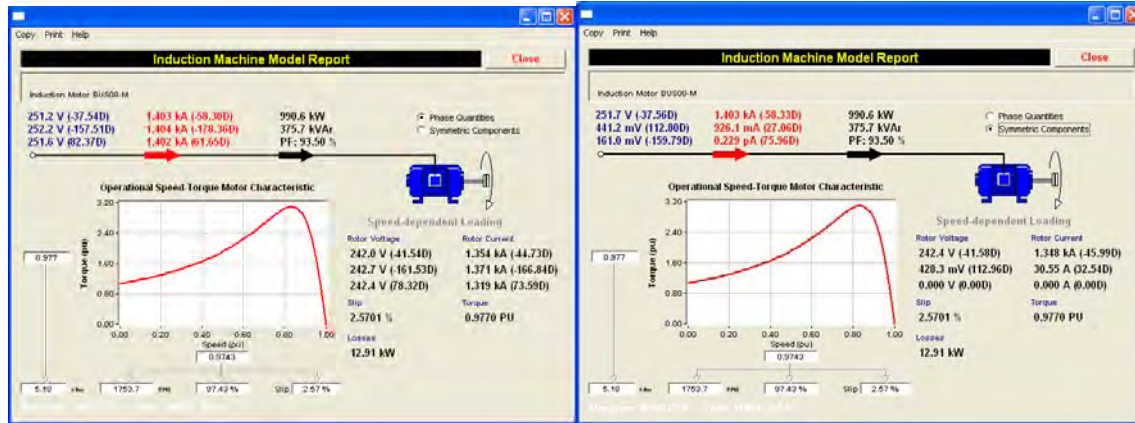


Figure 37. Steady-State Analysis Results for Induction Motor BUS08-M

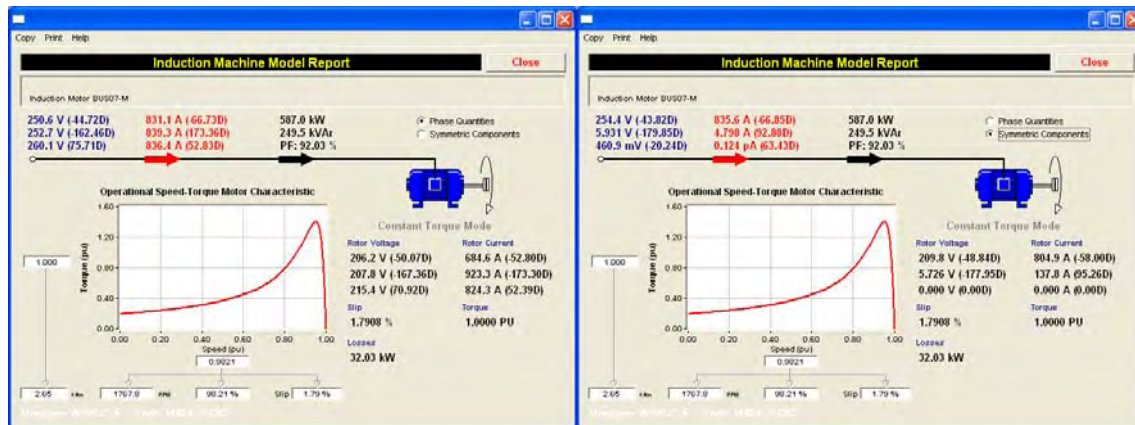


Figure 38. Steady-State Analysis Results for Induction Motor BUS07-M

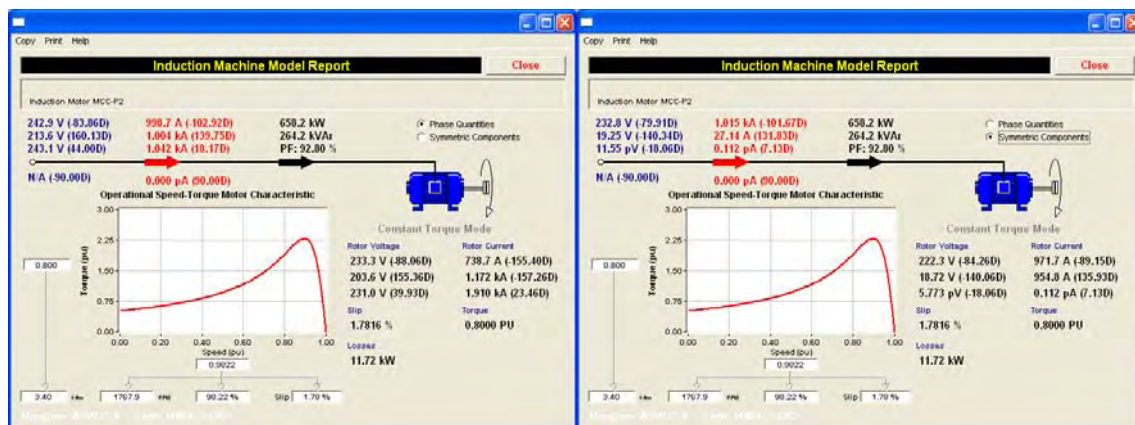


Figure 39. Steady-State Analysis Results for Induction Motor MCC-P2

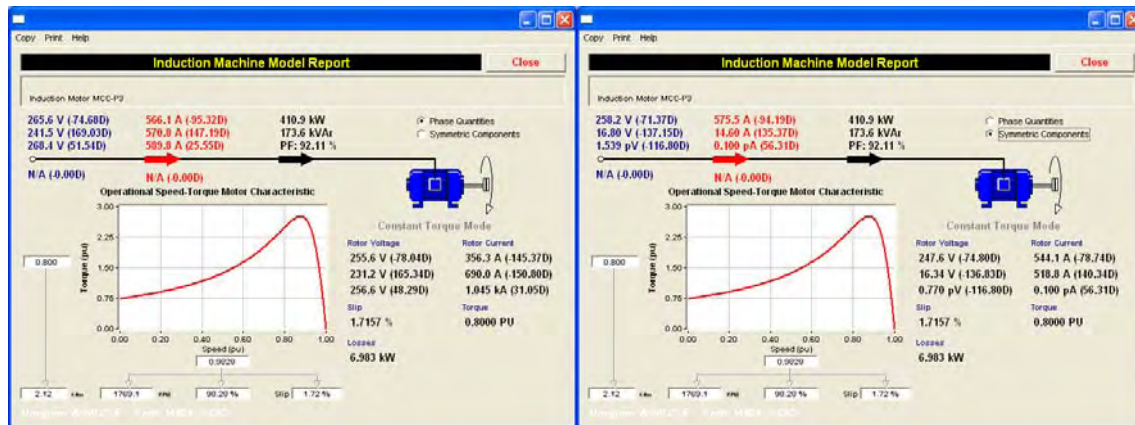


Figure 40. Steady-State Analysis Results for Induction Motor MCC-P3

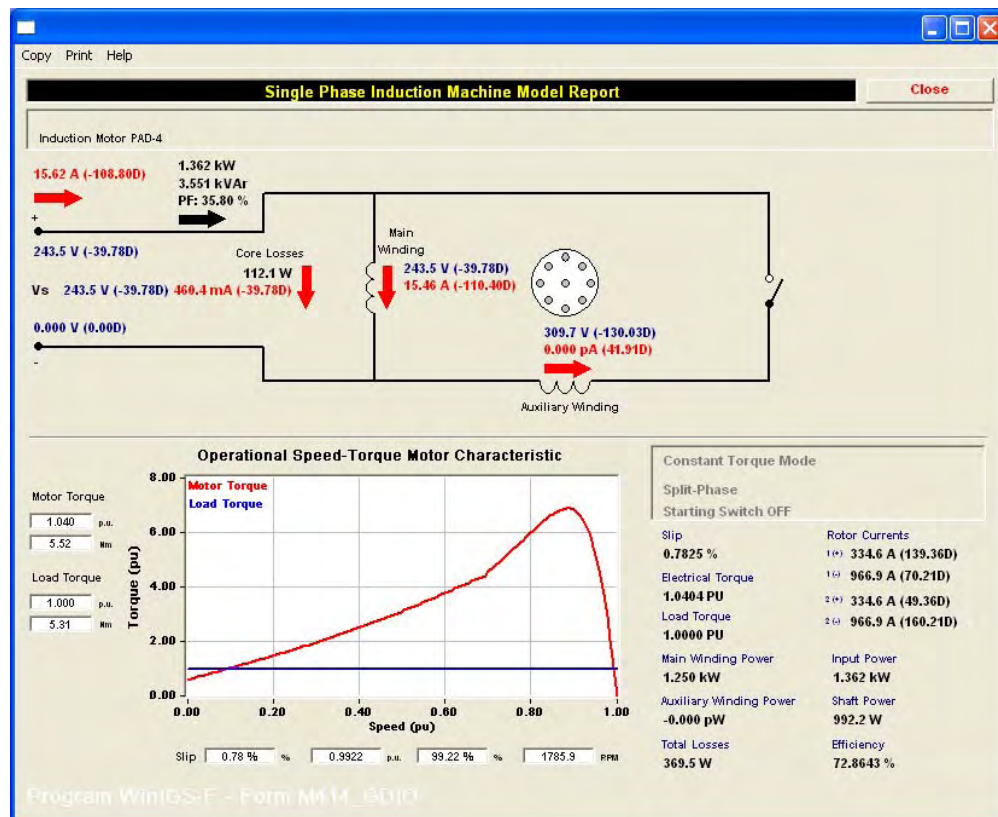


Figure 41. Steady-State Analysis Results for Induction Motor PAD-4

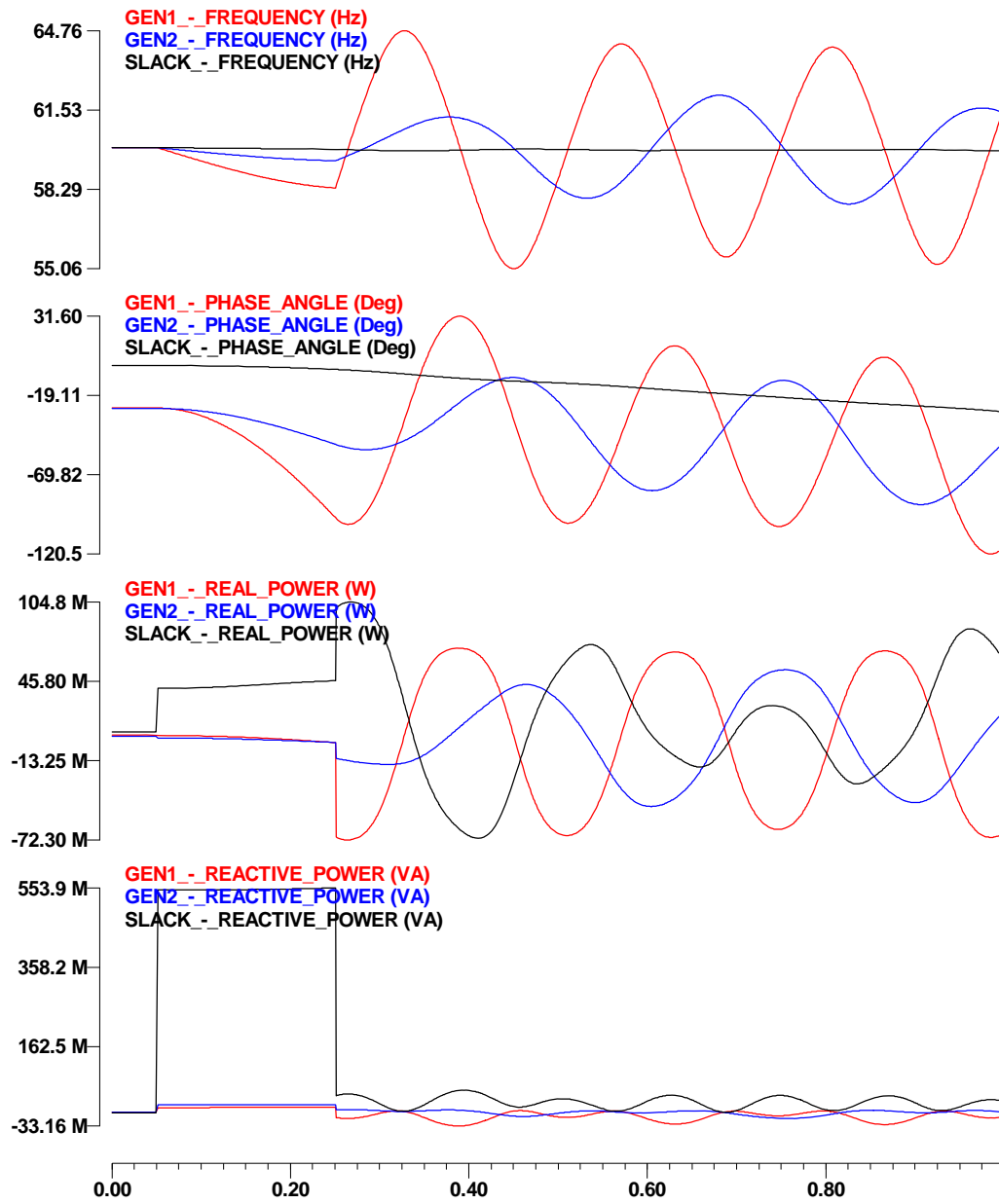


Figure 42. Generating Unit Response after a Three-Phase Fault

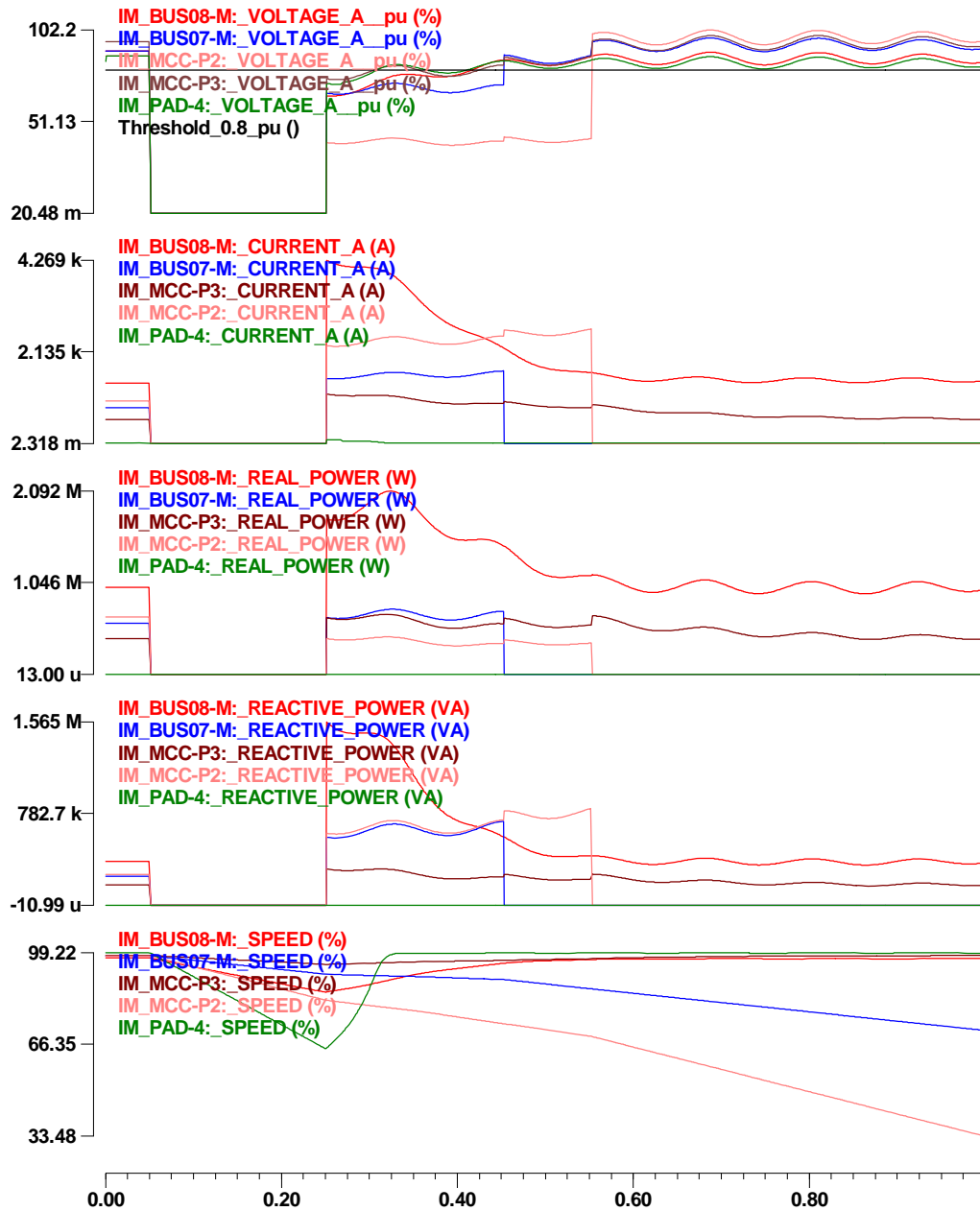


Figure 43. Induction Motor Response after a Three-Phase Fault

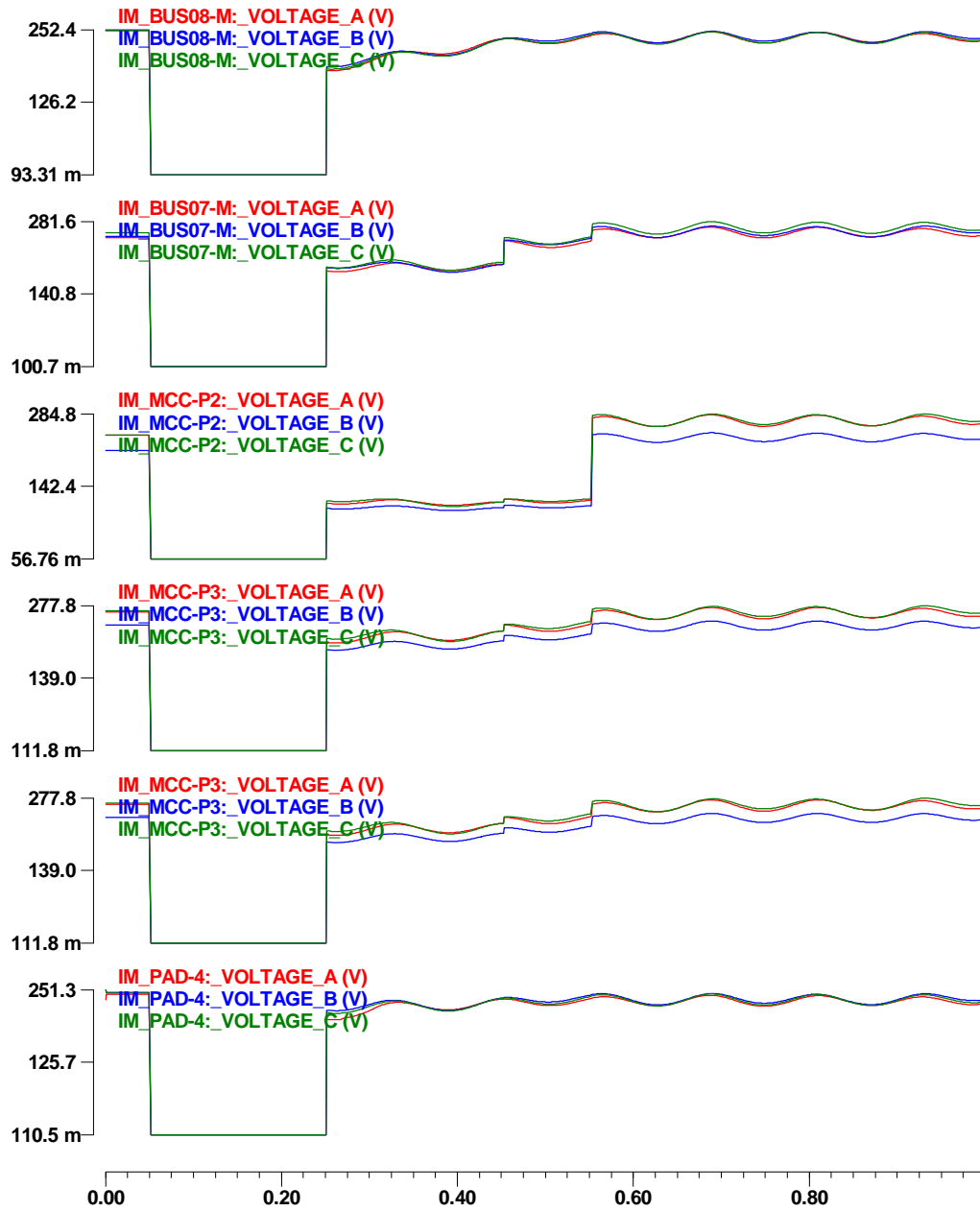


Figure 44. Terminal Voltages of Induction Motors at All Three Phases

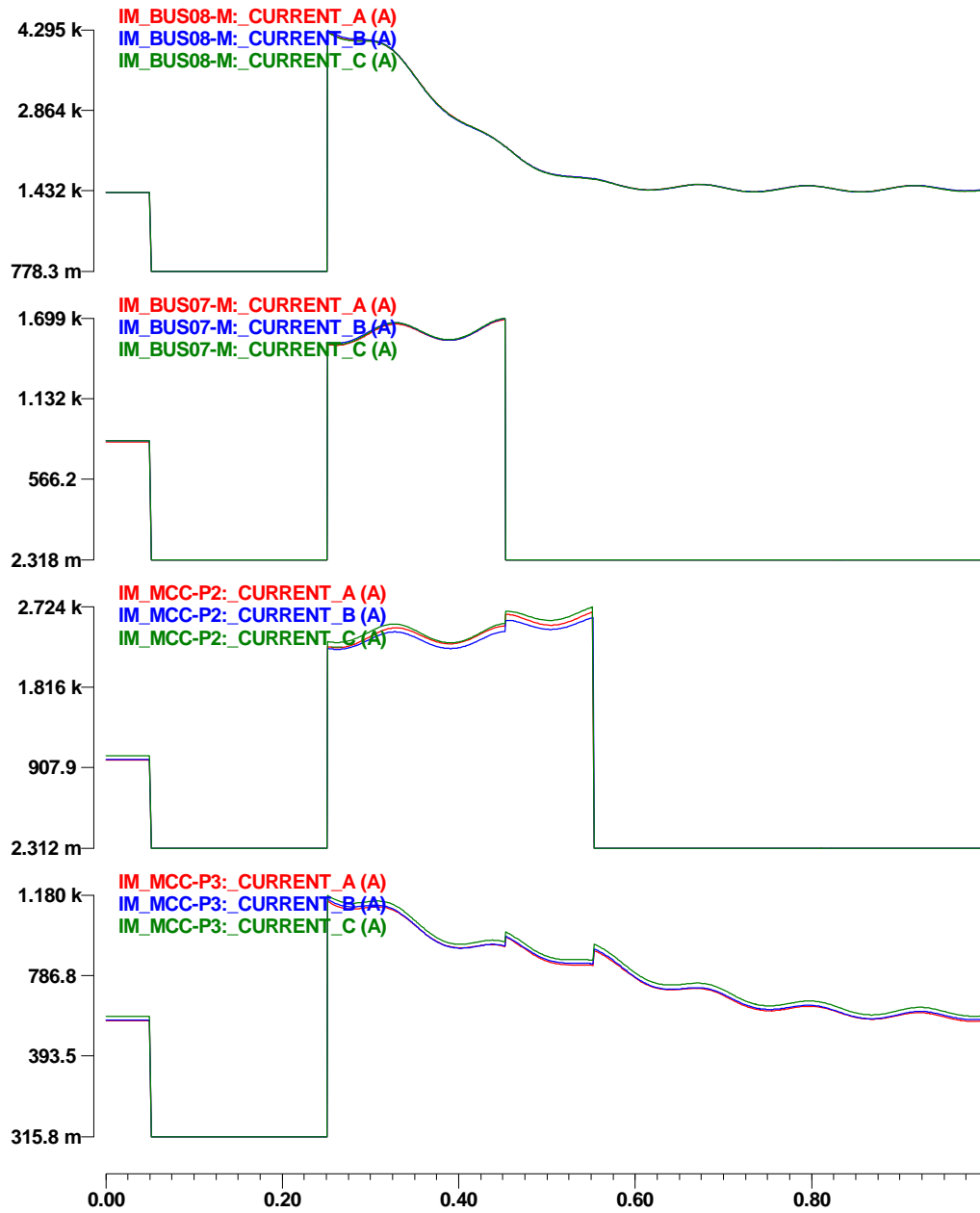


Figure 45. Current Absorption of Induction Motors at All Three Phases

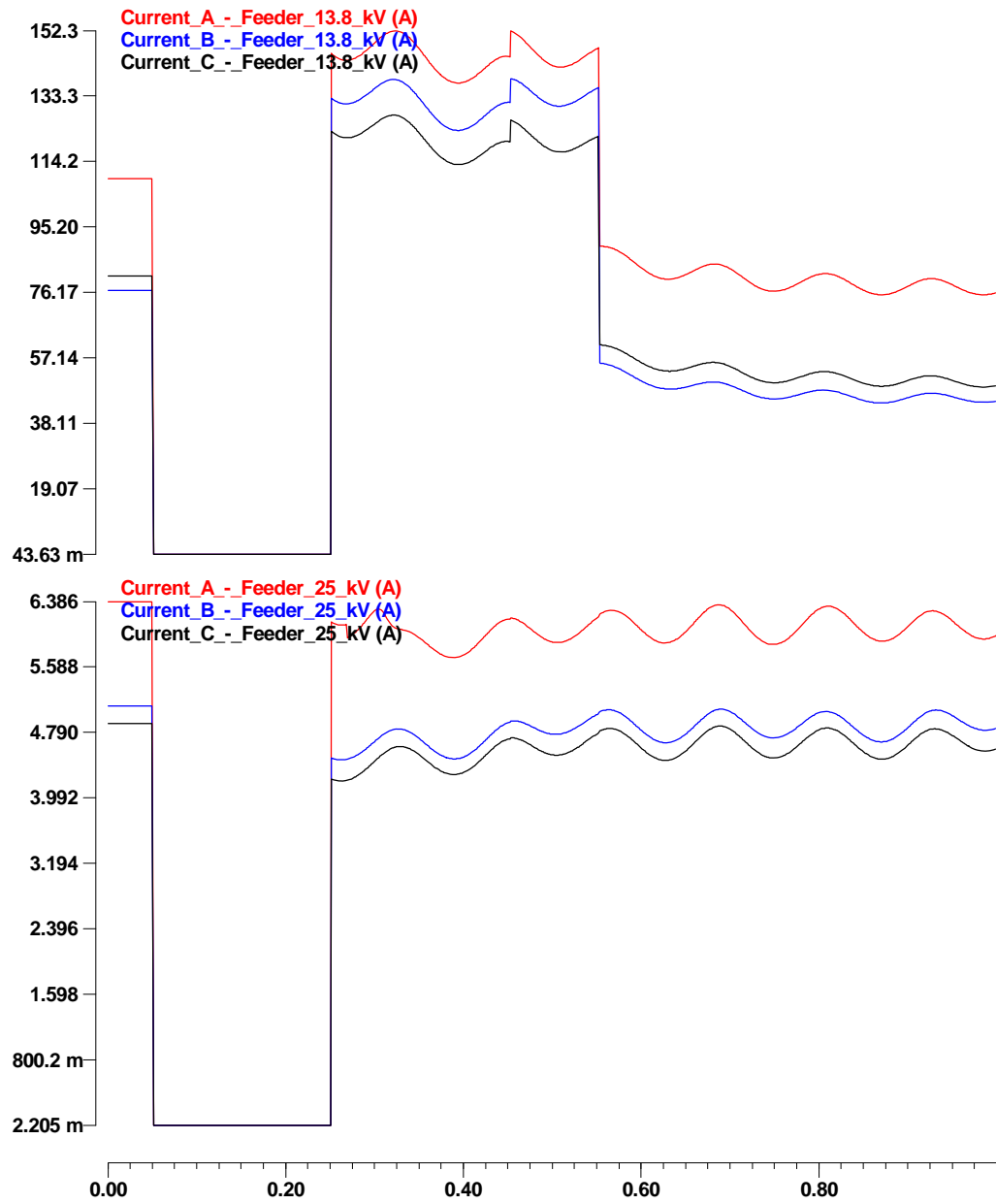


Figure 46. Current Absorption of Feeder Sections at All Three Phases

4.3 Summary

The simulation results clearly illustrate that voltage instabilities during recovery from disturbances can cause excessive current flow that may affect the operation of overcurrent relays as well as the impedance seen by distance relays. Distance relays are especially vulnerable since these phenomena exhibit simultaneously low voltage and high current creating the possibility of load encroachment.

The results presented in this section are preliminary. It is clear that they are dependent upon the specific parameters of the circuits involved and the type and magnitude of dynamic loads. Therefore it is difficult to develop general guidelines for predicting the level and impact of these phenomena. For this reason it is suggested that the proper way to apply the proposed methodology is to study specific systems that are heavily loaded with motor type loads.

References

- [1] M. H. J. Bollen, "Voltage recovery after unbalanced and balanced voltage dips in three-phase systems," *IEEE Trans. on Power Systems*, vol. 18, issue 4, Oct. 2003, pp. 1376-1381.
- [2] B. R. Williams, W. R. Schmus and D. C. Dawson, "Transmission voltage recovery delayed by stalled air conditioner compressors," *IEEE Trans. on Power Systems*, vol. 7, no. 3, Aug. 1992, pp. 1173-1181.
- [3] L. Y. Taylor, and S. -M. Hsu, "Transmission voltage recovery following a fault event in the Metro Atlanta area," *Proceedings of the 2000 IEEE-PES Summer Meeting*, July 16-20, 2000, pp. 537-542.
- [4] T. Sun, Z. Chen and F. Blaabjerg, "Voltage recovery of grid-connected wind turbines after a short-circuit fault," *Proceedings of the 29th Annual Conference of the IEEE Industrial Electronics Society (IECON '03)*, vol. 3, Nov. 2-6, 2003, pp. 2723-2728.
- [5] T. Sun, Z. Chen and F. Blaabjerg, "Voltage recovery of grid-connected wind turbines with DFIG after a short-circuit fault," *Proceedings of the 35th Annual IEEE Power Electronics Specialists Conference (PESC '04)*, vol. 3, June 20-25, 2004, pp. 1991-1997.
- [6] L. Haijun and H. W. Renzhen, "Preventing of transient voltage instability due to induction motor loads by static condenser," *Proceedings of the 1994 IEEE Conference on Industrial Technology*, Dec. 5-9, 1994, pp. 827-831.
- [7] A. E. Hammad and M. Z. El-Sadek, "Prevention of transient voltage instabilities due to induction motor loads by static VAR compensators," *IEEE Trans. on Power Systems*, vol. 4, no. 3, Aug. 1989, pp. 1182-1190.
- [8] I.A. Hamzah and J. A. Yasin, "Static VAR compensators (SVC) required to solve the problem of delayed voltage recovery following faults in the power system of the Saudi electricity company, western region (SEC-WR)," *Proceedings of the 2003 IEEE PowerTech Conference*, vol. 4, Bologna, Italy, June 23-26, 2003.
- [9] F. P. de Mello, and J. W. Feltes, "Voltage oscillatory instability caused by induction motor loads," *IEEE Trans. on Power Systems*, vol. 11, no. 3, Aug. 1996, pp. 1279-1285.
- [10] N. Martins, S. Gomes Jr., R. M. Henriques, C. B. Gomes, A. de Andrade Barbosa, and A. C. B. Martins, "Impact of induction motor loads in system loadability margins and damping of inter-area modes," *Proceedings of the 2003 IEEE-PES General Meeting*, Toronto, Canada, July 13-17, 2003.
- [11] J. Undrill, A. Renno, and G. Drobnjak, "Dynamics of a large induction motor load system," *Proceedings of the 2003 IEEE-PES General Meeting*, Toronto, Canada, July 13-17, 2003.
- [12] K. Morison, H. Hamadani, and L. Wang, "Practical issues in load modeling for voltage stability studies," *Proceedings of the 2003 IEEE-PES General Meeting*, Toronto, Canada, July 13-17, 2003.
- [13] K. Tomiyama, S. Ueoka, T. Takano, I. Iyoda, K. Matsuno, K. Temma, and J. J. Paserba, "Modeling of Load During and After System Faults Based on Actual Field Data," *Proceedings of the 2003 IEEE-PES General Meeting*, Toronto, Canada, July 13-17, 2003.

- [14] I. R. Navarro, O. Samuelsson, and S. Lindahi, "Automatic determination of parameters in dynamic load models from normal operation data," Proceedings of the 2003 IEEE-PES General Meeting, Toronto, Canada, July 13-17, 2003.
- [15] I. R. Navarro, O. Samuelsson, and S. Lindahi, "Influence of normalization in dynamics reactive load models," IEEE Trans. on Power Systems, vol. 18, issue 2, May 2003, pp. 972-973.
- [16] C. -J. Lin, A. Y. -T. Chen, C. -Y. Chiou, C. -H. Huang, H. -D. Chiang, J. -C. Wang and L. Fekih-Ahmed, "Dynamic load models in power systems using the measurement approach," IEEE Trans. on Power Systems, vol. 8, issue 1, Feb. 1993, pp. 309-315.
- [17] D. J. Hill, "Nonlinear dynamic load models with recovery for voltage stability studies," IEEE Trans. on Power Systems, vol. 8, no. 1, Feb. 1993, pp. 166-176.
- [18] D. Karlsson and D. J. Hill, "Modelling and identification of nonlinear dynamic loads in power systems," IEEE Trans. on Power Systems, vol. 9, no. 1, Feb. 1994, pp. 157-166.
- [19] A. P. Sakis Meliopoulos, Wenzhong Gao, Shengyuan Li, G. J. Cokkinides and Roger Dougal, "Quadratized induction machine model for power flow analysis," Proceedings of the Second IASTED International Conference, EuroPES, Crete, Greece, pp 194-199, June 25-28, 2002.
- [20] G. K. Stefopoulos and A. P. Meliopoulos, "Induction motor load dynamics: Impact on voltage recovery phenomena," to be presented at the 2005-2006 IEEE PES T&D Conference and Exposition, Dallas, TX, May 21-26, 2006.
- [21] A. P. Meliopoulos, G. J. Cokkinides, and G. K. Stefopoulos, "Voltage stability and voltage recovery: Effects of electric load dynamics," presented at the 2006 IEEE International Symposium on Circuits and Systems, Island of Kos, Greece, May 21-24, 2006.
- [22] A. P. Sakis Meliopoulos, G. J. Cokkinides, and G. K. Stefopoulos, "Symbolic integration of dynamical systems by collocation methods," Proceedings of the 2005 IEEE-PES General Meeting, San Francisco, CA, June 12-16, 2005, pp. 2387-2392.
- [23] G. K. Stefopoulos and A. P. Meliopoulos, "Quadratized Three-Phase Induction Motor Model for Steady-State and Dynamic Analysis," in Proc. of the 38th North America Power Symposium, Carbondale, IL, USA, Sept. 17-19, 2006, pp. 79-89.
- [24] A. P. Sakis Meliopoulos, G. J. Cokkinides, and G. K. Stefopoulos, "Quadratic integration method," Proceedings of the 8th Int. Conference on Power System Transients (IPST 05), Montréal, Canada, June 19-23, 2005.
- [25] P. Pillay, R. Nolan, and T. Haque, "Application of genetic algorithm to motor parameter determination for transient torque calculations," IEEE Trans. Ind. Applications, vol. 33, no 5, pp. 1273-1282, Sept./Oct. 1997.
- [26] H. Weatherford and C. W. Brice, "Estimation of induction motor parameters by a genetic algorithm," in Proc. 2003 Annu. Pulp and Paper Industry Technical Conference, pp. 21-28.
- [27] P. Nangsue, P. Pillay, S. Conry, "Evolutionary algorithms for induction motor parameter determinations," IEEE Trans. Energy Conversion, vol. 14, no 3, pp. 447-453, Sept./1999.

- [28] B. K. Johnson and J. R. Willis, "Tailoring induction motor analytical models to fit known motor performance characteristics and satisfy particular study needs," IEEE Trans. Power Systems, vol. 6, no 3, pp. 959-965, Aug. 1991.
- [29] J. Pedra and F. Corcoles, "Estimation of induction motor double-cage model parameters from manufacturer data," IEEE Trans. Energy Conversion, vol. 19, no 2, June 2004.
- [30] J. T. Betts, Practical Methods for Optimal Control Using Nonlinear Programming. SIAM 2001.
- [31] J. T. Betts, "Survey of numerical methods for trajectory optimization," AIAAJournal of Guidance, Control, and Dynamics, vol. 21, 1998, pp. 193-207.

Project Publications

G. K. Stefopoulos, A. P. Meliopoulos, and G. J. Cokkinides, “Voltage-Load Dynamics: Modeling and Control,” in Proceedings of the 2007 IREP Symposium on Bulk Power System Dynamics and Control – VII, (IREP 2007 Conference), Charleston, SC, USA, August 19-24, 2007.

G. K. Stefopoulos, G. J. Cokkinides, and A. P. Meliopoulos, “Voltage Recovery Phenomena in Distribution Feeders,” in Proceedings of the 2008 IEEE PES General Meeting, Pittsburgh, PA, USA, July 20-24, 2008.

A. P. Meliopoulos, V. Farantatos, G.J. Cokkinides, S. Mohagheghi, and G. K. Stefopoulos, “A New Out-of-Step Protection Scheme via GPS-Synchronized Data,” in Proceedings of the 16th Power Systems Computation Conference, Glasgow, Scotland, July 14-18, 2008.

G. K. Stefopoulos, G. J. Cokkinides, and A. P. Meliopoulos, “Optimal Operation of Dynamic VAR Sources for Mitigation of Delayed Voltage Recovery,” submitted to the 6th Mediterranean Conference and Exhibition on Power Generation, Transmission and Distribution, Thessaloniki, Greece, Nov. 2-5, 2008.